



This is to certify that the  
dissertation entitled

STRUCTURE AND FUNCTION RELATIONSHIPS OF  
DIHYDRONEOPTERIN ALDOLASES FROM *ESCHERICHIA  
COLI* AND *STAPHYLOCOCCUS AUREUS*

presented by

Yi Wang

has been accepted towards fulfillment  
of the requirements for the

Ph.D

degree in

Biochemistry & Molecular  
Biology



Major Professor's Signature

5/10/06

Date

*MSU is an Affirmative Action/Equal Opportunity Institution*



**PLACE IN RETURN BOX** to remove this checkout from your record.  
**TO AVOID FINES** return on or before date due.  
**MAY BE RECALLED** with earlier due date if requested.

DATE DUE	DATE DUE	DATE DUE
JUN 21 2007		

**STRUCTURE AND FUNCTION RELATIONSHIPS OF  
DIHYDRONEOPTERIN ALDOLASES  
FROM *ESCHERICHIA COLI* AND *STAPHYLOCOCCUS AUREUS***

By

Yi Wang

A DISSERTATION

Submitted to  
Michigan State University  
in partial fulfillment of the requirements  
for the degree of

DOCTOR OF PHILOSOPHY

Department of Biochemistry and Molecular Biology

2006

## ABSTRACT

### STRUCTURE AND FUNCTION RELATIONSHIPS OF DIHYDRONEOPTERIN ALDOLASES FROM *ESCHERICHIA COLI* AND *STAPHYLOCOCCUS AUREUS*

By

Yi Wang

Dihydroneopterin aldolase (DHNA) catalyzes the cleavage of 7,8-dihydro-D-neopterin (DHNP) to form 6-hydroxymethyl-7,8-dihydropterin (HP) and glycolaldehyde and the epimerization of DHNP to form 7,8-dihydro-L-monapterin (DHMP). NMR analysis of the reaction products in a D<sub>2</sub>O solvent suggests that the epimerization reaction follows the same intermediate as the aldol reaction. A complete set of kinetic constants for both the aldol and epimerization reactions according to a unified kinetic mechanism has been determined for DHNA from *Staphylococcus aureus* (SaDHNA) and DHNA from *Escherichia coli* (EcDHNA). The results show that they have significantly different binding and catalytic properties, in accordance with the significant sequence differences between them. EcDHNA is different from SaDHNA biochemically in several aspects. EcDHNA has much higher affinities for the substrate, products, and inhibitors measured in this work. EcDHNA has a much higher epimerase activity than SaDHNA. The rate-limiting step is product release for EcDHNA but is the chemical step for SaDHNA. EcDHNA has significantly higher rate constants for the chemical steps than SaDHNA.

The functional role of a conserved tyrosine residue at the active site of DHNA has been investigated by site-directed mutagenesis. Comprehensive analysis of the reactions catalyzed by Y54F-SaDHNA and Y53F-EcDHNA showed that the major reaction

product is dihydroxanthopterin (DHXP) rather than HP. DHXP is generated via the same enol intermediate as in the wild-type enzyme-catalyzed reaction. The mutants are impaired in the protonation of the enol intermediate to form HP. In addition to the normal products and DHXP, formic acid is also formed in the reaction. In addition to DHNP, molecular oxygen is also consumed in the reaction. The ligand-binding properties of the mutants are perturbed to a small extent. The results showed that the mutant enzymes are oxygenases, and the conserved tyrosine residue plays only a minor role in the physical steps of the enzymatic reaction and the formation of the enol reaction intermediate but a critical role in the protonation of the enol intermediate to form HP.

The functional roles of the conserved glutamate and lysine residues at the active site, E22, E74, and K100 in SaDHNA, E21, E73, and K98 in EcDHNA, have been investigated by site-directed mutagenesis in this work. The results showed that E74 of SaDHNA and E73 of EcDHNA are important for substrate binding, but their roles in catalysis are minor if any. In contrast, E22 and K100 of SaDHNA are important for catalysis, but their roles in substrate binding are minor. On the other hand, E21 and K98 of EcDHNA are important for both substrate binding and catalysis.

Copyright by  
YI WANG  
2006

To my parents

## ACKNOWLEDGEMENTS

I would like to express my sincere gratitude to my graduate advisor, Dr. Honggao Yan, for his constant guidance and support. I have benefited greatly from his wealth of knowledge and experience. I am grateful to my graduate committee members, Dr. Robert P. Hausinger for fruitful discussions on mechanistic issues about DHNA, Dr. J. Gregory Zeikus, Dr. Kathleen A. Gallo and Dr. James H. Geiger, for their discussion and suggestions. I thank Dr. Yue Li for her assistance in the site-directed mutagenesis experiments, and Yan Wu for binding and stopped-flow analysis of EcDHNA. Thanks also to Dr. Guangyu Li, Dr. Jaroslaw Blaszczyk and Dr. Krzysztof Felczak, Lishan Yao, Zhenwei Lu, and Jifeng Wang. I am also deeply thankful to Dr. Gavin Reid, Gwynyth Anne Scherperel, Dr. Kade D. Roberts and Katherine Rank for MS analysis, Dr. Denise Mills for assistance in the oxygen consumption assay, Mr. James B. McKinlay for assistance in the HPLC identification of formic acid, Dr. A. Daniel Jones for collecting GC-MS data of glycolaldehyde, Mr. Joseph Leykam for expert assistance in the HPLC analysis, Dr. Xinhua Ji and his coworkers for determinations of crystal structures of DHNAs. I am also indebted to Dr. Aizhou Liu, Dr. Daniel Holmes and Dr. Kermit Johnson for training on the operation of NMR, Dr. Zachary F. Burton for reading of the manuscript, Dr. Kaillathe Padmanabhan for solving computer problems. I would also like to thank my friends for their encouragement and grateful help.

And finally, I thank my parents and other family members for their support.

## TABEL OF CONTENTS

<b>LIST OF TABLES</b> .....	ix
<b>LIST OF FIGURES</b> .....	x
<b>ABBREVIATIONS</b> .....	xiii
<b>CHAPTER 1: INTRODUCTION</b>	
Folate biosynthesis pathway.....	1
Biomedical significance of DHNA.....	4
Uniqueness of DHNA.....	9
DHNA is a bifunctional enzyme	
DHNA is a novel type of aldolases	
Mechanism studies of DHNA.....	19
Structures of DHNAs.....	20
Active site residues of SaDHNA.....	25
References.....	27
<b>CHAPTER 2: NMR, EQUILIBRIUM AND TRANSIENT KINETIC STUDIES OF THE <i>STAPHYLOCOSSUS AUREUS</i> AND <i>ESCHERICHIA COLI</i> ENZYMES</b>	
Abstract.....	31
Introduction.....	33
Experimental Procedures.....	38
Results.....	43
Discussion.....	63
References.....	69
<b>CHAPTER 3: A POINT MUTATION CONVERTS THE ENZYME TO AN OXYGENASE</b>	
Abstract.....	72
Introduction.....	73
Experimental Procedures.....	74
Results.....	78
Discussion.....	109
References.....	118
<b>CHAPTER 4: FUNCTIONAL ROLES OF THE CONSERVED ACTIVE SITE GLUTAMATE AND LYSINE RESIDUES</b>	
Abstract.....	120

<b>Introduction.....</b>	<b>121</b>
<b>Experimental Procedures.....</b>	<b>123</b>
<b>Results.....</b>	<b>128</b>
<b>Discussion.....</b>	<b>141</b>
<b>References.....</b>	<b>146</b>

## LIST OF TABLES

### CHAPTER 2

- Table 2.1. Dissociation Constants of SaDHNA and EcDHNA Measured by Equilibrium Binding Experiments..... 53
- Table 2.2. Association and Dissociation Rate Constants of SaDHNA and EcDHNA Measured by Stopped-flow Experiments..... 57

### CHAPTER 3

- Table 3.1. Binding Constants of SaDHNA, EcDHNA and Y→F Mutants..... 84
- Table 3.2. Chemical Shifts of Selected Protons of Compounds Related to the Reactions Catalyzed by the Wild-Type and Mutant DHNAs ..... 88

### CHAPTER 4

- Table 4.1. The Forward and Reverse Primers for the PCR-Based Mutagenesis Experiments..... 125
- Table 4.2. Binding Constants of SaDHNA and Site-Directed Mutants..... 136
- Table 4.3. Binding Constants of EcDHNA and Site-Directed Mutants..... 137
- Table 4.4. Steady State Kinetic Constants of SaDHNA and Site-Directed Mutants..... 139
- Table 4.5. Steady State Kinetic Constants of EcDHNA and Site-Directed Mutants..... 140

## LIST OF FIGURES

### CHAPTER 1

- Figure 1.1. Folate biosynthesis pathway..... 3
- Figure 1.2. Amino acid sequence assignment of 11 DHNAs.....7
- Figure 1.3. The aldolase/epimerase reactions catalyzed by DHNA.....12
- Figure 1.4. Mechanisms of two types of aldolases.....15
- Figure 1.5. Proposed mechanism of reactions catalyzed by DHNA..... 18
- Figure 1.6. The crystal structure of the complex of SaDHNA and product HP.  
A) Top view, B) Side view..... 22
- Figure 1.7. The potential important residues around the product HP at the active site of SaDHNA..... 24

### CHAPTER 2

- Figure 2.1. The proposed catalytic mechanism for the DHNA  
-catalyzed reactions.....36
- Figure 2.2. Amino acid sequence alignment of DHNAs.....46

Figure 2.3.	The SaDHNA-catalyzed reactions in D <sub>2</sub> O monitored by NMR.....	49
Figure 2.4.	Binding of NP to SaDHNA at equilibrium.....	52
Figure 2.5.	Stopped-flow analysis of the binding of HPO to EcDHNA.....	56
Figure 2.6.	Quench-flow analysis of the SaDHNA-catalyzed reaction.....	60
Figure 2.7.	Quench-flow analysis of the EcDHNA-catalyzed reaction.....	62
Figure 2.8.	Summary of the kinetic constants for the SaDHNA-catalyzed (top panel) and EcDHNA-catalyzed (lower panel) reactions.....	65
 <b>CHAPTER 3</b>		
Figure 3.1.	Binding of HPO to EcY53F at equilibrium.....	81
Figure 3.2.	Stopped-flow analysis of the binding of MP to EcY53F.....	83
Figure 3.3.	NMR analysis of the reactions catalyzed by SaDHNA (A) and SaY54F (B) .....	86
Figure 3.4.	ESI MS analysis of the reaction mixtures generated by SaDHNA (A) and SaY54 (B) .....	90
Figure 3.5.	Multistage tandem mass spectrometry identification of the m/z 196 product from the reaction of DHNP with SaDHNA.....	92

Figure 3.6.	Multistage tandem mass spectrometry identification of the m/z 182 product from the reaction of DHNP with SaY54F.....	95
Figure 3.7.	MS spectra of the derivatives of GA Standard (A) and the DHNP reaction mixture generated SaY54F (B) .....	98
Figure 3.8.	Multistage tandem mass spectrometry identification of the substrate DHNP.....	100
Figure 3.9.	Multistage tandem mass spectrometry identification of the m/z 194 products from the DHNP reaction catalyzed by SaY54F.....	102
Figure 3.10.	Identification of formic acid by HPLC.....	105
Figure 3.11.	Time courses of DHNP reactions catalyzed by SaDHNA (A) and SaY54F (B) .....	108
Figure 3.12.	Oxygen consumption by the reactions catalyzed by SaDHNA and SaY54F.....	111
Figure 3.13.	The proposed chemical mechanism for the generation of DHXP and FDHP.....	117

#### **CHAPTER 4**

Figure 4.1.	Binding of MP to SaE22A at equilibrium.....	130
Figure 4.2.	Binding of HPO to EcK98A at equilibrium.....	132
Figure 4.3.	Stopped-flow analysis of the binding of HPO to SaE22A.....	135

## ABBREVIATIONS

CID	collision-induced dissociation
EcDHNA	dihydroneopterin aldolase from <i>Escherichia coli</i>
EcE21A	DHNA with E21 replaced with alanine
EcE73A	EcDHNA with E73 replaced with alanine
EcK98A	EcDHNA with K98 replaced with alanine
DEAE	diethylaminoethyl
DHFR	dihydrofolate reductase
DHMP	7, 8-dihydromonapterin
DHNA	dihydroneopterin aldolase
DHNP	7, 8-dihydroneopterin
DHNTF	7,8-dihydroneopterin triphosphate pyrophosphohydrolase
DHPS	dihydropteroate synthase
DHXP	dihydroxanthopterin
DSS	2,2-dimethyl-2-silapentane-5-sulfonate sodium salt
DTT	dithiothreitol
EcY53F	EcDHNA with Y53 replaced with a phenylalanine residue
EDTA	ethylenediaminetetraacetic acid
ESI	electrospray ionization
FDHP	6-formyl-7,8-dihydropterin
FID	free induction delay

FPGS	folylpolyglutamate synthetase
GA	glycolaldehyde
GC-MS	gas column with mass spectrometry
GTP	guanosine triphosphate
GTPCH	GTP cyclohydrolase
HEPES	4-(2-hydroxyethyl)piperazine-1-ethanesulfonic acid
HiDHNA	dihydroneopterin aldolase from <i>Haemophilus influenzae</i>
HMDP	6-hydroxymethyl-7,8-hydroxymethyl-pterin
HPO	6-hydroxymethyl-pterin
HPLC	high performance liquid chromatography
HPPK	hydroxymethyl-7,8-dihydropterin pyrophosphokinase
IPTG	isopropyl $\beta$ -D-thiogalactopyranoside
LC-MS	liquid column with mass spectrometry
Ni-NTA	nickel-nitrilotriacetic acid
NMR	nuclear magnetic resonance
NP	neopterin
MP	monapterin
MS	mass spectrometry
MtDHNA	dihydroneopterin aldolase from <i>Mycobacterium tuberculosis</i>
MTBSTFA	N-(t-butyldimethylsilyl)-N-methyltrifluoroacetamide
$K_d$	dissociation constant
$k_x$	rate constants
$pK_a$	ionization constant

SaDHNA	dihydroneopterin aldolase from <i>Staphylococcus aureus</i>
SaE22A	SaDHNA with E22 replaced with alanine
SaE74A	SaDHNA with E74 replaced with alanine
SaK100A	SaDHNA with K100 replaced with alanine
SaK100Q	SaDHNA with K100 replaced with glutamine
SaY54F	SaDHNA with Y54 replaced with a phenylalanine residue
THF	tetrahydrofolate
Tris	tris(hydroxymethyl)–aminomethane
TCEP	tris(2-carboxyethyl)phosphine

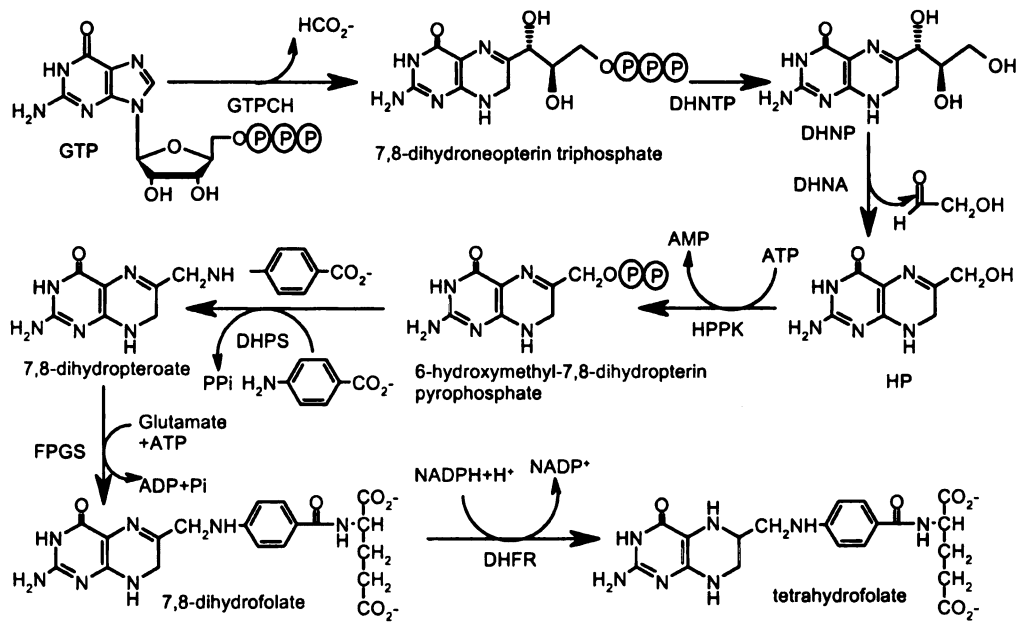
## CHAPTER 1: INTRODUCTION

### FOLATE BIOSYNTHESIS PATHWAY

Folate is essential to life. The entire folate synthesis pathway is shown in Figure 1.1. Plants and bacteria can synthesize folate, because they have all of the enzymes in the *de novo* synthesis pathway (1). Unlike plants and bacteria, humans and other vertebrates are unable to synthesize folate *de novo* (1). Instead, folic acid is an essential vitamin and humans have to obtain folate from their diet with an active transport system (1). This active transport system does not exist in bacteria. If the *de novo* folate synthesis pathway is shut down, bacteria can not survive. Therefore, the folate biosynthesis pathway is one of principal targets for the development of antimicrobial agents.

The first step in folate biosynthesis is the conversion of GTP into dihydroneopterin triphosphate, which is catalyzed by GTP cyclohydrolase (GTPCH). The triphosphate moiety of dihydroneopterin triphosphate is removed by 7,8-dihyroneopterin triphosphate pyrophosphohydrolase (DHNTP) (2), and the resulting DHNP is converted to 6-hydroxymethyl-7,8-dihydropterin (HP) by dihydroneopterin aldolase (DHNA). The enzyme 6-hydroxymethyl-7,8-dihydropterin pyrophosphokinase (HPPK) catalyzes the transfer of pyrophosphate from ATP to HP. The resulting product is converted to 7,8-dihydropteroate by replacing the pyrophosphate moiety with 4-aminobenzoate, a reaction that is catalyzed by dihydropteroate synthase (DHPS). 7,8-Dihydropteroate is converted to 7,8-dihydrofolate by folylpolyglutamate synthetase (FPGS).

**Figure 1.1: Folate biosynthesis pathway.** GTP, guanosine triphosphate. GTPCH, GTP cyclohydrolase. DHNTP, 7,8-dihydroneopterin triphosphate pyrophosphohydrolase. DHNA, dihydroneopterin aldolase. DHPS, dihydropteroate synthase. HPPK, hydroxymethyl-7,8-dihydropterin pyrophosphokinase. FPGS, folylpolyglutamate synthetase. DHFR, dihydrofolate reductase.



7,8-Dihydrofolate is reduced to tetrahydrofolate by dihydrofolate reductase (DHFR) using NADPH (3, 4).

The first class of antibiotics in clinical use for the treatment of infectious diseases was the sulfonamides, which target DHPS (5). Antibiotics such as trimethoprim have also been developed against DHFR (6). However, the folate pathway is under-explored as a target for developing antimicrobial agents. Both sulfonamides and trimethoprim are still in clinical use, but as for other antibiotics, their clinical use has been severely limited by the development of resistance (7). Antibiotic resistance naturally develops via natural selection through random mutation and plasmid exchange between bacteria of the same species. The mechanisms of resistance and of its spread among pathogenic bacteria show a remarkable evolutionary adaptation to the presence of trimethoprim and sulfonamide. This is reflected in the chromosomal pattern of changes in the structures and mechanisms of regulation of *dhps* and *dhfr* genes coding for the target enzymes DHPS and DHFR (7). The rapid development of microbial resistance against current antibiotic drugs requires renewed effort in developing new antimicrobial agents (8).

*Staphylococcus aureus* (*S. aureus*) has become resistant to many commonly used antibiotics. *S. aureus* frequently lives on the skin or in the nose of a healthy person. *S. aureus* can cause illnesses ranging from minor skin infections and abscesses, to life-threatening diseases such as pneumonia, meningitis, endocarditis and septicemia (9). Because of its importance in serious infections, I chose *S. aureus* as the target organism.

## **BIOMEDICAL SIGNIFICANCE OF DHNA**

Among the most promising strategies for the development of new antibacterial therapeutics is the targeting of proteins essential for bacterial growth but lacking mammalian counterparts (10). Of the enzymes in the folate pathway, DHNA, HPPK and DHPS are absent in human. Therefore, it is worthwhile to explore other folate biosynthesis enzymes such as DHNA besides DHPS and DHFR enzymes in the folate biosynthesis pathway. DHNA is a particularly attractive target for drug development also because the substrate has no phosphoryl group (11). Several other enzymes such as GTPCH and HPPK in the folate biosynthesis pathway use phosphorylated substrates (e.g. GTP and 6-hydroxymethylpterin pyrophosphate). Nonspecific inhibition of enzymes using substrates with phosphoryl groups is a major problem in developing inhibitors with high specificity (11). Inhibitors of one group of kinases might also inhibit other kinases and phosphatases, and bring global effects on signal transduction pathways.

DHNA exists widely in the bacterial kingdom. Generally, there are two types of bacteria: Gram-positive and Gram-negative. *S. aureus* is an important pathogenic Gram-positive bacterium, and *Escherichia coli* (*E. coli*) is a representative of the Gram-negative bacteria. Figure 1.2 shows the multiple sequence alignment of eleven DHNAs from different bacteria. The top five DHNAs are enzymes from Gram-positive bacteria including SaDHNA, and the bottom six DHNAs are enzymes from Gram-negative bacteria including EcDHNA. DHNAs from Gram-positive or Gram-negative bacteria share much similarity with DHNAs in their own group, but fewer similarities are observed between enzymes from the two classes. The identities between enzymes from Gram-positive bacteria range from 39% to 45% and those between Gram-negative bacteria are 49% to 91%, but the identities between Gram-positive and Gram-negative

**Figure 1.2: Amino acid sequence alignment of 11 bacteria DHNAs.** From top to bottom, the 11 DHNAs are from *Staphylococcus aureus* (SA), *Bacillus subtilis* (BS), *Streptococcus pyogenes* (SP), *Listeria innocua* (LI), *Streptomyces coelicolor* (SC), *Escherichia coli* (EC), *Salmonella typhi* (ST), *Yersinia pestis* (YP), *Vibrio cholerae* (VC), *Haemophilus influenzae* (HI), and *Pseudomonas aeruginosa* (PA). The First five DHNAs are from Gram-positive bacteria, and the next six DHNAs are from Gram-negative bacteria. The highly conserved residues among all Gram-positive and Gram-negative bacteria are shaded in black. Residues that are characteristics of the Gram-positive or Gram-negative bacteria are shaded in gray. The amino acid sequences are quite different between the enzyme from Gram-positive and Gram-negative bacteria. Many differences are at or near the active site of the enzyme.

```

*          0          *          20          *
SA : -----MCDITFLKGMRFYCYHGALSABNEIGCIIRKVDVTL : 35
BS : -----MDKVVVEGMEFYCYHGVFTBENKLGRRKVDLTA : 34
SP : -----MDKIVLEGCGRFYCYHGAYKBEQTLGGIIFLVDDEL : 34
LI : -----MDKHYLNLALAFYCYHCVLQEBETKLGCTFRVSLIL : 34
SC : -----MDRVALRGLKARCHEGVFPKEREDGGTFLVLDIVL : 34
EC : -----MDIVFIEQLSWITITICVYDNEQTHEKIVFDIEM : 34
ST : -----MMDIVFIEQLSWITITICVYDNEQTHEKIVFDIEM : 35
YP : -----MDIVFIEELSITITICVYDNEQTHEKIVFDIEM : 34
VC : MGIRPVNRKRLSMKVFIEQLSWITITICVYDNEQQKIKVLDLDM : 46
HI : -----MDRVFIEELTIFACICVYDNEQQKIKVFDIEM : 34
PA : -----MDRVFIEGLEMDTIVCIVYDNERGIRKCRLLDLTL : 34

```

```

          40          *          60          *          80
SA : KVDLAEAGRDTNVIDIVHYGCVFEEVKSIMEGKAVNLLHIAERFA : 81
BS : ELDLKAGQTDDEEQINVAELVHYCKDIVEGEPVKLVETLAERFA : 80
SP : SVDLQAASLSSQITDIVHGMVFDSDVRQLVEGEKFIIDGGLAGANC : 80
LI : GLSTKAGQSDSDVDIVSVADIVYETVKGIVEGTPFKLIBAIAERFA : 80
SC : GLDTRPAAADDDLAKIVHYGIVAEVVAVVEGEPVNLVETLAERFA : 80
EC : AWDNRKAASDDVADCLSVADIAETVVSHVGEGRFALVERVREBWA : 80
ST : AWDNRKSAKSDDVADCLSVADIAETVINHVGEGRFALVERVREBWA : 81
YP : GWDNRKAAGSDDVNDCLSVADIAEVAIVQHVSQRFALVERVREBWA : 80
VC : AHDNRAAGKSDDVADALDVAQVSAVLEHIEQGRFLLVERVREBWA : 92
HI : AWDCKQAAETDDVYVCLNVAEVSQAIIIDVYESKPFLLIERVREBWA : 80
PA : GWDNRPAAAGDDLALALDVAALSERVQEFARESHFQIVETFAERFA : 80

```

```

*          100          *          120
SA : NRINSQYNRVMEVKVRIITRENPEIPGHYDGVGHEIVRENK---- : 121
BS : GTVLGKFPQVQOCTVVKVIKPDPEIPGHYKSAIHEITRKKS---- : 120
SP : EQLFNEFPPIEAIKVAHKKENPPIAGHYKAVGHEIHERQR---- : 119
LI : SEVLTDPYLLLEEITVVKLIKPNPEIPGHYDSVAVEIKKRSDDLGD- : 124
SC : QVCLKHE-GVEEVEVGVHKPDAEITVFPDDVTVYTLIERSV---- : 119
EC : ELLLARF-NSPFWVRKLSKPGA-VA-RANVGVIIHERGNNLKENN : 122
ST : DLLLSRF-NSPFWVRKLSKPGA-VA-RANVGVIIHERGNNLK---- : 120
YP : ELLLSRF-NSPFWVRKLSKPGA-VA-QAKNVGVIIHERGQRLS--- : 119
VC : ELIMTRF-AVPWLRIRIRKPGA-VP-QAKGVGVIIHERG---- : 129
HI : DLLESRY-QLQGLKIKLSKPGA-VA-QARNVGVIIHERG-CLK---- : 118
PA : EVLMGER-GIPWLRIRIRKPGA-VP-ARGVGVIIHERGCR---- : 117

```

bacterial enzymes are less than 30%. SaDHNA and EcDHNA share only about 23% identity. Many differences between the enzymes from the two classes of bacteria might be at or near their active sites. The positions of their active sites are indicated by the crystal structures of SaDHNA. Lower sequence similarities indicate that Gram-positive and Gram-negative enzymes might have different characteristics. It may therefore be possible to design a “narrow spectrum” antibiotic drug for DHNA.

The major modification sites on the pterin ring for inhibitor design of DHNA are C6 and C7. Potent inhibitors of DHNA have been discovered using CrystaLEAD X-ray crystallographic high-throughput screening followed by structure-directed optimization (10). Several lead compounds with  $IC_{50}$  values of about 1  $\mu$ M against DHNA were identified among a 10,000 random compound library. Structure-directed optimization of one of the leads thus identified afforded potent inhibitors with submicromolar  $IC_{50}$  values (10). The potential problem with the crystallographic screening is that the binding pocket is fixed in one conformation in the crystallized form used for soaking-in of the ligand of interest. More inhibitors can be found when different conformations of DHNA are available in solution. A significant improvement of inhibition can be achieved by structure-based design and through additional cycles of screening (10)

## UNIQUENESS OF DHNA

### 1) DHNA is a bifunctional enzyme

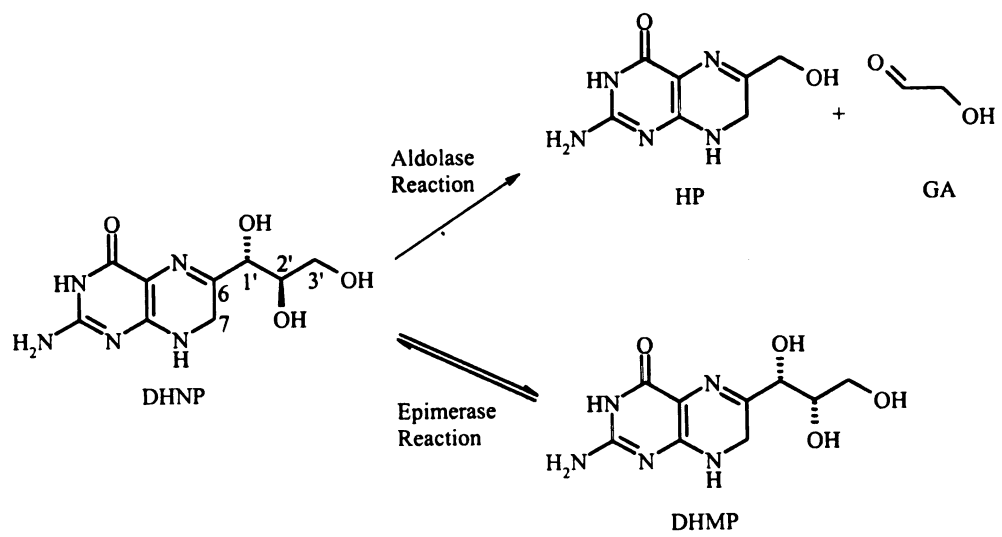
DHNA catalyzes both an aldolase and epimerase reaction as shown in Figure 1.3. As an aldolase, it converts the natural substrate DHNP to HP and glycolaldehyde (GA). As an epimerase, DHNA converts DHNP to 7,8-dihydromonapterin (DHMP), a stereoisomer of DHNP. The steady-state kinetic parameters of EcDHNA and DHNA from *Haemophilus influenzae* (HiDHNA) from the catalyzed reaction were determined in 1998 (12). DHNP and DHMP both can be used as substrates and their aldolase reaction activities  $k_{cat}$  are 127 and 158  $\mu\text{mol}/\text{mg}/\text{h}$ , respectively.  $K_m$  values for DHNP and DHMP are 64 and 36  $\mu\text{M}$ , respectively. HiDHNA has a higher aldolase reaction activity than EcDHNA with DHNP as substrate, but it has a lower aldolase activity than EcDHNA with DHMP as substrate. Its epimerase activity with DHNP and DHMP as substrates is also lower than that of EcDHNA (12).

The fact that DHNA has an epimerase activity is not totally surprising because the enzyme is homologous to dihydroneopterin triphosphate epimerase, which catalyzes the stereochemical conversion of dihydroneopterin triphosphate and dihydromonapterin triphosphate. The sequence identity between DHNA and dihydroneopterin triphosphate epimerases from *E. coli* is 30%, higher than the 23% identity between SaDHNA and EcDHNA. Furthermore, the two enzymes have a similar folding topology and quaternary structure (13). The epimerase also has a low level of aldolase activity.

Because these enzymes each have two activities, it is proposed that the aldolase and epimerase reactions share a common reaction intermediate. A retro-aldol cleavage of the C-C bond between C1' and C2' is proposed to be a crucial step in both reactions (12). For the epimerase reaction, the intermediate species stay long enough in the active site of the enzyme so that one of the cleaved products can rotate and reattach to form a new stereoisomer. For the aldolase reaction, two products may be released quickly from the active site of the enzyme. The overall products of these enzymatic reactions may be determined by the relative rates of these processes. It is reasonable to predict that aldolase could become an epimerase if the reaction intermediates are trapped at the active site to allow them to rotate and re-form the C-C bond.

Another pair of enzymes shares relationships with DHNA and dihydroneopterin triphosphate epimerase, namely L-fuculose-1-phosphate aldolase and ribulose-5-phosphate-epimerase. L-Fuculose-1-phosphate aldolase catalyzes the reversible cleavage of L-fuculose-1-phosphate to dihydroxyacetone phosphate and L-lactaldehyde (14). Ribulose-5-Phosphate-epimerase catalyzes the interconversion of L-ribulose-5-phosphate and D-xylulose-5-phosphate (15). The two enzymes both have a divalent cation at their active sites (16).

**Figure 1.3: The aldolase/epimerase reactions catalyzed by DHNA.**

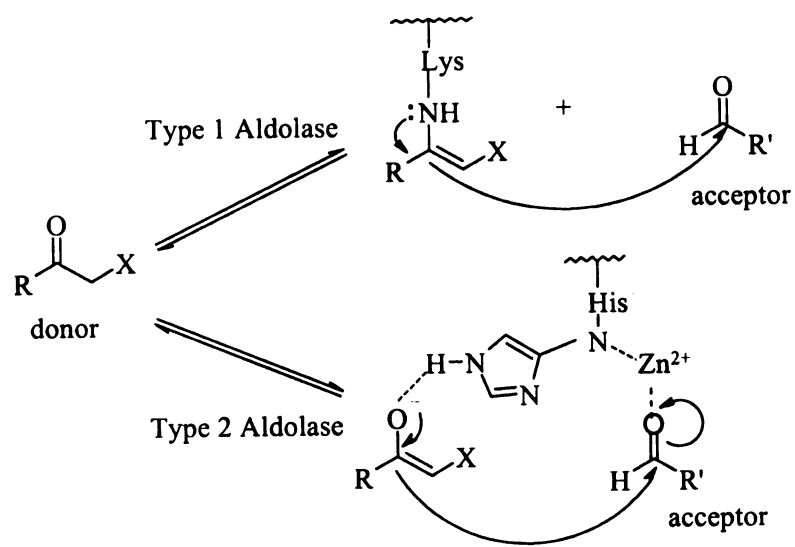


Moreover, L-ribulose 5-phosphate 4-epimerase uses a retroaldol/aldol mechanism for the epimerization of L-ribulose 5-phosphate. The evidence for the mechanism is solid: (a) No solvent isotope incorporation ( $^2\text{H}$  or  $^{18}\text{O}$ ) could be detected, indicating that any mechanism involving nonstereospecific deprotonation/reprotonation is highly unlikely (15). (b) There were no primary deuterium isotope effects on the protons at either C-3 or C4 (17). (c)  $^{13}\text{C}$  kinetic isotope effects were observed on both the C3 carbon (1.85%) and the C4 carbon (1.5%) of L-ribulose 5-phosphate, which is consistent with a mechanism involving C-C bond cleavage (17). (d) There is a detectable aldolase activity (18). (e) The epimerase shares 26% sequence identity with L-fuculose-1-phosphate aldolase as described earlier (14). When the structures of the epimerase and the aldolase are superimposed, 93% of the  $\alpha$ -carbons align with a root-mean square deviation of only 1.5 Å, indicating that the two enzymes belong to a superfamily of aldolases/epimerases and have evolved from a common ancestor (19).

## **2) DHNA is a novel aldolase**

There are two known classes of aldolases (20, 21). Class I aldolases utilize an active-site lysine to form a Schiff base to activate their substrates, while class II enzymes require a divalent metal ion, usually zinc, for catalysis as shown in Figure 1.4 (22). Type I aldolases include fructose-1,6-bisphosphate aldolase (23), 2-keto-3-deoxy-6-phosphogluconate aldolase (24), and *N*-acetylneuraminate aldolase (25). Type II enzymes

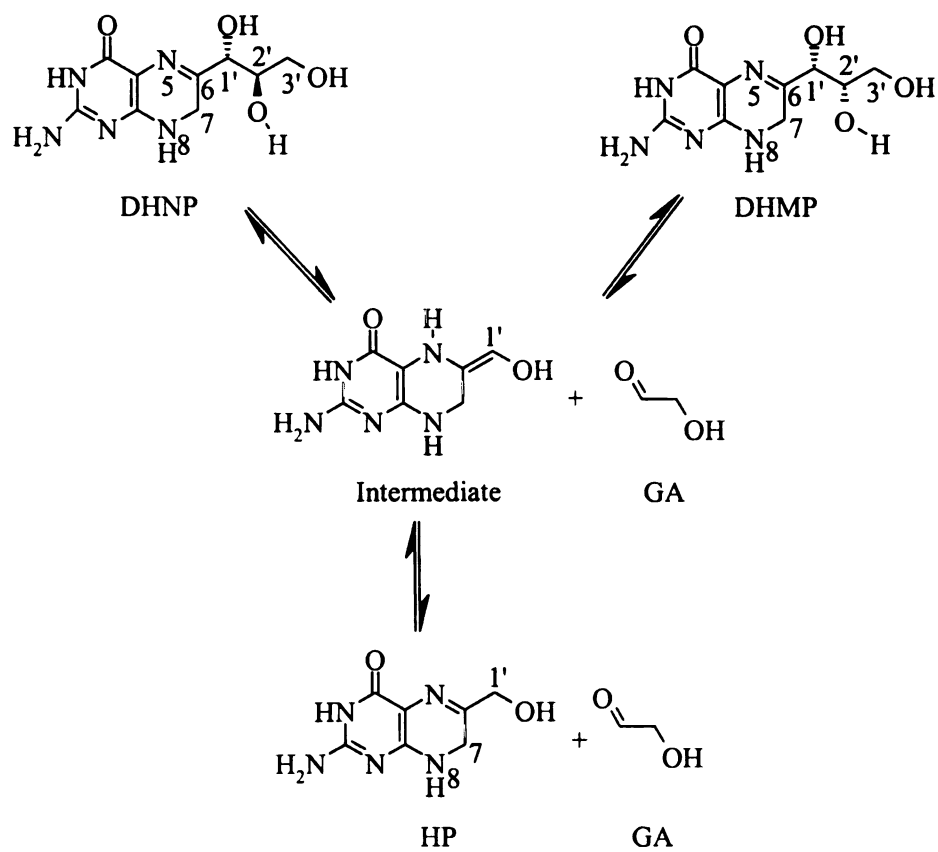
**Figure 1.4: Mechanisms of two types of aldolases.**



include L-fuculose-1-phosphate aldolase (26), fructose-1,6-bisphosphate aldolase (27, 28) and L-rhamnulose-1-phosphate aldolase (29, 30).

DHNA does not form a Schiff base with its substrate as found in type I aldolases nor does it need a metal ion for catalysis as for type II aldolases. Instead, the Schiff base appears to be embedded in the substrate DHNP/DHMP itself as shown in Figure 1.5. Specifically, the protonation of N5 in the substrate helps to stabilize the enol reaction intermediate. Without the imine group at N5 functioning as a Schiff base, the aldolase reaction would not proceed. NP is the oxidized form of substrate DHNP and tetrahydroneopterin is the reduced form of substrate DHNP. They cannot produce a protonated imine group at N5 and neither NP nor tetrahydroneopterin can be used as a substrate (31). Tetrahydroneopterin does not contain the imine required by the reaction and the aromatic nature of neopterin would deactivate the imine through delocalization (32).

**Figure 1.5: Proposed mechanism of reactions catalyzed by DHNA.**



## MECHANISTIC STUDIES OF DHNA

Although the proposed chemical mechanism of the DHNA-catalyzed reaction is reasonable, no experimental evidence has been reported and how the enzyme catalyzes the reaction is largely unknown (32). In the proposed reaction mechanism, C2'-C3' cleavage occurs with formation of an enol and a proton is transferred to the enol intermediate to form the product HP as shown in Figure 1.5 (33). The mechanism of the protonation transfer was studied by NMR in 2002 (9). In order to determine how a proton is transferred in the step between the enol intermediate and the product HP, the incorporation of deuterium from the solvent D<sub>2</sub>O into the heterocyclic reaction product was measured by multinuclear NMR spectroscopy by dissolving the enzyme and substrate in D<sub>2</sub>O. The data indicated that the protonation of the intermediate by DHNA occurs preferentially in the pro-*S* position. Although the data do not answer the question of whether or not the proton donor is an acidic group of the protein or solvent water, it is clear that the protonation of the enol intermediate does not occur by a return of the proton that had been abstracted from the substrate (9). A study using Raman difference spectroscopy of the electronic structure of dihydrobiopterin, the analogue of DHNP, bound to SaDHNA indicates that the p*K*<sub>a</sub> of N5 is not significantly increased in the enzyme-bound form (34). Dihydrobiopterin stays in an unprotonated form. This result suggested that N5 of DHNP might not be protonated before the bond cleavage of DHNP during the DHNA-catalyzed reaction (34).

## STRUCTURES OF DHNAS

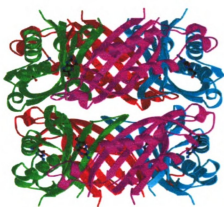
The study of the structure and function relationship of DHNA is based on the high resolution X-ray crystal structure. DHNA was first identified in *E. coli* in 1970 (31). The genes of both EcDHNA (12) and SaDHNA (32) were cloned and overproduced in *E. coli* by recombinant DNA methods in 1998. Crystal structure of the binary complex form of SaDHNA and product HP was determined at 1.65 Å resolution by Hennig and coworkers (32). SaDHNA is a homooctamer with 121 residues of 13.8 kDa per subunit. The octameric structure is composed of two stacked rings each composed of four subunits. Each subunit contains a “T-fold” structure with one antiparallel  $\beta$  sheet and two  $\alpha$  helices. For each tetramer, the subunits are placed “head to head” to form a circular “donut”-shaped ring with a big hole in the middle. The overall quaternary structure is similar in appearance to two stacked “donuts”. The top-down view and side view of the protein in complex with the product HP are shown in Figure 1.6A and 1.6B, respectively. The crystal structure of active site residues is shown in Figure 1.7. Figures 1.6 and 1.7 are from the Protein Data Bank structure of 2dhn (32).

In 2000, the sequential resonance assignment of the 110 kDa SaDHNA was determined by NMR. The protein was labeled with  $^2\text{H}$ ,  $^{13}\text{C}$ , and  $^{15}\text{N}$  uniformly to increase the sensitivity of the measurements. The complete sequence assignment of the octamer was obtained, and the regular secondary structures in the solution conformation were found to coincide nearly identically with those in the crystal structure (35).

**Figure 1.6: The crystal structure of the complex of SaDHNA and product HP. A) Top view, B) Side view. The small molecules located at the interface between two adjacent subunits are product HP at active sites.**

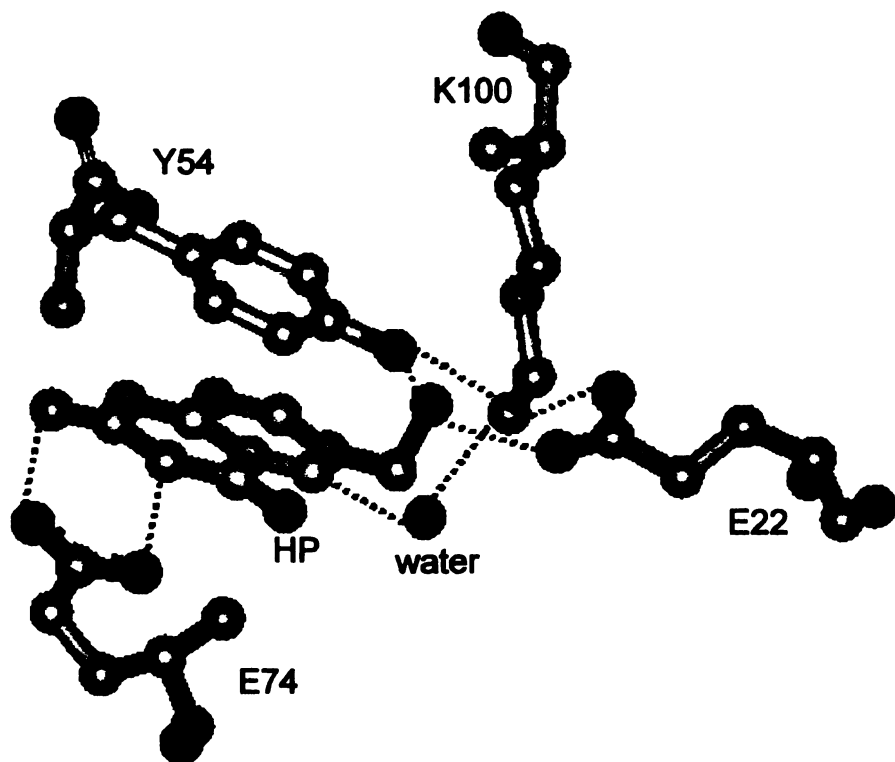


A)



B)

**Figure 1.7: The potentially important residues around the product HP at the active site of SaDHNA. The residues shown are E22, Y54, E74, and K100. A water molecule is found close to N5 of HP. The dotted lines represent hydrogen bonds.**



The crystal structure of DHNA from *Arabidopsis thaliana* (AtDHNA) has been determined at 2.2 Å resolution (33). The enzyme forms a D<sub>4</sub>-symmetric homooctamer, structurally similar to SaDHNA. It has 126 residues in each monomer, each of 14.1 kDa. The enzyme is bound with guanine. The spatial arrangements of active site residues of AtDHNA are superimposable to those of SaDHNA (33).

The 1.6 Å X-ray crystal structure of DHNA from *Mycobacterium tuberculosis* (MtDHNA) complexed with the product HP reveals an octameric assembly similar to SaDHNA (28). However, the 2.5 Å crystal structure of unliganded MtDHNA reveals a novel tetrameric oligomerization state, with only partially formed active sites. Unlike SaDHNA and EcDHNA, MtDHNA displays cooperativity in substrate binding, which is proposed to regulate the cellular concentration of DHNP so that it may function not only as a precursor for folate biosynthesis but also as an antioxidant for the survival of the organism against host defense (36).

### **ACTIVE SITE RESIDUES OF SADHNA**

The octameric protein contains eight active sites with each active site located at the interface of two adjacent subunits (Figures 1.6 and 1.7) (32). Each active site contains four conserved residues, E22, E74, and K100 from one subunit and Y54 from the adjacent subunit (SaDHNA numbering, Figure 1.7). HP is stacked with the phenol ring of Y54 and is fixed at the active site by five hydrogen bonds with the protein (including the two hydrogen bonds with main chain amides, not shown). The carboxyl group of E22 forms a hydrogen bond with the hydroxyl group of HP and with the amino group of K100.

The hydroxyl group of the phenol ring of Y54 forms a hydrogen bond with the hydroxyl group of HP as well as with the amino group of K100. The carboxyl group of E74 forms two hydrogen bonds with HP. In addition to the hydrogen bonds with E22 and Y54, K100 also forms a hydrogen bond with a water molecule, which is in turn hydrogen bonded to N5 of HP. It is noted that there is no residue in SaDHNA that can form hydrogen bond directly with N5 of HP. While the crystal structures of SaDHNA, AtDHNA and MtDHNA have provided a three-dimensional view of the active sites of the enzymes, the functional roles of the active site residues are yet to be established. In order to answer how DHNA catalyzes the aldolase and epimerase reactions, thermodynamic and kinetic analyses of SaDHNA and EcDHNA were carried out first (Chapter 2). Subsequently, site-directed mutagenesis was used to remove the functional groups at the active sites of the enzymes, and changes in the binding and catalytic properties of the enzymes were measured to determine the functional roles of these residues (Chapter 3 and 4). Of particular interest, mutations involving the active site Tyr residue were found to confer unique new chemistry to the enzyme such that oxygenase activity was identified (Chapter 3).

## REFERENCES

- (1) Young, D. W. (1986) The biosynthesis of the vitamins thiamin, riboflavin, and folic acid. *Nat. Prod. Rep.* 3, 395-419.
- (2) Klaus, S. M. J., Wegkamp, A., Sybesma W., Hugenholtz, J., Gregory, J. F. III, and Hanson A. D. (2005) A Nudix Enzyme Removes Pyrophosphate from Dihydroneopterin Triphosphate in the Folate Synthesis Pathway of Bacteria and Plants. *J. Biol. Chem.* 280, 5274-5280.
- (3) Bermingham, A., and Derrick, J. P. (2002) The folic acid biosynthesis pathway in bacteria: evaluation of potential for antibacterial drug discovery. *Bioassays.* 24, 637-648.
- (4) Kompis, I. M., Islam, K., and Then, R. L. (2005) DNA and RNA Synthesis: Antifolates. *Chem. Rev.* 105, 593-620.
- (5) Chio, L. C., Bolyard, L. A., Nasr, M., and Queener, S. F. (1996) Identification of a class of sulfonamides highly active against dihydropteroate synthase from *Toxoplasma gondii*, *Pneumocystis carinii*, and *Mycobacterium avium*. *Antimicrob. Agents Chemother.* 40, 727-733.
- (6) Garg, S. K., Ghosh, S. S., and Mathur, V. S. (1986) Comparative pharmacokinetic study of four different sulfonamides in combination with trimethoprim in human volunteers. *Int. J. Clin. Pharmacol. Ther. Toxicol.* 24, 23-25.
- (7) Huovinen, P., Sundström, L. Swedberg, G., and Sköld, O. (1995) Trimethoprim and sulfonamide resistance. *Antimicrob. Agents Chemother.* 39, 279-289.
- (8) Illarionova, V., Eisenreich, W., Fischer, M., Haussmann, C., Romisch, W., Richter, G., and Bacher, A. (2002) Biosynthesis of tetrahydrofolate - stereochemistry of dihydroneopterin aldolase. *J. Biol. Chem.* 277, 28841-28847.
- (9) Todar, K. (2005) *Todar's Online Textbook of Bacteriology. University of Wisconsin-Madison Department of Bacteriology.*
- (10) Sanders, W. J., Nienaber, V. L., Lerner, C. G., McCall, J. O., Merrick, S. M., Swanson, S. J., Harlan, J. E., Stoll, V. S., Stamper, G. F., Betz, S. F., Condroski, K. R., Meadows, R. P., Severin, J. M., Walter, K. A., Magdalinos, P., Jakob, C. G., Wagner, R., and Beutel, B. A. (2004) Discovery of potent inhibitors of dihydroneopterin aldolase using CrystaLEAD high-throughput X-ray crystallographic screening and structure-directed lead optimization. *J. Med. Chem.* 47, 1709-1718.

- (11) Zimmerman, M., Tolman, R. L., Morman, H., Graham, D. W., and Rogers, E. F. (1977) Inhibitors of folate biosynthesis .1. Inhibition of dihydroneopterin aldolase by pteridine derivatives. *J. Med. Chem.* 20, 1213-1215.
- (12) Haußmann, C., Rohdich, F., Schmidt, E., Bacher, A., and Richter, F. (1998) Biosynthesis of pteridines in *Escherichia coli* - structural and mechanistic similarity of dihydroneopterin-triphosphate epimerase and dihydroneopterin aldolase. *J. Biol. Chem.* 273, 17418-17424.
- (13) Ploom, T., Haussmann, C., Hof, P., Steinbacher, S., Bacher, A., Richardson, J., and Huber, R. (1999) Crystal structure of 7,8-dihydroneopterin triphosphate epimerase. *Structure* 7, 509-16.
- (14) Dreyer, M. K., and Schulz, G. E. (1993) The spatial structure of the class II l-fucose-1-phosphate aldolase from *Escherichia coli*. *J. Mol. Biol.* 231, 549-533.
- (15) Tanner, M. E., and Kenyon, G. L. (1998) *Inversion of stereocenters.*, Vol. II, Academic Press, San Diego.
- (16) Samuel, J., Luo, Y., Morgan, P. M., Strynadka, N. C. J., and Tanner, M. E. (2001) Catalysis and binding in l-ribulose-5-phosphate 4-epimerase: A comparison with l-fucose-1-phosphate aldolase. *Biochemistry* 40, 14772-14780.
- (17) Lee, L. V., Vu, M. V., and Cleland, W. W. (2000) <sup>13</sup>C and deuterium isotope effects suggest an aldol cleavage mechanism for l-ribulose-5-phosphate 4-epimerase. *Biochemistry* 39, 4808-4820.
- (18) Johnson, A. E., and Tanner, M. E. (1998) Epimerization via carbon-carbon bond cleavage. L-ribulose-5-phosphate 4-epimerase as a masked class II aldolase. *Biochemistry* 37, 5746-5754.
- (19) Tanner, M. E. (2002) Understanding nature's strategies for enzyme-catalyzed racemization and epimerization. *Acc. Chem. Res.* 35, 237-46.
- (20) Horecker, B. L., Tsolas, O., and Lai, C.-Y. (1975) Aldolases, in *The enzymes* (Boyer, P. D., Ed.) pp 213-258, Academic Press, San Diego.
- (21) Allen, K. N. (1998) Reactions of enzyme-derived enamines, in *Comprehensive biological catalysis* (Sinnott, M., Ed.) pp 135-172, Academic Press, San Diego.
- (22) Silverman, R. B. (2000) *The organic chemistry of enzyme-catalyzed reactions* pp 455, Academic Press, San Diego.
- (23) Lorentzen, E., Siebers, B., Hensel, R., and Pohl, E. (2005) Mechanism of the Schiff base forming fructose-1,6-bisphosphate aldolase: Structural analysis of reaction intermediates. *Biochemistry* 44, 4222-9.

- (24) Mavridis, I. M., Hatada, M. H., Tulinsky, A., and Lebioda, L. (1982) Structure of 2-keto-3-deoxy-6-phosphogluconate aldolase at 2.8 Å resolution. *J. Mol. Biol.* 162, 419-444.
- (25) Lawrence, M. C., Barbosa, J. A. R. G., Smith, B. J., Hall, N. E., Pilling, P. A., Ooi, H. C., and Marcuccio, S. M. (1997) Structure and mechanism of a sub-family of enzymes related to N-acetylneuraminidase. *J. Mol. Biol.* 266, 381-399.
- (26) Dreyer, M. K., and Schulz, G. E. (1996) Refined high-resolution structure of the metal-ion dependent l-fucose-1-phosphate aldolase (class II) from *Escherichia coli*. *Acta Crystallogr., Sect. D* 52, 1082-1091.
- (27) Hall, D. R., Leonard, G. A., Reed, C. D., Watt, C. I., Berry, A., and Hunter, W. N. (1999) The crystal structure of *Escherichia coli* class II fructose-1,6-bisphosphate aldolase in complex with phosphoglycolohydroxamate reveals details of mechanism and specificity. *J. Mol. Biol.* 287, 383-394.
- (28) Cooper, S. J., Leonard, G. A., McSweeney, S. M., Thompson, A. W., Naismith, J. H., Qamar, S., Plater, A., Berry, A., and Hunter, W. N. (1996) The crystal structure of a class II fructose-1,6-bisphosphate aldolase shows a novel binuclear metal-binding active site embedded in a familiar fold. *Structure* 4, 1303-1315.
- (29) Schwartz, N. B., Abram, D., and Feingold, D. S. (1974) L-Rhamnulose 1-phosphate aldolase of *Escherichia coli*. The role of metal in enzyme structure. *Biochemistry* 13, 1726-30.
- (30) Chiu, T. H., and Feingold, D. S. (1969) L-Rhamnulose 1-phosphate aldolase from *Escherichia coli*. Crystallization and properties. *Biochemistry* 8, 98-108.
- (31) Mathis, J. B., and Brown, G. M. (1970) The biosynthesis of folic acid XI. Purification and properties of dihydroneopterin aldolase. *J. Biol. Chem.* 245, 3015-3025.
- (32) Hennig, M., D'Arcy, A., Hampele, I. C., Page, M. G. P., Oefner, C., and Dale, G. E. (1998) Crystal structure and reaction mechanism of 7,8-dihydroneopterin aldolase from *Staphylococcus aureus*. *Nature Struct. Biol.* 5, 357-362.
- (33) Bauer, S., Schott, A. K., Illarionova, V., Bacher, A., Huber, R., and Fischer, M. (2004) Biosynthesis of tetrahydrofolate in plants: Crystal structure of 7,8-dihydroneopterin aldolase from *Arabidopsis thaliana* reveals a novel aldolase class. *J. Mol. Biol.* 339, 967-79.
- (34) Deng, H., Callender, R., and Dale, G. E. (2000) A vibrational structure of 7,8-dihydrobiopterin bound to dihydroneopterin aldolase. *J. Biol. Chem.* 275, 30139-30143.

- (35) Salzmann, M., Pervushin, K., Wider, G., Senn, H., and Wüthrich, K. (2000) NMR assignment and secondary structure determination of an octameric 110 kDa protein using TROSY in triple resonance experiments. *J. Am. Chem. Soc.* 122, 7543-7548.
- (36) Goulding, C. W., Apostol, M. I., Sawaya, M. R., Phillips, M., Parseghian, A., and Eisenberg, D. (2005) Regulation by oligomerization in a mycobacterial folate biosynthetic enzyme. *J. Mol. Biol.* 349, 61-72.

## CHAPTER 2: NMR, EQUILIBRIUM AND TRANSIENT KINETIC STUDIES OF STAPHYLOCOCCUS AUREUS AND ESCHERICHIA COLI ENZYMES

### ABSTRACT

Dihydroneopterin aldolase (DHNA) catalyzes both the cleavage of 7,8-dihydro-D-neopterin (DHNP) to form 6-hydroxymethyl-7,8-dihydropterin (HP) and glycolaldehyde and the epimerization of DHNP to form 7,8-dihydro-L-monapterin (DHMP). Whether the epimerization reaction uses the same reaction intermediate as in the aldol reaction or the deprotonation and re-protonation of the 2'-carbon of DHNP has been investigated by NMR analysis of the reaction products in a D<sub>2</sub>O solvent. No deuteration of the 2'-carbon was observed for the newly formed DHMP, while there was a significant deuteration of the 6-hydroxymethyl carbon of HP. The results strongly suggest that the epimerization reaction uses the same reaction intermediate as the aldol reaction. The binding and catalytic properties of DHNAs from both *Staphylococcus aureus* (SaDHNA) and *Escherichia coli* (EcDHNA) have been determined by equilibrium binding and transient kinetic studies. The DHNA-catalyzed reaction is reversible in contrast to an early observation. A complete set of kinetic constants for both the aldol and epimerization reactions according to a unified kinetic mechanism has been determined for both SaDHNA and EcDHNA. The results show that the two enzymes have significantly different binding and catalytic properties, in accordance with the significant sequence differences between them. EcDHNA is different from SaDHNA biochemically in several aspects. (1) EcDHNA has much higher affinities for the

substrate, products, and inhibitors measured in this work. (2) EcDHNA has a much higher epimerase activity than SaDHNA. (3) The rate-limiting step in the forward reaction (the formation of HP) is the product release for EcDHNA but is the formation of the reaction intermediate for SaDHNA. (4) The reverse reaction is very slow with EcDHNA but very fast with SaDHNA.

## INTRODUCTION

Infectious diseases are the leading causes of death and the main causes of premature death (0-44 years) (2). Widespread and persistent antibiotic resistance has caused a worldwide health care crisis (3-5). The crisis has been aggravated by the decisions by many major pharmaceutical companies to abandon or curtail their antibacterial programs for business reasons (6-8), and the fact that most new antibiotics are chemical modifications of existing antimicrobial agents (9). These compounds act against old targets and are therefore less effective in dealing with widespread antibiotic resistance. New targets for the development of novel antimicrobial agents are thus urgently needed for combating the antibiotic crisis.

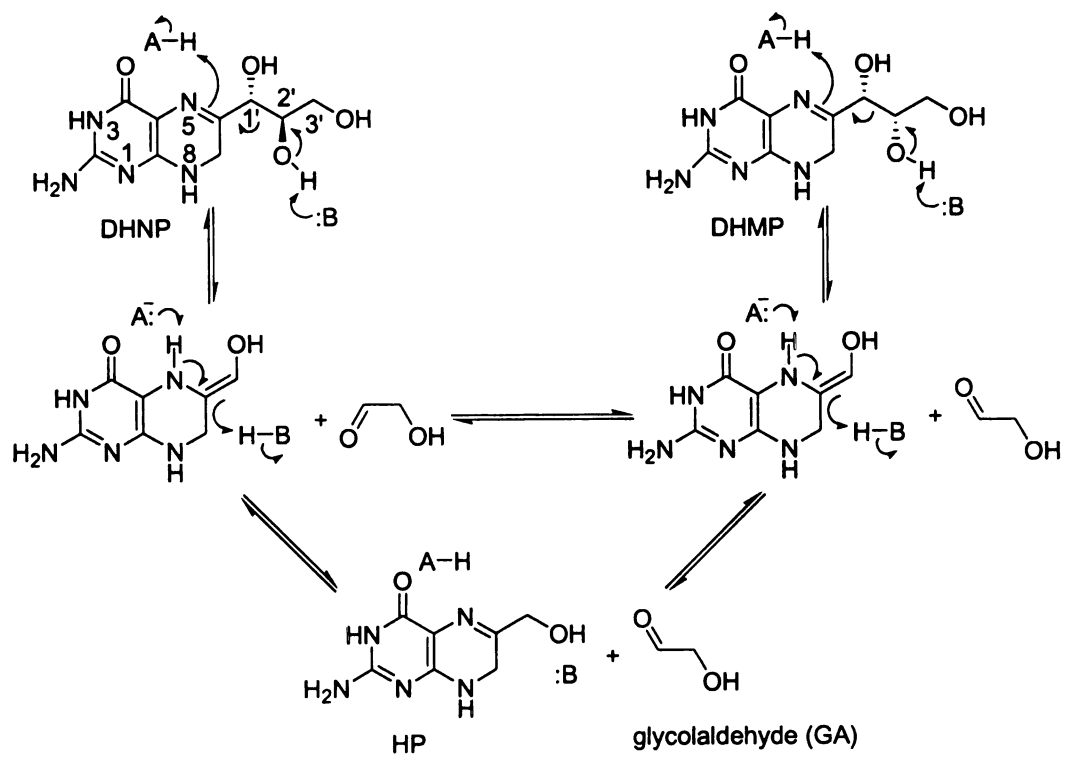
Dihydroneopterin aldolase (DHNA) catalyzes the conversion of 7,8-dihydroneopterin (DHNP) to 6-hydroxymethyl-7,8-dihydropterin (HP) in the folate biosynthetic pathway, one of principal targets for developing antimicrobial agents (3). Folate cofactors are essential for life (10). Most microorganisms must synthesize folates *de novo*. In contrast, mammals cannot synthesize folates because of the lack of three enzymes in the middle of the folate pathway and obtain folates from the diet. DHNA is the first of the three enzymes that are absent in mammals and therefore an attractive target for developing antimicrobial agents (11).

DHNA is a unique aldolase in two respects. First, DHNA requires neither the formation of a Schiff's base between the substrate and enzyme nor metal ions for catalysis (12). Aldolases can be divided into two classes based on their catalytic mechanisms (13, 14). Class I aldolases require the formation of a Schiff's base between

an amino group of the enzyme and the carbonyl of the substrate, whereas class II aldolases require a  $Zn^{2+}$  ion at their active sites for catalysis. The proposed catalytic mechanism for DHNA (12, 15, 16) is similar to that of class I aldolases, but the Schiff's base is embedded in the substrate (Figure 2.1). Secondly, in addition to the aldolase reaction, DHNA also catalyzes the epimerization at the 2'-carbon of DHNP to generate 7,8-dihydromonapterin (DHMP) (15), but the biological function of the epimerase reaction is not known at present. The aldolase and epimerase reactions are believed to involve a common intermediate as shown in Figure 2.1 (12, 15, 16). Both reactions involve the retroaldol cleavage of the C-C bond between C1' and C2'. Epimerization results from the re-formation of the C-C bond after the rotation of glycolaldehyde. The mechanism of the epimerization reaction is very similar to that catalyzed by L-ribulose-5-phosphate 4-epimerase (17), which also follows aldol chemistry (18), but the two enzymes are different in structure and have no apparent sequence identity. L-ribulose-5-phosphate 4-epimerase has 26% identity with the class II L-fuculose-1-phosphate aldolase and requires a  $Zn^{2+}$  ion for catalysis (17). DHNA is unique because it catalyzes both aldolase and epimerase reactions, whereas L-ribulose-5-phosphate 4-epimerase and L-fuculose-1-phosphate aldolase catalyze only one type of reaction.

Interestingly, DHNAs from Gram-positive and Gram-negative bacteria have some unique sequence motifs. Figure 1.2 shows the amino acid sequence alignment of DHNAs from 11 bacteria. The first five enzymes are from Gram-positive bacteria, and the rest are from Gram-negative bacteria. The identities between enzymes from Gram-positive bacteria range from 39% to 45% and those between Gram-negative bacteria are 49-91%, but the identities between Gram-positive and Gram-negative bacterial enzymes are

**Figure 2.1: The proposed catalytic mechanism for the DHNA-catalyzed reactions.**



<30%. Many differences between enzymes from Gram-positive and Gram-negative bacteria are at or near their active centers (16).

DHNA was first identified in *Escherichia coli* (EcDHNA) by Mathis and Brown in 1970 (12). There were few studies on DHNA until 1998, when Hennig and coworkers determined the crystal structures of DHNA from *Staphylococcus aureus* (SaDHNA) and its complex with the product HP (16). In the same year, Haußmann and coworkers demonstrated that the enzyme has both aldolase and epimerase activities and determined the steady-state kinetic parameters for both reactions (15). In 2000, the Wüthrich group published the total sequential resonance assignment of the 110 kDa homooctameric SaDHNA (19), which was a model system for the development of TROSY NMR spectroscopy (20-22). Also in 2000, Deng and coworkers measured the  $pK_a$  of nitrogen 5 of SaDHNA-bound 7,8-dihydrobiopterin by Raman spectroscopy (23). In 2002, Illarionova and coworkers showed that the protonation of the reaction intermediate prefers the pro-S position (24). Most recently, we studied the dynamic properties of apo SaDHNA and the product complex SaDHNA•HP by molecular dynamics simulations (1). How DHNA catalyzes both aldol and epimerization reactions is however largely unknown at present.

We are interested in understanding the catalytic mechanism of DHNA and the biochemical consequences of the significant sequence differences described above. To this end, we performed a comprehensive equilibrium and kinetic study of SaDHNA and EcDHNA, representing DHNAs from Gram-positive and Gram-negative bacteria, respectively. We also addressed the issue of whether the epimerase reaction uses the same reaction intermediate as that of the aldolase reaction or an alternative mechanism

via the deprotonation and re-protonation of 2'-carbon. The results showed that the epimerase reaction follows the same reaction intermediate as that of the aldolase reaction and that SaDHNA and EcDHNA have significantly different equilibrium and kinetic constants, which form the basis for elucidating the catalytic mechanism of DHNA and developing antimicrobial agents specifically against Gram-positive or Gram-negative bacteria.

## EXPERIMENTAL PROCEDURES

*Materials.* 6-Hydroxymethylpterin (HPO), 6-hydroxymethyl-7,8-dihydropterin (HP), 7,8-dihydro-D-neopterin (DHNP), 7,8-dihydro-L-monapterin (DHMP), D-neopterin (NP), and L-monapterin (MP) were purchased from Schircks Laboratories. Restriction enzymes and T4 ligase were purchased from New England Biolabs. *Pfu* DNA polymerase and the pET-17b vector were purchased from Stratagene and Novagen, respectively. Other chemicals were from Sigma or Aldrich.

*Cloning.* The SaDHNA gene was cloned into the prokaryotic expression vector pET-17b and a home-made derivative (pET17H) by PCR from *S. aureus* genomic DNA. The pET17H vector was used for the production of a His-tagged SaDHNA. The primers for the PCR reaction were 5'-G GAA TTC CAT ATG CAA GAC ACA ATC TTT CTT AAA G -3'(forward primer with a *Nde* I site) and 5'- CG GGA TCC TCA TTT ATT CTC CCT CAC TAT TTC-3' (reverse primer with an *Bam*H I site). The EcDHNA gene was cloned into the prokaryotic expression vector pET-17b by PCR from *E. coli* genomic DNA. The primers for the PCR reaction were 5'-G GAA TTC CAT ATG GAT ATT

GTA TTT ATA GAG CAA C -3' (forward primer with a *Nde* I site) and 5'- CG GGA TCC TTA ATT ATT TTC TTT CAG ATT ATT GCC-3' (reverse primer with an *Bam*H I site). The expression constructs were transformed into the *E. coli* strain DH5 $\alpha$ . The correct coding sequences of the cloned genes were verified by DNA sequencing. The verified SaDHNA expression constructs were transformed into the *E. coli* strain BL21(DE3)pLysS for over-production of SaDHNA. The verified EcDHNA expression construct was transformed into the *E. coli* strain BL21 (DE3) for over-production of EcDHNA.

*Expression and Purification.* The non-tagged SaDHNA was purified by ion exchange chromatography on a DEAE-cellulose column and gel filtration on a Bio-Gel A-0.5m gel column. One liter of LB medium containing 100 mg ampicillin and 20 mg chloramphenicol was inoculated with 5 mL of overnight seed culture and incubated at 37 °C with vigorous shaking. The production of the SaDHNA was induced when the OD<sub>600</sub> of the culture reached 0.8-1.0. The culture was further incubated for 4 h and harvested by centrifugation. The *E. coli* cells were re-suspended in 20 mM Tris-HCl, pH 8.0 (buffer A) and lysed by a French press. The lysate was centrifuged for 20 min at ~27,000 g. The supernatant was loaded onto a DEAE-cellulose column equilibrated with buffer A. The column was washed with buffer A until OD<sub>280</sub> of the effluent was <0.05 and eluted with a 0-500 mM linear NaCl gradient in buffer A. Fractions containing DHNA were identified by OD<sub>280</sub> and SDS-PAGE and concentrated to ~15 mL by an Amicon concentrator using a YM30 membrane. The concentrated protein solution was centrifuged, and the supernatant was applied to a Bio-Gel A-0.5m gel column equilibrated with buffer A containing 150 mM NaCl. The column was developed with the same buffer. Fractions

from the gel filtration column were monitored by OD<sub>280</sub> and SDS-PAGE. Pure DHNA fractions were pooled and concentrated to 10-20 mL. The concentrated DHNA was dialyzed against 5 mM TrisHCl, pH 8.0, lyophilized, and stored at -80 °C. EcDHNA was purified essentially the same way except that the *E. coli* cells that over-produced EcDHNA were from overnight cultures from single colonies without the IPTG induction. The His-tagged SaDHNA was purified by a Ni-NTA column and a Bio-Gel A-0.5m gel column. The cells were harvested and lysed as described above except that buffer was replaced with 50 mM sodium phosphate, 300 mM NaCl, pH 8.0 (buffer B) and 10 mM imidazole. The lysate was loaded onto the Ni-NTA column equilibrated with buffer B containing 10 mM imidazole. The column was washed with 20 mM imidazole in buffer B and eluted with 250 mM imidazole in buffer B. The concentrated protein was further purified by gel filtration, concentrated again, dialyzed, lyophilized, and stored at -80 °C as described earlier.

*Equilibrium Binding Studies.* The procedures for the equilibrium binding studies of DHNAs were essentially the same as previously described for the similar studies of 6-hydroxymethyl-7,8-dihydropterin pyrophosphokinase using a Spex FluoroMax-2 fluorometer (25, 26). Briefly, proteins and ligands were all dissolved in 100 mM Tris-HCl, pH 8.3, and the titration experiments were performed in a single cuvette at 24 °C. For the NP, MP, and HPO experiments, a DHNA solution was titrated with a stock solution of one of the ligands. Fluorescence intensities were measured at an emission wavelength of 446 nm with a slit of 5 nm. The excitation wavelength and slit were 400 nm and 1 nm, respectively. A set of control data was obtained in the absence of the protein. The data set obtained in the absence of the protein was then subtracted from the

corresponding data set obtained in the presence of the protein after correcting inner filter effects. The  $K_d$  value was obtained by nonlinear least square fitting of the titration data as previously described (25).

To determine the  $K_d$  values for HP, a solution containing 1  $\mu$ M HP was titrated with the proteins. The fluorescence of HP was measured at an emission wavelength of 430 nm and an excitation wavelength of 330 nm. The emission and excitation slits were both 5 nm. A control titration experiment was performed in the absence of HP. The control data set obtained in the absence of HP was subtracted from the corresponding data set obtained in the presence of HP. The  $K_d$  values were obtained by nonlinear least square fitting of the titration data as previously described (25).

*Stopped-Flow Analysis.* Stopped-flow experiments were performed on an Applied Photophysics SX.18MV-R stopped-flow spectrofluorometer at 25 °C. One syringe contained the protein (SaDHNA or EcDHNA), and the other contained NP, MP, HP or HPO. The protein concentrations were 1 or 2  $\mu$ M, and the ligand concentrations ranged 5-60  $\mu$ M. All concentrations were those after the mixing of the two syringe solutions. Fluorescence traces for NP, MP and HPO were obtained with an excitation wavelength of 360 nm and a filter with a cutoff of 395 nm for emission. Fluorescence traces for HP were obtained with an excitation wavelength of 330 nm and the same filter for emission. Apparent rate constants were obtained by nonlinear squares fitting of the data to a single exponential equation and were re-plotted against the ligand concentrations. The association and dissociation constants were obtained by linear regression of the apparent rate constants vs. ligand concentration data.

*Quench-Flow Analysis.* Quench-flow experiments were carried out on a KinTek RQF-3 rapid quench-flow instrument. One syringe was loaded with a protein solution (SaDHNA or EcDHNA), and the other loaded with a substrate solution (DHNP or DHMP). All components were dissolved in a buffer containing 100 mM Tris-HCl, 1 mM EDTA, and 5 mM DTT, pH 8.3. For the forward reaction with DHNP or DHMP as the substrate, the enzyme concentrations were 15-20  $\mu\text{M}$ , and the substrate concentrations were 10, 20, and 30  $\mu\text{M}$ , all referred to those immediately after the mixing of the two syringe solutions. For the reverse reaction, the enzyme (SaDHNA or EcDHNA) was 10  $\mu\text{M}$ , HP was 100  $\mu\text{M}$ , and GA ranged from 1 to 100 mM. All reactions were initiated by mixing of the two solutions, one containing the enzyme and the other the substrate(s), and quenched with 1 N HCl. The quenched reaction mixtures were processed as previously described (15). Briefly, the reaction mixtures (115  $\mu\text{L}$  each) were mixed with 50  $\mu\text{L}$  1%  $\text{I}_2$  (w/v) and 2% (w/v) KI in 1 N HCl for 5 min at room temperature to oxidize the pterin compounds. Excess iodine was reduced by mixing with 25  $\mu\text{L}$  2% ascorbic acid (w/v). The samples were then centrifuged at room temperature for 5 min using a microcentrifuge. The oxidized reactant and products in the supernatants were separated by HPLC using a Vydac RP18 column. The column was equilibrated with 20 mM  $\text{NaH}_2\text{PO}_4$  made with MilliQ water and eluted at the flow rate of 0.8 mL/min with the same solution. The oxidized reactant and products were quantified by online fluorometry with excitation and emission wavelengths of 365 and 446 nm, respectively. The quench-flow data were analyzed by global fitting using the program DYNAFIT (27) according to Scheme 1.

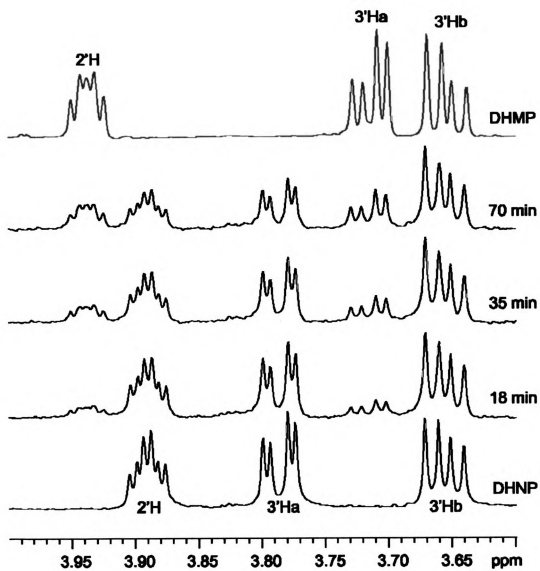
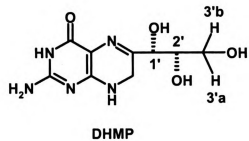
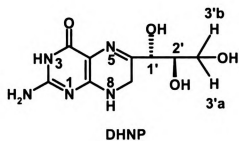
*NMR Spectroscopy.* NMR measurements were made at 25 °C with a Varian Inova 600 spectrometer. The initial NMR sample contained 2 mM DHNP and 1 mM tris(2-carboxyethyl) phosphine (TCEP) in 50 mM sodium phosphate buffer, pH 8.3 (pH meter reading without correction for deuterium isotope effects), made with D<sub>2</sub>O. The reaction was initiated with 3 μM SaDHNA. NMR spectra were recorded before and after the addition of the enzyme. A spectrum of DHMP was also acquired for comparison. The spectral width for the NMR data was 8000 Hz with the carrier frequency at the HDO resonance. The solvent resonance was suppressed by presaturation. Each FID was composed of 16 k data points with 16 transients. The delay between successive transients was 6 s. The time domain data were processed by zero-filling to 32 k points, multiplication with a 90°-shifted sine bell function, and Fourier transformation. Chemical shifts were referenced to the internal standard sodium 2-dimethyl-2-silapentane-5-sulfonate sodium salt (DSS). The relative proton populations were calculated based on the integrals of their NMR signals.

## RESULTS

*NMR Analysis.* Although it is reasonable that the epimerase reaction follows the same reaction intermediate as that of the aldolase reaction as described earlier (Figure 2.1), it is also possible that the epimerase reaction follows an alternative mechanism, i.e., the deprotonation and re-protonation of 2'-carbon. The alternative reaction can be initiated by deprotonation of 1'-carbon and protonation of 5-nitrogen to form an enol

intermediate, which can turn into a keto intermediate by tautomerization for the subsequent deprotonation and re-protonation of 2'-carbon. Whether the epimerase reaction follows the same reaction intermediate as that of the aldolase reaction or the mechanism of deprotonation and re-protonation of 2'-carbon can be tested by NMR. The key difference between the two reaction mechanisms is that 2'-proton is always attached to 2'-carbon if the epimerase reaction follows the same reaction intermediate as that of the aldolase reaction (Figure 2.1), while it has to be extracted by a base if the epimerase reaction follows the mechanism of deprotonation and re-protonation of 2'-carbon. Therefore, when the reaction is run in D<sub>2</sub>O, the 2'-proton occupancy will change if the epimerase reaction involves the deprotonation and re-protonation of 2'-carbon but will not change if it follows the same reaction intermediate as that of the aldolase reaction. The proton occupancy can be quantified by NMR. It was noticed in this context that the 6-hydroxymethyl group of the aldolase reaction product HP can be significantly deuterated (at least half of the -CH<sub>2</sub>- protons of the hydroxymethyl group) if the reaction occurs in D<sub>2</sub>O (24). The result of such an experiment is shown in Figure 2.2. The NMR signals were assigned based on their multiplicity patterns, decoupling experiments, and comparison with the NMR spectrum of authentic DHMP (the top spectrum in Figure 2.2). As shown in Figure 2.2, the NMR signals of all 2'- and 3'-protons of DHNP and DHMP are well separated, except those of the 3'H<sub>b</sub> protons of the two compounds, which are overlapping. The proton occupancy at the 2'-position of the newly formed DHMP could be quantified by comparing the integrals of the 2'H and 3'Ha NMR signals of DHMP, because 3'-protons do not participate in the chemical reaction in either mechanism and cannot be replaced with deuterons. The result showed that the intensities of the 2'H and

**Figure 2.2: The SaDHNA-catalyzed reactions in D<sub>2</sub>O monitored by NMR.** The bottom spectrum was obtained before the addition of the enzyme and the middle three spectra were obtained 18, 35, and 70 min after the addition of the enzyme. The top spectrum is that of DHMP for comparison. Only the NMR signals of 2' and 3' protons of DHNP and DHMP are shown. The chemical structures of DHNP and DHMP are also shown at the top with atom numbering labeled for DHNP. For clarity, the NMR signals of the aldolase reaction products HP and GA are not shown.

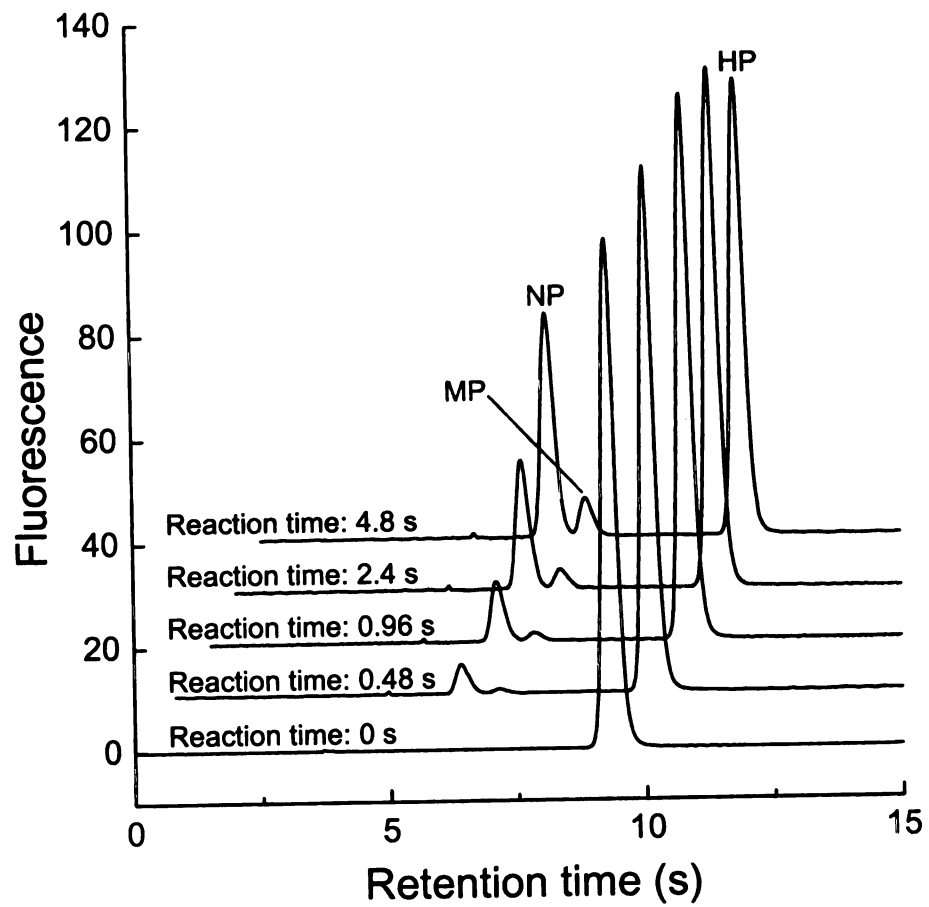


3'Ha NMR signals were the same throughout the time course of the reaction (18, 35, and 70 min). The 1:1 intensities of the 2'H and 3'Ha NMR signals indicated a 100% proton occupancy at 2'-position, strongly suggested that there is no deprotonation and re-protonation at 2'-carbon and the epimerase reaction follows the aldol chemistry.

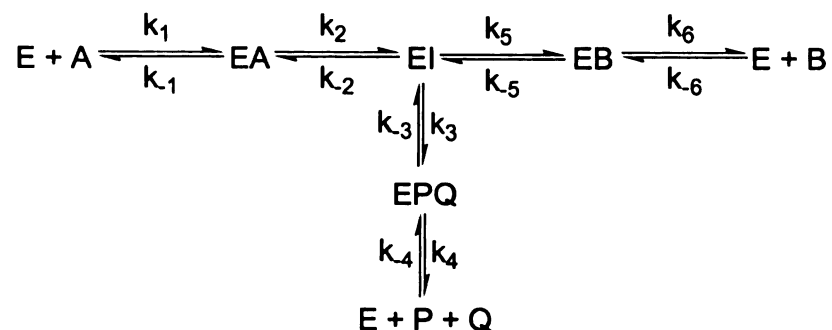
*Is the DHNA-catalyzed reaction reversible?* Although aldolase-catalyzed reactions are generally reversible, the DHNA-catalyzed reaction was shown previously to be irreversible (12). However, it was noticed that the *E. coli* enzyme preparation used in the experiment had a low activity and furthermore, the GA concentration (150  $\mu$ M) was rather low, especially considering that GA exists in various forms in solution and only a small fraction is in the correct form for the reaction (28, 29). To further investigate the issue of the reversibility of the DHNA-catalyzed reaction, we ran the reverse reaction with our recombinant enzymes and high concentrations of GA. One such result obtained with SaDHNA is shown in Figure 2.3. Clearly, the SaDHNA-catalyzed reaction was reversible. Furthermore, the reverse reaction was rather rapid in the presence of SaDHNA. The apparent  $K_m$  for GA obtained by varying GA at a fixed HP concentration (100  $\mu$ M) was  $\sim$ 10 mM. The EcDHNA-catalyzed reaction was also reversible, but the reverse reaction catalyzed EcDHNA was much slower than that catalyzed by SaDHNA (data not shown).

*Equilibrium Binding Studies.* Since the epimerase reaction uses the same reaction intermediate as that of the aldolase reaction and the aldolase reaction is reversible, we can draw a unified kinetic scheme for the DHNA-catalyzed reactions as shown in Scheme 1, where A, B, I, P, and Q represent DHNP, DHMP, the reaction intermediate, HP, and glycolaldehyde, respectively.

**Figure 2.3: Reverse reaction catalyzed by SaDHNA.** The initial reaction mixture in 100 mM Tris-HCl, pH 8.3, contained 100  $\mu$ M HP and 20 mM GA. The reaction was initiated with 10  $\mu$ M SaDHNA at 25 °C, quenched with 1 N HCl, and processed as described in the Experimental Procedures section. The HPLC chromatograms only show the oxidized pterin substrate (HPO) and products (NP and MP), because GA has no fluorescence.



Scheme 1



The major goal of this work was to determine the rate constants of the individual steps of the reactions. Our strategy to achieve this goal was a comprehensive one, involving the measurements of both equilibrium and kinetic constants of the physical steps by equilibrium and stopped-flow fluorometric analysis and the determination of the rate constants of the chemical steps by quench-flow analysis of both forward and reverse reactions. We first measured the dissociation constants by fluorometry. A typical fluorometric titration curve is shown in Figure 2.4. The results are summarized in Table 2.1. To facilitate the purification of SaDHNA, we engineered a His-tag at the N-terminal of the enzyme. The binding properties of the His-tagged and untagged enzymes were essentially the same (data not shown), and the binding data for SaDHNA in Table 2.1 are those of the His-tagged enzyme. NP, MP, and HPO are the oxidized forms of DHNP, DHMP, and HP, respectively. The only difference between the two sets of the pterin compounds is that between C7 and N8 is a single bond in the reduced pterins, but a double bond in the oxidized pterins. Consequently, there is a hydrogen atom attached to N8 in the reduced pterins and the NH group can serve as a hydrogen bond donor, while in the oxidized pterins, there is no hydrogen attached to N8 and it can only serve as a

**Figure 2.4: Binding of NP to SaDHNA at equilibrium.** A 2 mL solution containing 15  $\mu\text{M}$  SaDHNA in 100 mM Tris-HCl, pH 8.3 was titrated with NP by adding aliquots of a 1.94 mM NP stock solution at 24 °C. The final enzyme concentration was 14  $\mu\text{M}$ . The top axis indicates the NP concentrations during the titration. A set of control data was obtained in the absence of the enzyme and was subtracted from the corresponding data set obtained in the presence of the enzyme. The solid line was obtained by nonlinear least-squares regression as previously described (25).

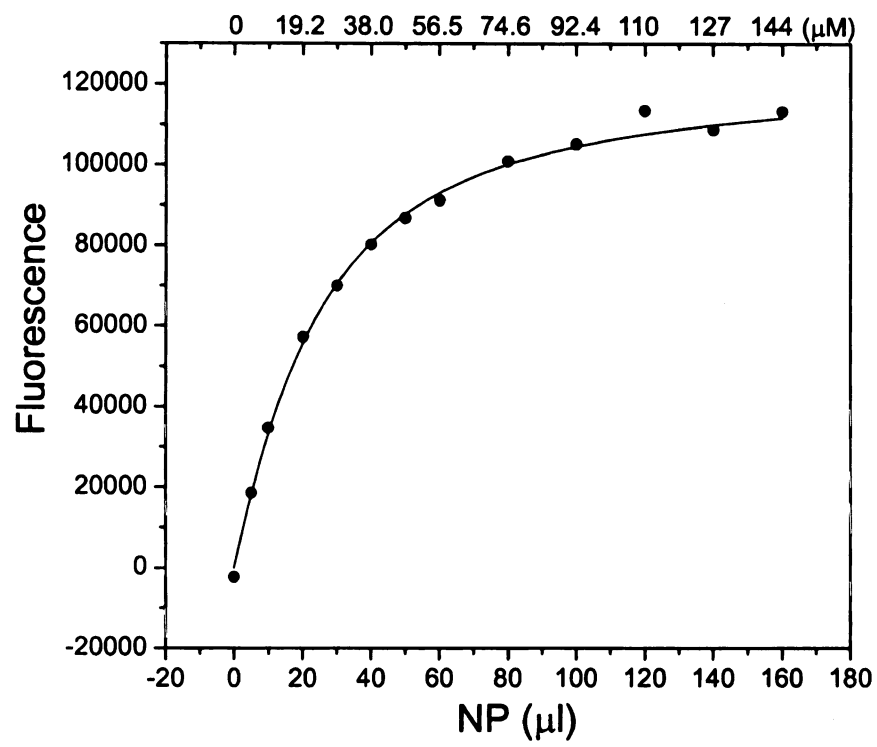
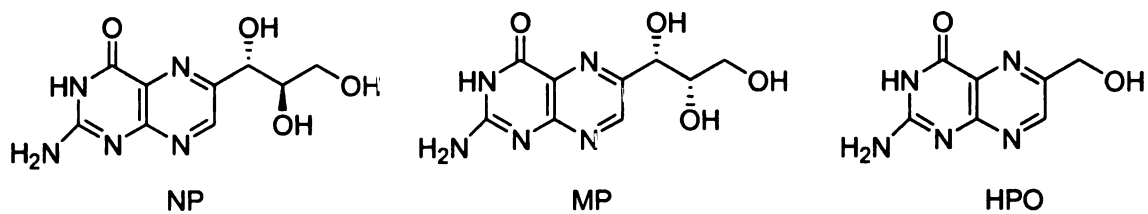


Table 2.1: Dissociation Constants of *S. aureus* and *E. coli* DHNAs Measured by  
Equilibrium Binding Experiments

	SaDHNA <sup>a</sup>	EcDHNA
$K_{d(NP)}$ ( $\mu\text{M}$ )	18 $\pm$ 2	0.77 $\pm$ 0.06
$K_{d(MP)}$ ( $\mu\text{M}$ )	13 $\pm$ 1	2.6 $\pm$ 0.06
$K_{d(HP)}$ ( $\mu\text{M}$ )	24 $\pm$ 0.2	0.43 $\pm$ 0.04
$K_{d(HPO)}$ ( $\mu\text{M}$ )	24 $\pm$ 0.2	0.10 $\pm$ 0.007

<sup>a</sup>The chemical structures of the measured compounds are as follows.



<sup>b</sup>SaDHNA has a His-tag at the N-terminus.

hydrogen bond acceptor. NP, MP, and HPO are all DHNA inhibitors. The results of the equilibrium binding studies showed that in comparison with EcDHNA, SaDHNA has significantly higher  $K_d$  values for the measured pterin compounds, particularly HPO, whose the  $K_d$  value for SaDHNA was 240 times that for EcDHNA. Furthermore, while the  $K_d$  values of SaDHNA for the reduced and oxidized pterin compounds (HP and HPO respectively) were the same, the  $K_d$  value of EcDHNA for the reduced pterin compound (the product HP) was higher than that for the oxidized pterin compound (the oxidized product HPO). Finally, the  $K_d$  value of SaDHNA for NP was slightly higher than that for MP, while the  $K_d$  value of EcDHNA for NP is lower than that for MP.

*Stopped-Flow Analysis.* We then measured the rate constants of the physical steps of the reaction by stopped-flow fluorometric analysis. Because glycolaldehyde (GA) has a very low affinity for the enzymes (data not shown) and exists in solution in multiple forms, of which the correct form for the reaction is a minor one (28, 29), we focused our analysis of product binding and dissociation on HP. Because DHNP and DHMP undergo chemical reactions in the presence DHNA, we measured the binding and dissociation of the structurally-related DHNA inhibitors NP and MP. To assess the differences in the rate constants of the reduced and oxidized pterins, we also measured the association and dissociation rate constants of HPO and compared them with those of HP. A typical result of the stopped-flow analysis is shown in Figure 2.5. The rate constants measured by the stopped-flow experiments are summarized in Table 2.2, where  $k_1$  and  $k_{-1}$  are the association and dissociation rate constants, respectively. The  $K_d$  values calculated as  $k_{-1}/k_1$  were in excellent agreement with those measured by equilibrium binding studies

**Figure 2.5: Stopped-flow analysis of the binding of HPO to EcDHNA.** The concentration of EcDHNA was 0.2  $\mu\text{M}$ , and the concentrations of HPO were 1, 2, 4 and 8  $\mu\text{M}$  for traces 1, 2, 3, and 4, respectively. All concentrations were those immediately after the mixing of the two syringe solutions. Both EcDHNA and HPO were dissolved in 100 mM Tris-HCl, pH 8.3. The fluorescent signals were rescaled so that they could be fitted into the figure with clarity. The solid lines were obtained by nonlinear regression as described in the Experimental Procedures section. The inset is a replot of the apparent rate constants vs. the HPO concentrations. The solid line was obtained by linear regression.

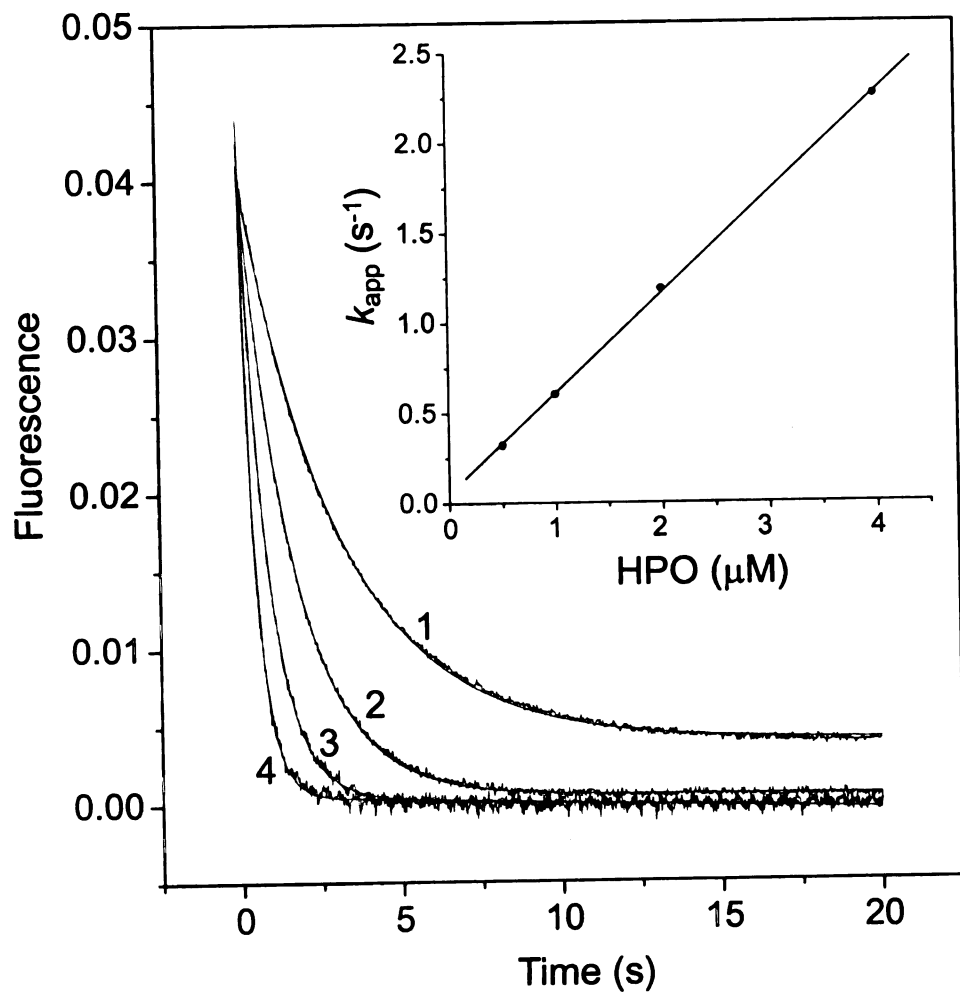


Table 2.2: Association and Dissociation Rate Constants of *S. aureus* and *E. coli* DHNAs  
Measured by Stopped-flow Experiments

	SaDHNA <sup>a</sup>			EcDHNA		
	$k_1$ ( $\mu\text{M}^{-1}\text{s}^{-1}$ )	$k_{-1}$ ( $\text{s}^{-1}$ )	$K_d^b$ ( $\mu\text{M}$ )	$k_1$ ( $\mu\text{M}^{-1}\text{s}^{-1}$ )	$k_{-1}$ ( $\text{s}^{-1}$ )	$K_d^b$ ( $\mu\text{M}$ )
NP	0.24±0.01	4.5±0.1	19	0.32±0.02	0.29±0.03	0.88
MP	0.29±0.02	4.2±0.2	15	0.26±0.01	0.58±0.03	2.3
HP	0.47±0.04	13±1	28	0.65±0.08	0.26±0.02	0.4
HPO	0.45±0.02	10±0.5	24	0.55±0.04	0.062±0.006	0.11

<sup>a</sup>SaDHNA has a His-tag at the N-terminus.

<sup>b</sup>The  $K_d$  values were calculated as  $k_{-1}/k_1$ .

(Table 2.1). The results showed that the association rate constants for NP and MP are very similar and slightly lower than those for HP and HPO, which are very similar. This phenomenon is presumably related to the sizes of the molecules. NP and MP are the same size and are slightly larger than HP and HPO. Furthermore, the results also showed that for SaDHNA, the association and dissociation rate constants of the reduced pterin HP are the same as those of the oxidized pterin (HPO), in accordance with the same  $K_d$  value for the two pterin compounds. On the other hand, for EcDHNA, the association rate constants for HP and HPO are essentially the same, but the dissociation constant of HP is larger than that of HPO, in agreement with a larger  $K_d$  value for HP. Finally, the higher  $K_d$  values are all mainly due to the higher dissociation rate constants.

*Quench-Flow Analysis.* The rate constants of the chemical steps were measured by quench-flow experiments. We ran the forward reaction (the formation of HP) using both DHNP and DHMP as the substrates and the reverse reaction (the formation of DHNP and DHMP) with HP and GA. For the forward reaction, three concentrations each for DHNP and DHMP were used. For the reverse reaction, the concentration of HP was fixed, and eight concentrations of GA were used for the SaDHNA-catalyzed reaction and six concentrations of GA for the EcDHNA-catalyzed reaction. Each reaction generated three curves, one each for DHNP, DHMP, and HP. The multitude of the quench-flow data was then fitted globally to Scheme 1 by nonlinear least squares regression using the program DYNAFIT (27). The initial values for the physical steps were from the stopped-flow analysis described in the previous section. Typical results of the forward reaction are shown in Figures 2.6 and 2.7 for the SaDHNA- and EcDHNA-catalyzed reactions, respectively, and for clarity, only the formation of HP was plotted. The results of the

**Figure 2.6: Quench-flow analysis of the SaDHNA-catalyzed reaction.** Data 1, 2, and 3 were obtained with DHNP as the substrate. Because the commercial DHNP contained a minute amount of DHMP, the reaction mixtures contained both DHNP and DHMP. The concentrations of DHNP and DHMP for data 1, 2, and 3 were 29.7 and 0.3, 19.8 and 0.2, 9.9 and 0.1  $\mu\text{M}$ , respectively. Data 4, 5, and 6 were obtained with DHMP as the substrate. The DHMP concentrations were 10, 20, and 30  $\mu\text{M}$ , respectively. The enzyme concentration was 20  $\mu\text{M}$  for all reactions. All concentrations were those immediately after the mixing of the two syringe solutions. The buffer contained 100 mM Tris-HCl, 5 mM DTT, pH 8.3. The solid lines were obtained by global nonlinear least squares regression using the program DYNAFIT (27). For clarity, the changes in the concentrations of DHNP and DHMP were not plotted.

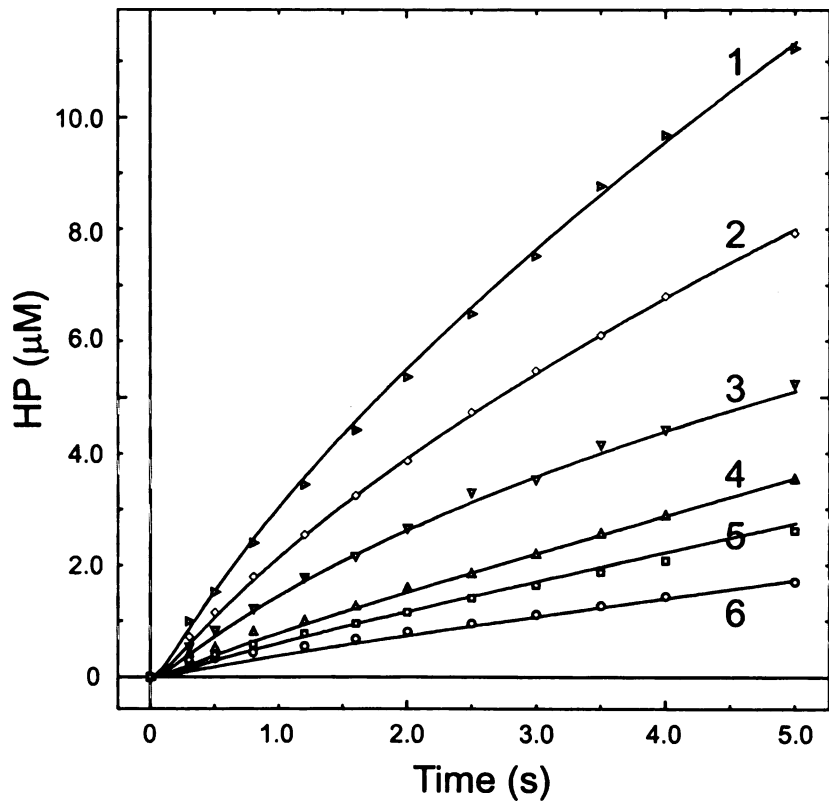
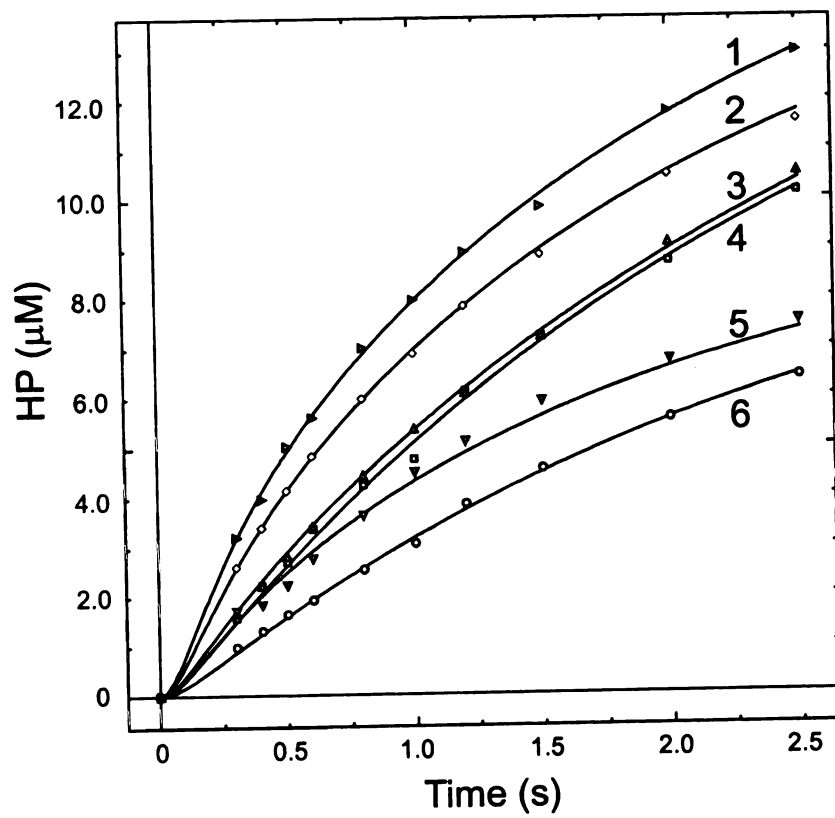


**Figure 2.7: Quench-flow analysis of the EcDHNA-catalyzed reaction.** The reaction conditions and substrate concentrations were the same as those described in the legend for Figure 2.6. The EcDHNA concentration was 15  $\mu\text{M}$  for all data sets. The solid lines were obtained by global nonlinear least squares regression using the program DYNAFIT. For clarity, the changes in the concentrations of DHNP and DHMP were not plotted.

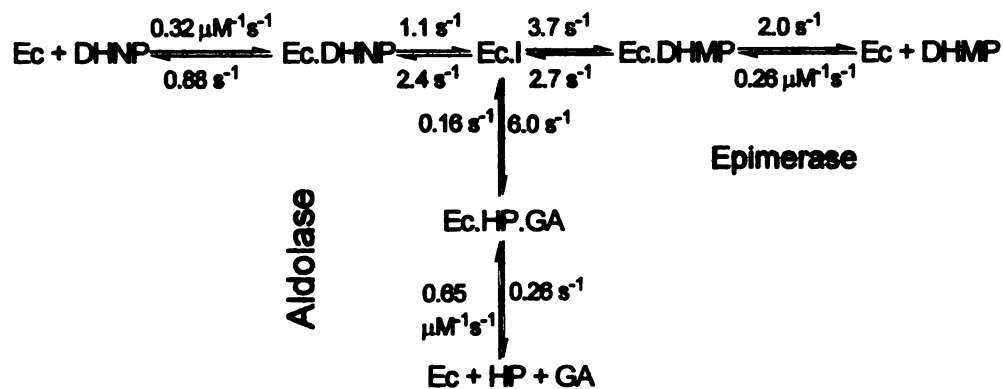
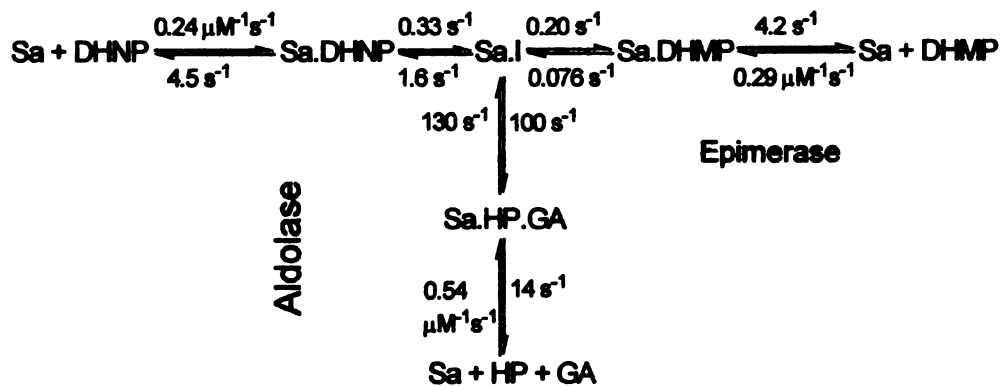


quench-flow analysis are summarized in Figure 2.8. For SaDHNA, the epimerase activity is insignificant in comparison with its aldolase activity, only a small fraction of the aldolase activity, the rate-limiting step in the formation of HP is the generation of the reaction intermediate, and the reverse reaction is faster than the forward reaction. For EcDHNA, in contrast, the epimerase activity is highly significant, comparable to the aldolase activity, the rate-limiting step in the formation of HP is the product release, and the reverse reaction is much slower than the forward reaction.

## DISCUSSION

Despite its fundamental significance as a unique aldolase and its biological significance as an attractive target for developing antimicrobial agents, how the enzyme catalyzes both the aldolase and epimerase reactions are largely unknown beyond the crystal structures (11, 16, 30, 31). While it is reasonable to assume that the epimerase reaction follows the same reaction intermediate as that of the aldolase reaction, one cannot exclude *a priori* the alternative mechanism of deprotonation and re-protonation of 2-carbon. Our NMR analysis of DHMP generated in the reaction in D<sub>2</sub>O clearly indicated that there is no deuteration of 2-carbon of the epimerase product. In contrast, the 6-hydroxymethyl group of the aldolase product HP is deuterated to the extent of having at least one equivalent of deuterons added to the 6-hydroxymethyl carbon (24). Obviously, the lack of deuteration of the 2'-carbon of DHMP is not due to the lack of deuterons, rather it suggests that the epimerase reaction follows the aldol chemistry and the 2'-proton is not extracted during the course of the reaction. The NMR data strongly supports

**Figure 2.8: Summary of the kinetic constants for the SaDHNA-catalyzed (top panel) and EcDHNA-catalyzed (lower panel) reactions. The chemical steps are highlighted with blue ovals, and the aldolase and epimerase activities with blue arrows.**



the hypothesis that the aldolase and epimerase activities follows the same reaction intermediate as depicted in Figure 2.1.

Because DHNA catalyzes both aldol and epimerization reactions and the epimerization product DHMP can also be converted to the aldol reaction product HP, it is particularly important to determine the rate constants for elementary steps if one intends to determine how the enzyme catalyzes the two reactions. Furthermore, steady-state kinetic analysis is insufficient for DHNA, because the steady-state kinetic parameters cannot adequately describe the two reactions catalyzed by the enzyme and the formation of DHMP will be underestimated because of its conversion to HP. Haußmann and coworkers previously determined the steady-state kinetic constants for EcDHNA (15). According to the steady-state kinetic data, the epimerase activity is 1/6 of the aldolase activity, which significantly underestimates the epimerase activity of EcDHNA (see Figure 2.8, lower panel). Furthermore, the  $k_{\text{cat}}$  values for the aldolase and epimerase activities are significantly lower than the rate constants of the chemical steps.

A critical issue in the kinetic analysis is whether the reaction is reversible or not. Although in general aldolase-catalyzed reactions are readily reversible, it was shown earlier that DHNA was an exception and the DHNA-catalyzed reaction is apparently irreversible. The apparent irreversibility is probably due to the low activity of the enzyme preparation used in the experiment, the low concentration of GA, and the low reaction rate of the EcDHNA-catalyzed reverse reaction. With pure recombinant enzymes and high concentrations of GA, it is clear that DHNA-catalyzed reaction is reversible. In fact for SaDHNA, the reverse reaction is much faster than the forward reaction. Our strategy for determining the rate constants of individual steps is a comprehensive one. The

philosophy behind the strategy is to isolate the different steps of the reaction whenever possible and design experiments to determine rate constants for the specific steps. Stopped-flow fluorometry is rapid and suitable for the physical steps of the enzymatic reaction, but is not suitable for the chemical steps because of the lack of significant optical changes in the chemical steps. On the other hand, quench-flow analysis is laborious but provides an accurate measurement of the rates of the chemical steps. Because the reaction is reversible, it can be run in three directions with DHNP, DHMP, or HP and GA as the substrates. One can then derive a complete set of rate constants for the enzymatic reaction by the global analysis of the multitude of data. The determination of a complete set of kinetic constants for both SaDHNA and EcDHNA provides a firm basis for dissecting their catalytic mechanisms.

Our equilibrium and kinetic data show that SaDHNA and EcDHNA have significantly different binding and catalytic properties, in accordance with the significant sequence differences between the two enzymes. EcDHNA is different from SaDHNA biochemically in several aspects. (1) EcDHNA has much higher affinities for the substrate, products, and inhibitors measured in this work, particularly for HPO. (2) EcDHNA has a much higher epimerase activity than SaDHNA. (3) The rate-limiting step in the forward reaction (the formation of HP) is the product release for EcDHNA but is the formation of the reaction intermediate for SaDHNA. (4) The reverse reaction is very slow with EcDHNA but very fast with SaDHNA. The marked differences in the ligand-binding properties of SaDHNA and EcDHNA, which must stem from the significant differences in the structures of their active sites, suggest that it may be possible to develop antimicrobial agents specifically against DHNA from *S. aureus* or *E. coli*.

Indeed, we have developed potent inhibitors for SaDHNA or EcDHNA (Felczak et al., unpublished). Because many DHNAs from Gram-positive and Gram-negative bacteria are highly homologous within their own groups but significantly different between the two groups, it may be possible to develop antimicrobial agents specifically against Gram-positive or Gram-negative bacteria by targeting respective DHNAs.

## REFERENCES

- (1) Yao, L. S., Yan, H. G., and Cukier, R. I. (2006) Mechanism of dihydroneopterin aldolase: A molecular dynamics study of the apo enzyme and its product complex. *J. Phys. Chem. B* 110, 1443-1456.
- (2) World Health Organization (1999) World Health Organization Report on Infectious Diseases: Removing Obstacles to Healthy Development. World Health Organization, Geneva.
- (3) Walsh, C. (2003) Where will new antibiotics come from? *Nature Rev. Microbiol.* 1, 65-70.
- (4) Cohen, M. L. (2000) Changing patterns of infectious disease. *Nature* 406, 762-767.
- (5) Murray, B. E. (1997) Antibiotic resistance. *Ad. Intern. Med.* 42, 339-367.
- (6) Projan, S. J. (2003) Why is big pharma getting out of antibacterial drug discovery? *Curr. Opin. Microbiol.* 6, 427-430.
- (7) Spellberg, B., Powers, J. H., Brass, E. P., Miller, L. G., and Edwards, J. E. (2004) Trends in antimicrobial drug development: Implications for the future. *Clin. Infect. Dis.* 38, 1279-1286.
- (8) Wenzel, R. P. (2004) Business and medicine - the antibiotic pipeline - challenges, costs, and values. *N. Engl. J. Med.* 351, 523-526.
- (9) Barrett, C. T., and Barrett, J. F. (2003) Antibacterials: Are the new entries enough to deal with the emerging resistance problems? *Curr. Opin. Biotechnol.* 14, 621-626.
- (10) Blakley, R. L., and Benkovic, S. J. (1984) in *Folates and pterins*, John Wiley & Sons, New York.
- (11) Sanders, W. J., Nienaber, V. L., Lerner, C. G., McCall, J. O., Merrick, S. M., Swanson, S. J., Harlan, J. E., Stoll, V. S., Stamper, G. F., Betz, S. F., Condroski, K. R., Meadows, R. P., Severin, J. M., Walter, K. A., Magdalinos, P., Jakob, C. G., Wagner, R., and Beutel, B. A. (2004) Discovery of potent inhibitors of dihydroneopterin aldolase using crystalLEAD high-throughput X-ray crystallographic screening and structure-directed lead optimization. *J. Med. Chem.* 47, 1709-1718.

- (12) Mathis, J. B., and Brown, G. M. (1970) The biosynthesis of folic acid XI. Purification and properties of dihydroneopterin aldolase. *J. Biol. Chem.* 245, 3015-3025.
- (13) Horecker, B. L., Tsolas, O., and Lai, C.-Y. (1975) Aldolases, in *The enzymes* (Boyer, P. D., Ed.) pp 213-258, Academic Press, San Diego.
- (14) Allen, K. N. (1998) Reactions of enzyme-derived enamines, in *Comprehensive biological catalysis* (Sinnott, M., Ed.) pp 135-172, Academic Press, San Diego.
- (15) Haußmann, C., Rohdich, F., Schmidt, E., Bacher, A., and Richter, F. (1998) Biosynthesis of pteridines in *Escherichia coli* - structural and mechanistic similarity of dihydroneopterin-triphosphate epimerase and dihydroneopterin aldolase. *J. Biol. Chem.* 273, 17418-17424.
- (16) Hennig, M., D'Arcy, A., Hampele, I. C., Page, M. G. P., Oefner, C., and Dale, G. E. (1998) Crystal structure and reaction mechanism of 7,8- dihydroneopterin aldolase from *Staphylococcus aureus*. *Nature Struct. Biol.* 5, 357-362.
- (17) Luo, Y., Samuel, J., Mosimann, S. C., Lee, J. E., Tanner, M. E., and Strynadka, N. C. J. (2001) The structure of l-ribulose-5-phosphate 4-epimerase: An aldolase-like platform for epimerization. *Biochemistry* 40, 14763-14771.
- (18) Samuel, J., Luo, Y., Morgan, P. M., Strynadka, N. C. J., and Tanner, M. E. (2001) Catalysis and binding in l-ribulose-5-phosphate 4-epimerase: A comparison with l-fuculose-1-phosphate aldolase. *Biochemistry* 40, 14772-14780.
- (19) Salzmann, M., Pervushin, K., Wider, G., Senn, H., and Wüthrich, K. (2000) NMR assignment and secondary structure determination of an octameric 110 kDa protein using TROSY in triple resonance experiments. *J. Am. Chem. Soc.* 122, 7543-7548.
- (20) Wider, G., and Wüthrich, K. (1999) NMR spectroscopy of large molecules and multimolecular assemblies in solution. *Curr. Opin. Struct. Biol.* 9, 594-601.
- (21) Riek, R., Pervushin, K., and Wüthrich, K. (2000) TROSY and CRINEPT: NMR with large molecular and supramolecular structures in solution. *Trends Biochem. Sci.* 25, 462-468.
- (22) Pervushin, K. (2000) Impact of transverse relaxation optimized spectroscopy (TROSY) on NMR as a technique in structural biology. *Q. Rev. Biophys.* 33, 161-197.
- (23) Deng, H., Callender, R., and Dale, G. E. (2000) A vibrational structure of 7,8-dihydrobiopterin bound to dihydroneopterin aldolase. *J. Biol. Chem.* 275, 30139-30143.

- (24) Illarionova, V., Eisenreich, W., Fischer, M., Haussmann, C., Romisch, W., Richter, G., and Bacher, A. (2002) Biosynthesis of tetrahydrofolate - stereochemistry of dihydroneopterin aldolase. *J. Biol. Chem.* 277, 28841-28847.
- (25) Li, Y., Gong, Y., Shi, G., Blaszczyk, J., Ji, X., and Yan, H. (2002) Chemical transformation is not rate-limiting in the reaction catalyzed by *Escherichia coli* 6-hydroxymethyl-7,8-dihydropterin pyrophosphokinase. *Biochemistry* 41, 8777-8783.
- (26) Shi, G., Gong, Y., Savchenko, A., Zeikus, J. G., Xiao, B., Ji, X., and Yan, H. (2000) Dissecting the nucleotide binding properties of *Escherichia coli* 6-hydroxymethyl-7,8-dihydropterin pyrophosphokinase with fluorescent 3'(2)'-o-anthraniloyladenine 5'-triphosphate. *Biochim. Biophys. Acta* 1478, 289-299.
- (27) Kuzmic, P. (1996) Program DYNAFIT for the analysis of enzyme kinetic data: Application to HIV proteinase. *Anal. Biochem.* 237, 260-273.
- (28) Yaylayan, V. A., Harty-Majors, S., and Ismail, A. A. (1998) Investigation of the mechanism of dissociation of glycolaldehyde dimer (2,5-dihydroxy-1,4-dioxane) by ftir spectroscopy. *Carbohydr. Res.* 309, 31-38.
- (29) Collins, G. C. S., and George, W. O. (1971) Nuclear magnetic resonance spectra of glycolaldehyde. *J. Chem. Soc. B*, 1352-1355.
- (30) Bauer, S., Schott, A. K., Illarionova, V., Bacher, A., Huber, R., and Fischer, M. (2004) Biosynthesis of tetrahydrofolate in plants: Crystal structure of 7,8-dihydroneopterin aldolase from *Arabidopsis thaliana* reveals a novel adolase class. *J. Mol. Biol.* 339, 967-979.
- (31) Goulding, C. W., Apostol, M. I., Sawaya, M. R., Phillips, M., Parseghian, A., and Eisenberg, D. (2005) Regulation by oligomerization in a mycobacterial folate biosynthetic enzyme. *J. Mol. Biol.* 349, 61-72.

### **CHAPTER 3: MECHANISM OF DIHYDRONEOPTERIN ALDOLASE: A POINT MUTATION CONVERTS THE ENZYME TO A COFACTOR-INDEPENDENT OXYGENASE**

#### **ABSTRACT**

Dihydroneopterin aldolase (DHNA) catalyzes the conversion of 7,8-dihydroneopterin to 6-hydroxymethyl-7,8-dihydropterin (HP) in the folate biosynthetic pathway. Substitution of a conserved tyrosine residue at the active site of DHNA by phenylalanine converts the enzyme to a cofactor-independent oxygenase, which generates mainly dihydroxanthopterin (DHXP) rather than HP. DHXP is generated via the same enol intermediate as in the wild-type enzyme-catalyzed reaction, but this species undergoes an oxygenation reaction to form DHXP. The conserved tyrosine residue plays only a minor role in the formation of the enol reaction intermediate, but a critical role in the protonation of the enol intermediate to form HP.

## INTRODUCTION

Dihydroneopterin aldolase (DHNA) catalyzes the conversion of 7,8-dihydroneopterin (DHNP) to 6-hydroxymethyl-7,8-dihydropterin (HP) in the folate biosynthetic pathway, one of principal targets for developing antimicrobial agents (1). Like other enzymes such as dihydropteroate synthase and dihydrofolate reductase in the folate pathway (2, 3), DHNA is an attractive target for developing antimicrobial agents (4). DHNA is also a unique aldolase in that it requires neither the formation of a Schiff base between the substrate and the enzyme nor metal ions for catalysis (5) and in addition to the aldolase reaction, DHNA also catalyzes the epimerization at the 2'-carbon of DHNP to generate 7,8-dihydroneopterin (DHMP, Figure 1.3) (6). Interestingly, DHNAs from *Staphylococcus aureus* (SaDHNA) and *Escherichia coli* (EcDHNA), representatives of DHNAs from Gram-positive and Gram-negative bacteria respectively, have significant differences in binding and catalytic properties.

One of the conserved residues at the active site of DHNA is a tyrosine residue, Y54 in SaDHNA and Y53 in EcDHNA. According to the crystal structure of SaDHNA in complex with HP (7), the pterin ring is stacked with the phenol ring of Y54 (Figure 1.7). The hydroxyl group of the phenol ring of Y54 is hydrogen bonded to the amino group of the putative general base of K100 and the hydroxyl of the 6-hydroxymethyl group of the bound HP. To investigate the role of the conserved tyrosine residue in catalysis, we replaced Y54 of SaDHNA and Y53 of EcDHNA with a phenylalanine residue by site-directed mutagenesis. The single point mutations convert the aldolases to oxygenases, which generate mainly dihydroxanthopterin (DHXP) rather than HP. DHXP is generated

via the same enol intermediate as in the wild-type enzyme-catalyzed reaction, but this species undergoes an oxygenation reaction to form DHXP. The conserved tyrosine residue plays only a minor role in the formation of the enol reaction intermediate, but a critical role in the protonation of the enol intermediate to form HP.

## EXPERIMENTAL PROCEDURES

*Materials.* 6-Hydroxymethylpterin (HPO), 6-Hydroxymethyl-7,8-dihydropterin (HP), 7,8-dihydro-D-neopterin (DHNP), 7,8-dihydro-L-monapterin (DHMP), D-neopterin (NP), L-monapterin (MP), 7,8-dihydroxanthopterin (DHXP), and 6-formyl-7,8-dihydropterin (FDHP) were purchased from Schircks Laboratories. *Pfu* DNA polymerase was purchased from Stratagene. Other chemicals were from Sigma or Aldrich.

*Site-Directed Mutagenesis and Protein Purification.* The mutants SaY54F and EcY53F, where Y54 of SaDHNA and Y53 of EcDHNA were replaced by Phe, respectively, were made by a PCR-based method using high-fidelity *pfu* DNA polymerase according to a protocol developed by Stratagene. The forward and reverse primers for making the SaY54F mutant were 5'-GTT ATTGATACAGTTCATTTTGGTGAAGTGTTCGAAGAG G-3' and 5'-CCTCTTCGAACA CTTCACCAAATGAACTGTATCAATAAC-3, respectively. The forward and reverse primers for making the EcY53F mutant 5'-CGGATTGCCTCAGTTCGCTGACATTGCAGAAAC-3' and 5'-GTTTCTGCAATGTCAGCGAACTGAGGCAATCCG-3', respectively. The mutants were selected by DNA sequencing. In order to ensure that there were no unintended

mutations in the mutants, the entire coding sequences of the mutated genes were determined.

The mutant proteins were purified as previously described (Wang et al., unpublished). Briefly, SaY5F was purified to homogeneity by a Ni-NTA column followed by a Bio-Gel A-0.5m gel column. EcY53F was purified by a DEAE-cellulose column followed by a Bio-Gel A-0.5m gel column. The purities of the protein preparations were checked by SDS-PAGE. The amino acid sequence of the purified proteins were confirmed by 'top-down' tandem mass spectrometry (8). The purified proteins were concentrated, dialyzed, lyophilized, and stored at -80 °C.

*Equilibrium Binding Studies.* The procedures for the equilibrium binding studies of the DHNA mutants were essentially the same as described previously for the wild-type enzymes (Wang et al., unpublished). Briefly, proteins and ligands were all dissolved in 100 mM Tris-HCl, pH 8.3, and the titration experiments were performed in a single cuvette with a Spex FluoroMax-2 fluorometer at 24 °C. To determine the  $K_d$  values of the binding of NP and MP to SaY54F, a 2 mL solution containing 10  $\mu$ M SaY54F was titrated with a NP or MP stock solution of one of the ligands (NP, MP, or HPO). To determine the  $K_d$  values of the binding of HPO to SaY54F and the binding of NP, MP, and HP to EcY53F, a 2 mL solution containing 1  $\mu$ M of one of the ligands (NP, MP, or HPO) was titrated with a stock solution of SaY54F or EcY53F. The  $K_d$  values were obtained by nonlinear least square fitting of the titration data as previously described (9).

*Stopped-Flow Analysis.* Stopped-flow experiments were performed on an Applied Photophysics SX.18MV-R stopped-flow spectrofluorometer at 25 °C as described previously for the wild-type enzymes (Wang et al., unpublished). Apparent rate constants

were obtained by nonlinear least squares fitting of the data to a single exponential equation and were re-plotted against the ligand concentrations. The association and dissociation constants were obtained by linear regression of the apparent rate constants vs. ligand concentration data.

*Kinetic assay.* The kinetic experiments were performed manually. Both DHNP and DHNA were dissolved in a buffer containing 100 mM Tris-HCl, 1 mM EDTA, and 5 mM DTT, pH 8.3. The reactions were initiated by the addition of DHNA and stopped with 1 N HCl. The stopped reaction mixtures were processed and separated by HPLC as described (6).

*NMR Spectroscopy.* NMR measurements were made at 25 °C with a Varian Inova 600 spectrometer. The initial NMR sample contained 1 mM DHNP and 1 mM tris(2-carboxyethyl) phosphine (TCEP) in 100 mM sodium phosphate buffer, pH 8.3 (pH meter reading without correction for deuterium isotope effects), made with 90% H<sub>2</sub>O and 10% D<sub>2</sub>O. The reaction was initiated with 1 μM SaDHNA or 3 μM SaY54F. NMR spectra were recorded before and after the addition of the enzyme. The spectral width for the NMR data was 12000 Hz with the carrier frequency at the HDO resonance. The solvent resonance was suppressed by presaturation. Each FID was composed of 16 k data points with 64 transients. The delay between successive transients was 1.7 s. The time domain data were processed by zero-filling to 32 k points, exponential multiplication (1 Hz), and Fourier transformation. Chemical shifts were referenced to the internal standard sodium 2-dimethyl-2-silapentane-5-sulfonate sodium salt (DSS).

*Mass Spectrometry (MS).* All MS experiments were performed using a Thermo model LTQ linear ion trap mass spectrometer. The initial 300 μl samples contained 200

$\mu\text{M}$  DHNP and 4  $\mu\text{M}$  SaDHNA or 10  $\mu\text{M}$  SaY54F in 5 mM ammonium carbonate, pH 8. Twenty  $\mu\text{L}$  aliquots of the reaction mixtures were taken out at 1-min intervals and mixed with 80  $\mu\text{L}$  of a solution containing 50% acetic acid and 1% methanol. The samples were further diluted with the same solution and then introduced to the mass spectrometer at a flow rate of 0.5  $\mu\text{L}/\text{min}$  by nanoelectrospray ionization (nESI). The nESI conditions used were: spray voltage 1.8 kV, heated capillary temperature 200 °C, capillary voltage -10 V, and tube lens voltage -50 V. Collision induced dissociation (CID) tandem mass spectrometry (MS/MS and MS<sup>3</sup>) spectra were acquired at an activation q value of 0.25 using an isolation width of 1 or 2 Da (to monoisotopically isolate the precursor ion), a normalized collision energy of 30% to 40%, and an activation time of 30 ms or 300 ms. The values were chosen such that the gentlest conditions were used in order to completely dissociate the selected precursor ion (i.e., some precursor ions required a larger normalized collision energy and/or longer activation time). The MS, MS/MS and MS<sup>3</sup> product ion spectra shown are the average of 60 individual mass analysis scans.

*Gas Chromatography/Mass Spectrometry (GC/MS) of GA.* The reaction contained 200  $\mu\text{M}$  DHNP and 4  $\mu\text{M}$  SaDHNA or 6.3  $\mu\text{M}$  SaY54F in 5 mM ammonium carbonate, pH 8.3. The reaction was stopped after 20 min by adding 1 N HCl and centrifuged for 5 min with a microcentrifuge. The supernatant collected was then lyophilized overnight to dryness. The dried residue was incubated for 1 h with 10  $\mu\text{L}$  methoxyamine hydrochloride in pyridine (10 mg/mL) and N-(t-butyltrimethylsilyl)-N-methyltrifluoroacetamide (MTBSTFA). GC/MS analyses were performed on an Agilent 5973 mass spectrometer coupled to a model 6890 gas chromatograph. All analyses were performed using 70 eV electron ionization. Separations were performed using a 30 meter

HP-5MS column and helium (36 cm/s) as carrier gas. The column temperature was programmed from 50 °C (4 min hold) to 285 °C at 10 degrees/min.

*HPLC Identification of Formic Acid.* The reaction mixtures in 1 mL contained 200  $\mu$ M DHNP and 10  $\mu$ M SaDHNA or SaY54F in 100 mM HEPES-KOH, pH 8.3, and were mixed with 100  $\mu$ l 3.2 M H<sub>2</sub>SO<sub>4</sub> after 20 min incubation at 24 °C. The solutions were centrifuged, filtered through a 0.45 micron syringe filter, and injected into a 7.8 $\times$ 300 mm Aminex HPX-87H column. Standard compounds, including formic acid, acetic acid, glycolic acid, glyceric acid, succinic acid, formaldehyde, glycolaldehyde, and glyceraldehyde, were treated the same way as the enzymatic reaction mixture. The column was eluted with 4 mM H<sub>2</sub>SO<sub>4</sub> at a flow rate of 0.6 mL/min, and the elution was monitored by a Waters 2487 UV detector at 210 nm and a Waters 410 differential refractometer.

*Oxygen Consumption Assay.* Oxygen consumption was measured using a Gilson 5/6H oxygraph with a Clark oxygen electrode at 25 °C. The initial samples in 1.8 mL contained 200  $\mu$ M DHNP in 100 mM HEPES-KOH, pH 8.2. The reactions were initiated by 8  $\mu$ M SaDHNA or SaY54F at 25 °C. The turnover number for SaY54F was calculated using the slope of the initial linear part of the data obtained by linear regression.

## RESULTS

*Biochemical Analysis.* Previously we established the thermodynamic and kinetic framework for the structure-function studies of SaDHNA and EcDHNA (Wang et al., unpublished). We performed the biochemical characterizations of the mutants SaY54F

and EcY53F using the same strategy. The binding steps were mimicked with the substrate and product analogues NP, MP, and HPO. The only difference between the substrate and product analogues and the corresponding substrate and products is that between C7 and N8 is a double bond in the analogues and a single bond in the substrate and products. NP, MP, and HPO are excellent substrate and product analogues (Wang et al., unpublished). The  $K_d$  values were measured by equilibrium binding experiments using fluorometry. The association and dissociation rate constants were determined by kinetic binding experiments using stopped-flow fluorometry. Representative results are shown in Figures 3.1 and 3.2 for the equilibrium and kinetic binding experiments, respectively. The complete results are summarized in Table 3.1. For SaY54F, the mutation increased the affinities of the ligands for the enzyme by a factor of ~4-6. For EcY53F, the mutation increased the affinities of NP and MP by a factor of 4-6, but decreased the affinity of HPO by a factor of 4. The changes were mainly caused by the changes in the dissociation rate constants. The results suggested that neither Y54 of SaDHNA nor Y53 of EcDHNA is critically important for the binding of substrate or products. To our surprise, there was a dramatic drop in the total fluorescence intensity in the HPLC analysis of the reaction mixtures generated by either SaY54F or EcY53F as the reaction progressed, suggesting that the substrate was converted to a non-fluorescent compound at the chosen excitation and emission wavelengths and the mutant enzyme-catalyzed reactions generated different products.

*NMR Analysis.* In order to identify the products of the mutant-catalyzed reactions, we analyzed the reaction mixtures by NMR. Representative spectra are shown in Figure 3.3, and the chemical shifts of selected protons of related compounds are summarized in

**Figure 3.1: Binding of HPO to EcY53F at equilibrium.** A 2 mL solution containing 1  $\mu\text{M}$  HPO in 100 mM Tris-HCl, pH 8.3 was titrated with EcY53F by adding aliquots of a 60  $\mu\text{M}$  EcY53F stock solution at 24 °C. The final HPO concentration was 0.93  $\mu\text{M}$ . The top axis indicates the EcY53F concentrations during the titration. A set of control data was obtained in the absence of HPO and was subtracted from the corresponding data set obtained in the presence of HPO. The solid line was obtained by nonlinear least-squares regression as previously described (9).

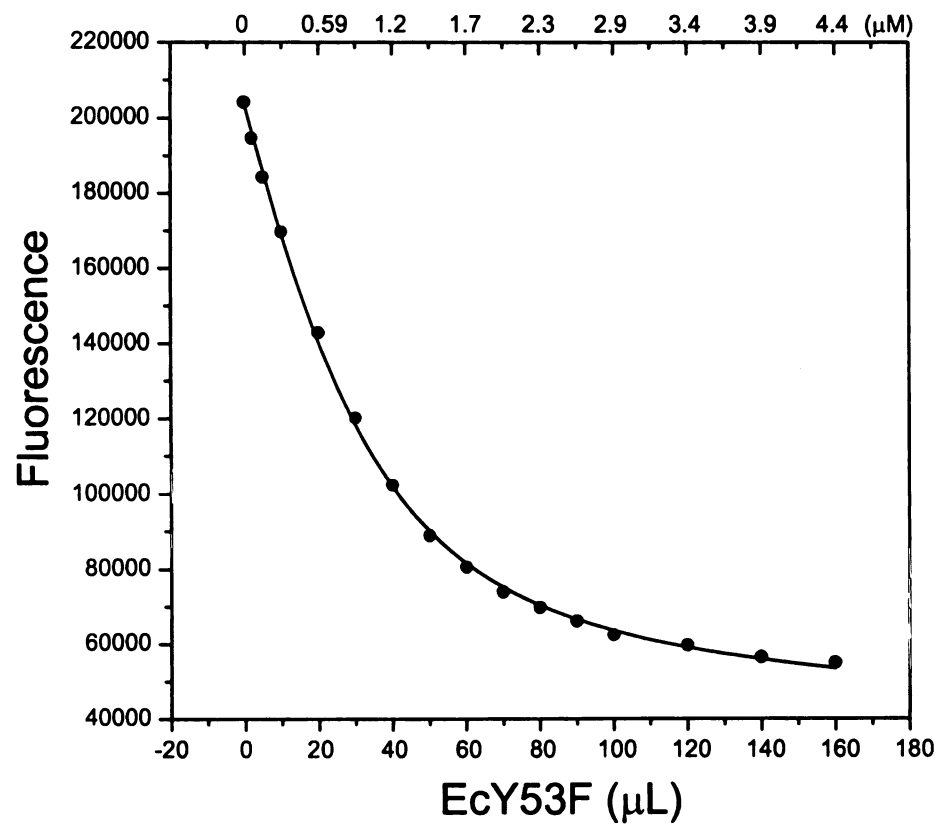


**Figure 3.2: Stopped-flow analysis of the binding of MP to EcY53F.** The concentration of EcY53F was 0.2  $\mu\text{M}$ , and the concentrations of MP were 1, 2, 4 and 8  $\mu\text{M}$  for traces 1, 2, 3, and 4, respectively. All concentrations were those immediately after the mixing of the two syringe solutions. Both EcY53F and MP were dissolved in 100 mM 100 mM Tris-HCl, pH 8.3. The fluorescent signals were rescaled so that they could be fitted into the figure with clarity. The solid lines were obtained by nonlinear regression as described in the Experimental Procedures section. The inset is a replot of the apparent rate constants vs. the MP concentrations. The solid line was obtained by linear regression.

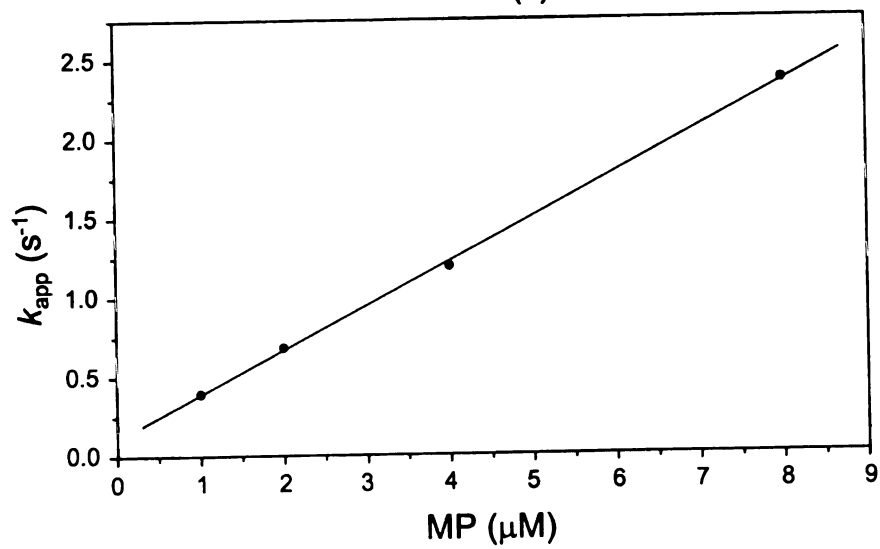
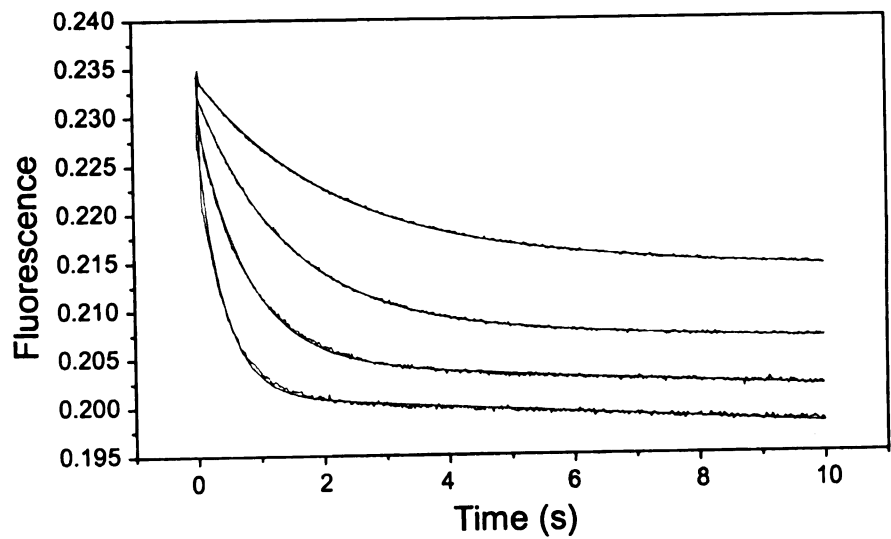


Table 3.1: Binding Constants of *S. aureus* and *E. coli* DHNAs and Y→F Mutants

		SaDHNA	SaY54F	EcDHNA	EcY53F
NP	$K_d$ ( $\mu\text{M}$ )	18±2	4.5±0.9	0.77±0.06	0.2±0.009
	$k_1$ ( $\mu\text{M}^{-1}\text{s}^{-1}$ )	0.24±0.01	0.099±0.005	0.32±0.02	0.26±0.003
	$k_{-1}$ ( $\text{s}^{-1}$ )	4.5±0.1	0.44±0.05	0.29±0.03	0.060±0.006
MP	$K_d$ ( $\mu\text{M}$ )	13±1	3.7±0.5	2.6±0.06	0.40±0.01
	$k_1$ ( $\mu\text{M}^{-1}\text{s}^{-1}$ )	0.29±0.02	0.13±0.003	0.26±0.01	0.28±0.003
	$k_{-1}$ ( $\text{s}^{-1}$ )	4.2±0.2	0.80±0.09	0.58±0.03	0.11±0.006
HPO	$K_d$ ( $\mu\text{M}$ )	24±0.2	3.8±0.9	0.10±0.007	0.40±0.02
	$k_1$ ( $\mu\text{M}^{-1}\text{s}^{-1}$ )	0.45±0.02	0.68±0.003	0.55±0.04	0.79±0.005
	$k_{-1}$ ( $\text{s}^{-1}$ )	10±0.5	2.9±0.06	0.062±0.006	0.26±0.0001

**Figure 3.3: NMR analysis of the reactions catalyzed by SaDHNA (A) and SaY54F (B).** The initial NMR sample contained 1 mM DHNP and 1 mM tris(2-carboxyethyl) phosphine (TCEP) in 100 mM sodium phosphate buffer, pH 8.3, made with 90% H<sub>2</sub>O and 10% D<sub>2</sub>O. The reaction was initiated with 1 μM SaDHNA (A) or 3 μM SaY54F (B).

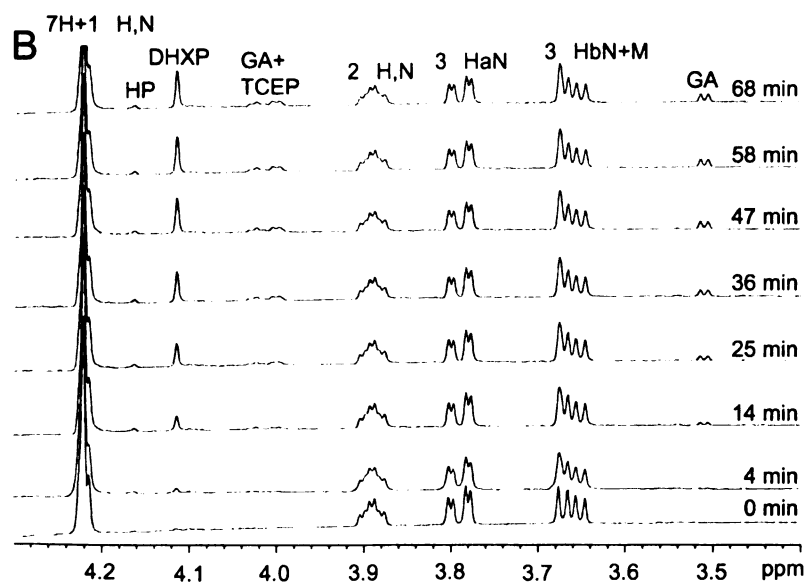
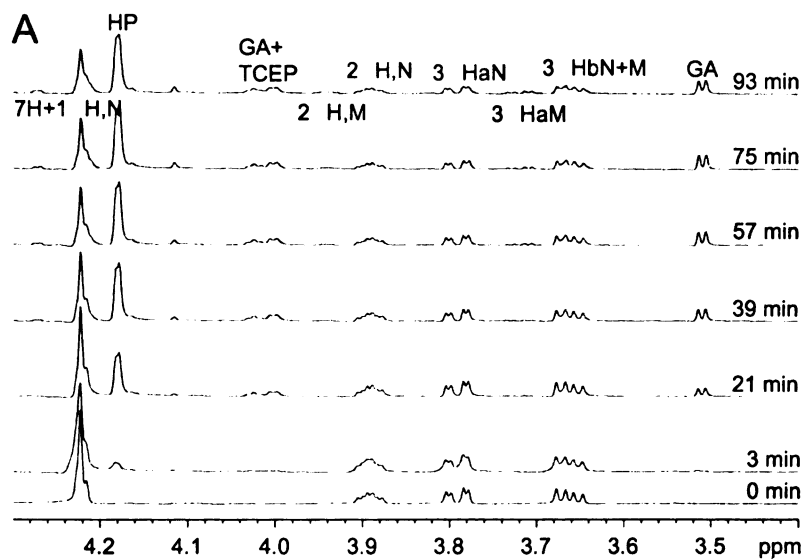


Table 3.2. As shown in Figure 3.3, GA was generated by both the wild-type enzyme- and the mutant-catalyzed reactions. While the wild-type enzyme catalyzed reaction generated HP along with GA (Figure 3.3A), the mutant-catalyzed reaction generated little HP (Figure 3.3B). The major product of the mutant-catalyzed reaction was a peak at 4.12 ppm. The NMR spectra of the reaction mixtures generated by the *E. coli* enzymes (data not shown) were very similar to those of the reaction mixtures generated by the *S. aureus* enzymes. Because both SaDHNA and SaY54F were saturated with the substrate DHNP under the experimental conditions, their turnover numbers ( $k_{\text{cat}}$ ) could be calculated on the basis of the enzyme concentration, the initial substrate concentration, and the NMR peak intensities of the substrate and products. The calculated  $k_{\text{cat}}$  values for the formation of HP were  $0.2 \text{ s}^{-1}$  for SaDHNA and  $3.4 \times 10^{-4} \text{ s}^{-1}$  for SaY54F.

*MS Analysis.* The identity of the major product of the SaY54F-catalyzed reaction that gave rise to the 4.12 ppm peak in the NMR spectrum could not be determined by 1D proton NMR. In order to identify the reaction product, we analyzed the reaction mixtures generated by both the wild-type and the mutant enzymes by MS. As expected, the primary product generated by SaDHNA was different from that generated by SaY54F (Figures 3.4A and B). The mass spectrum of the reaction involving SaDHNA showed the formation of a product ion at  $m/z$  196, while the spectrum of the reaction involving SaY54F showed the formation of a product ion at  $m/z$  182.

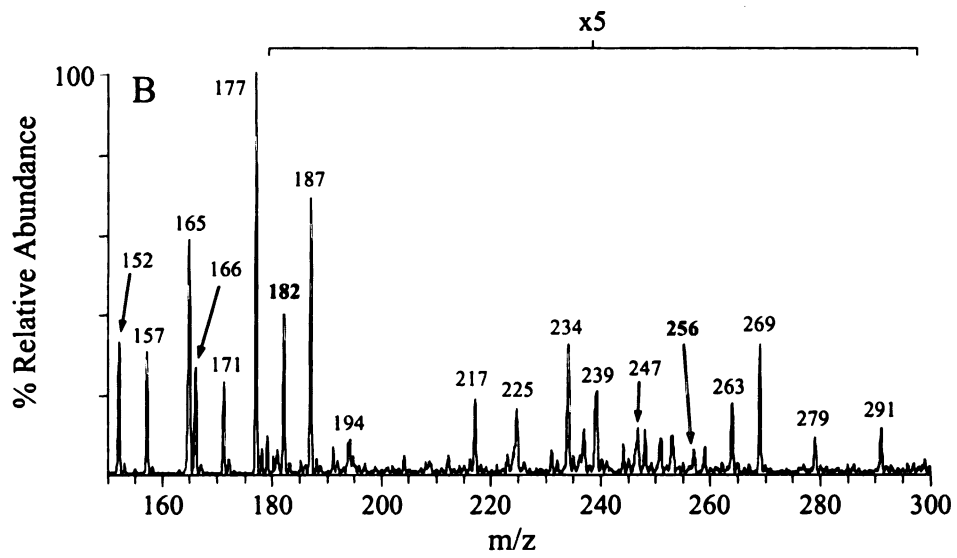
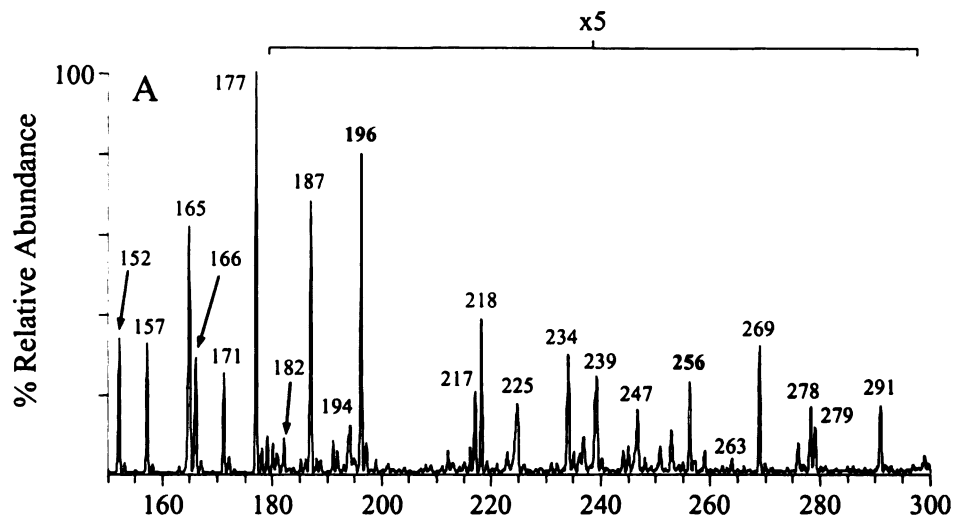
In order to determine the identity of the  $m/z$  196 ion in Figure 3.4A, MS/MS and MS<sup>3</sup> spectra were obtained and compared to those of the expected reaction product HP. As shown in Figure 3.5, the major ions observed by CID MS/MS of the ion at  $m/z$  196 obtained from the SaDHNA-catalyzed reaction were identical to the major product ions

Table 3.2: Chemical Shifts of Selected Protons of Compounds Related to the Reactions  
Catalyzed by the Wild-Type and Mutant DHNAs<sup>a</sup>

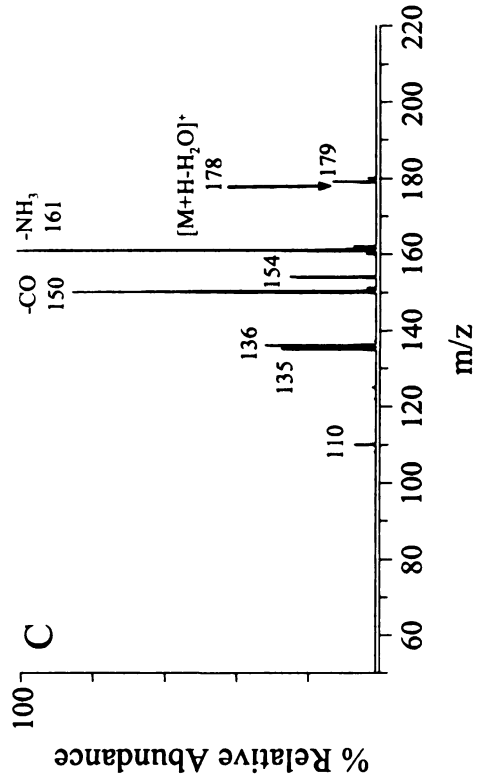
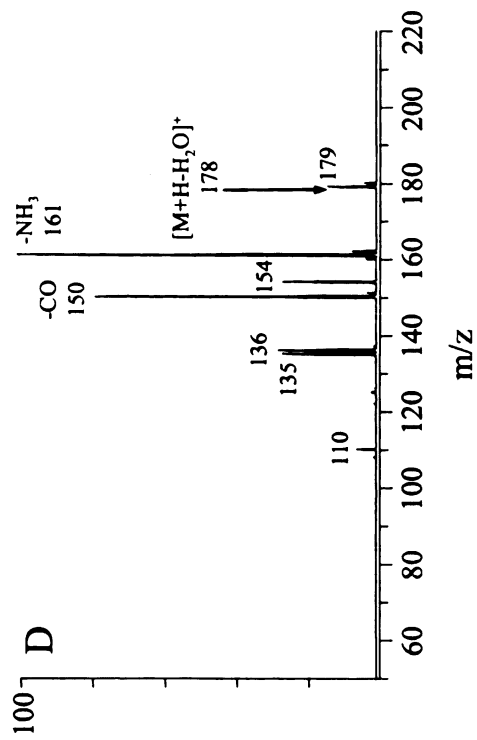
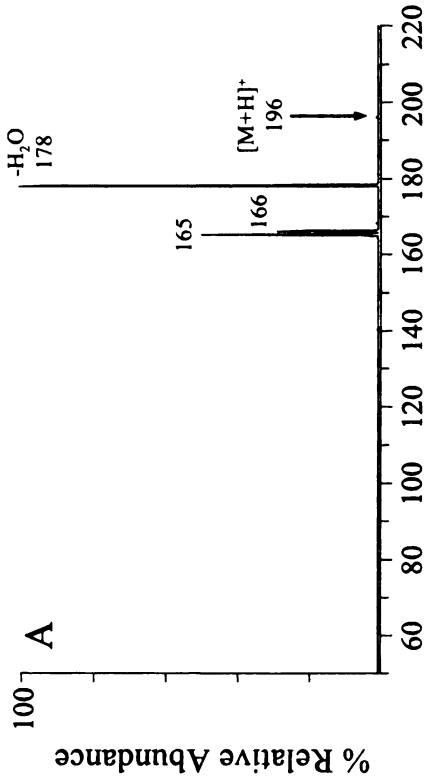
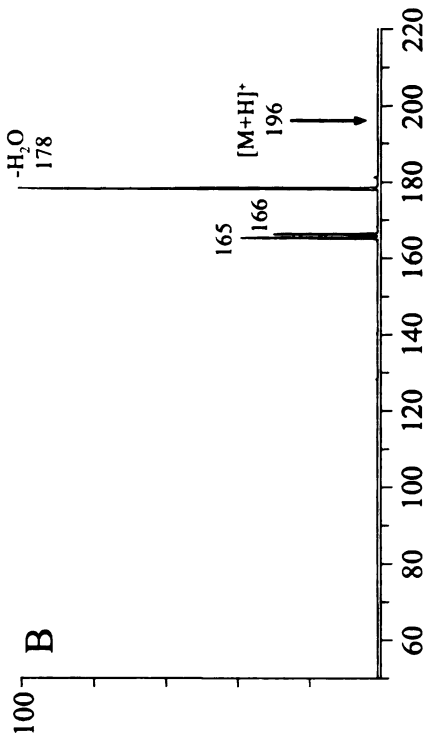
Compounds	7H	1'H	2'H	3'Ha	3'Hb	Others
DHNP	4.22 (d)	4.22 (d)	3.90 (m)	3.80 (m)	3.66 (m)	
DHMP	4.22 (d)	4.27 (d)	3.94 (m)	3.72 (m)	3.66 (m)	
HP	4.18 (s)					4.18 (s)
DHXP	4.12 (s)					
GA						3.50 (d)
GA+TCEP						4.02 (m)

<sup>a</sup>The chemical shifts were from those of the commercial compounds in 50 mM sodium phosphate buffer, pH 8.3 (pH meter reading without correction for deuterium isotope effects), made with 90% H<sub>2</sub>O and 10% D<sub>2</sub>O. The peak at 4.02 ppm was present only in the presence of both GA and TCEP. The 4.18 ppm peak of HP also belongs to the 6-hydroxymethyl group.

**Figure 3.4: ESI MS analysis of the mixtures generated by a 10 min reaction of SaDHNA (A) and SaY54F (B).** The substrate, DHNP, is observed at  $m/z$  256 in both spectra. The region from  $m/z$  180-300 has been magnified (x5) for clarity.



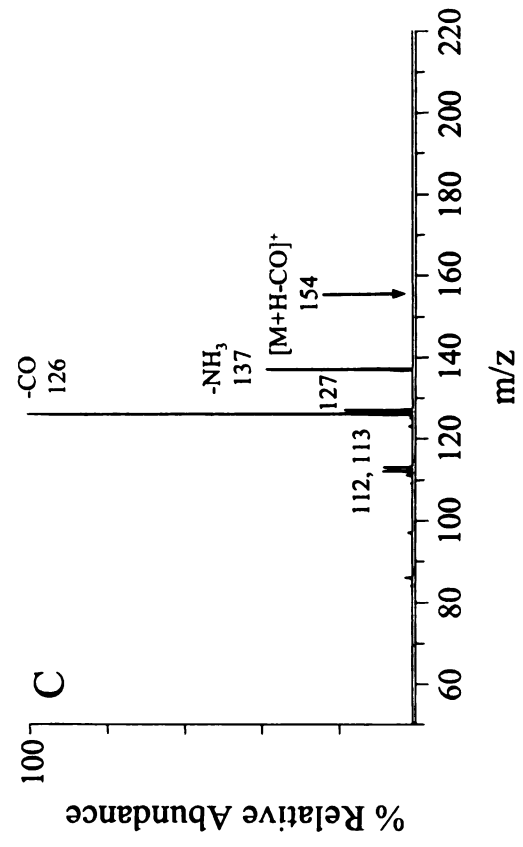
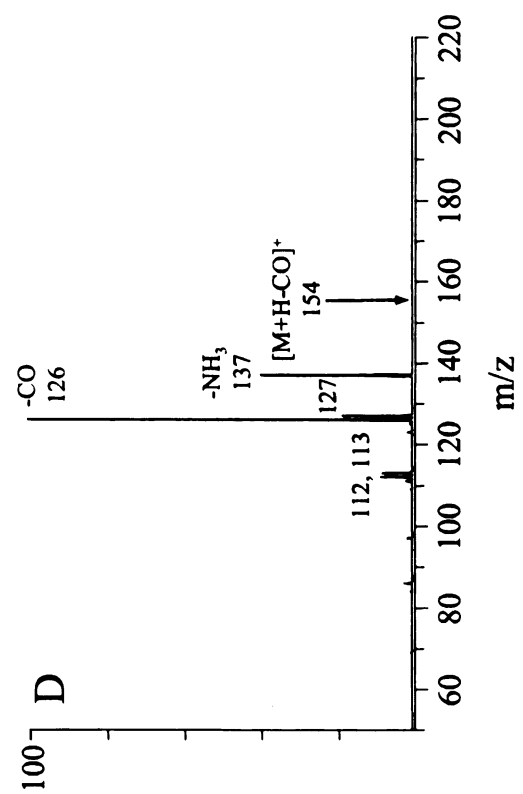
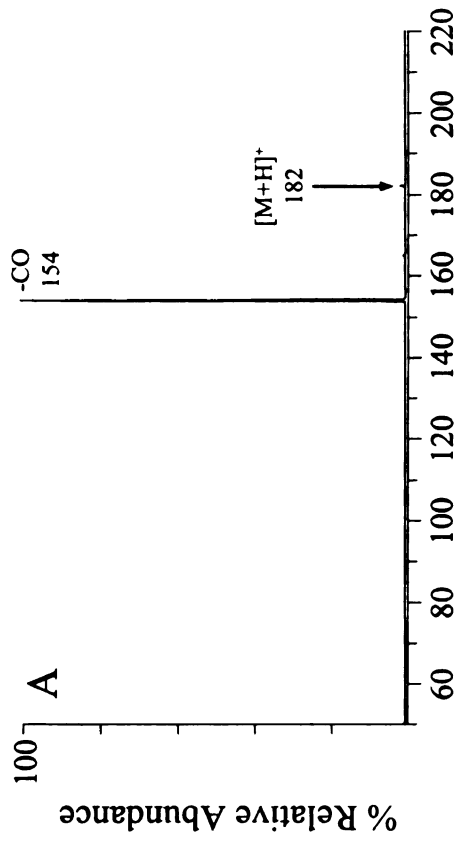
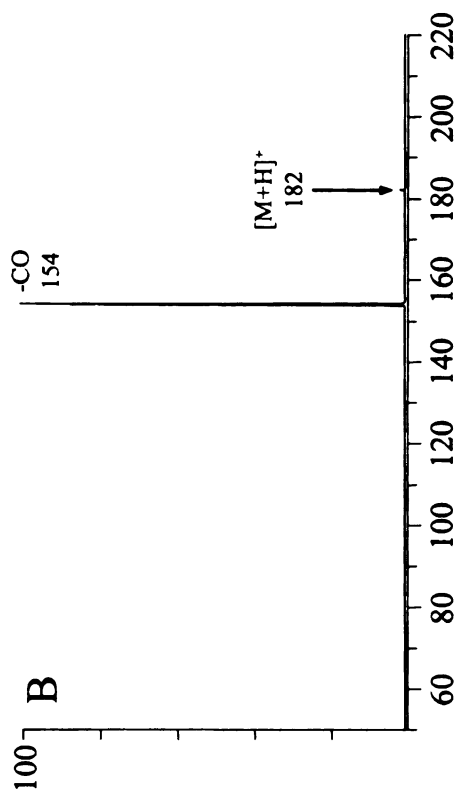
**Figure 3.5: Multistage tandem mass spectrometry identification of the m/z 196 product from the reaction of DHNP with SaDHNA.** (A) CID MS/MS product ion spectrum of the ion at m/z 196 obtained from Figure 3.4A. (B) CID MS/MS product ion spectrum of the m/z 196 precursor ion obtained from a solution of commercially available HP. (C) CID MS<sup>3</sup> product ion spectrum of the ion at m/z 178 in panel A. (D) CID MS<sup>3</sup> product ion spectrum of the ion at m/z 178 in panel B.



seen in the MS/MS product ion spectrum obtained from the standard (compare Figures 3.5A and B). The most abundant product ion in Figures 3.5A and B at  $m/z$  178 is most likely due to the loss of water from the precursor ion. To obtain further confirmation of the expected product ion structure,  $MS^3$  was then performed on the  $m/z$  178 product ion (Figures 3.5C and D). As expected, the experimental and standard  $MS^3$  spectra were essentially identical. The most abundant product ions at  $m/z$  161 and 150 are most likely due to the loss of  $NH_3$  and CO, respectively. Based on an  $MS^4$  experiment (data not shown), the  $MS^3$  product ion seen at  $m/z$  179 was formed via an ion-molecule reaction between the ion at  $m/z$  161 and a water molecule. Taken together, the MS/MS and  $MS^3$  spectra provided strong evidence that the product seen at  $m/z$  196 from the reaction of DHNP with SaDHNA is HP.

This same type of analysis was also performed in order to determine the identity of the  $m/z$  182 ion in Figure 5B. MS/MS and  $MS^3$  spectra of the ion were obtained and compared to those of the proposed reaction product, DHXP. An examination of Figure 3.6 indicated that the major ion observed by CID MS/MS of the ion at  $m/z$  182 obtained from the SaY54F-catalyzed reaction is identical to the major ion seen in the MS/MS product ion spectrum obtained from the standard (compare Figures 3.6A and B). The  $m/z$  154 product ion in Figures 3.6A and B is most likely due to the loss of CO from the precursor ion.  $MS^3$  was then performed on the  $m/z$  154 ion (Figures 3.6C and D). Again, the experimental and standard spectra were essentially the same. The major  $MS^3$  product ion, seen at  $m/z$  126, corresponds to the loss of CO, while the second most intense ion, seen at  $m/z$  137, corresponds to the loss of  $NH_3$ . As was the case for the previous analysis of the SaDHNA-catalyzed reaction, these spectra together provided strong

**Figure 3.6: Multistage tandem mass spectrometry identification of the m/z 182 product from the reaction of DHNP with SaY54F.** (A) CID MS/MS product ion spectrum of the ion at m/z 182 obtained from Figure 3.4B. (B) CID MS/MS product ion spectrum of the m/z 182 precursor ion obtained from a solution of commercially available DHXP. (C) CID MS<sup>3</sup> product ion spectrum of the ion at m/z 154 in panel A. (D) CID MS<sup>3</sup> product ion spectrum of the ion at m/z 154 in panel B.



evidence that the product seen at  $m/z$  182 from the reaction of DHNP with SaY54F is DHXP.

The  $m/z$  256 ion (Figure 3.4) was found to correspond to DHNP (Figure 3.7), as well as probably partly due to DHMP, which was generated by the enzymatic reactions. DHNP and DHMP differ only in the stereochemistry of 2'-carbon and have the same molecular weight. The  $m/z$  194 ion (Figure 3.4) was found to correspond to HPO and FDHP, because the MS/MS and MS<sup>3</sup> spectra of the  $m/z$  194 species were the sum of those of HPO and FDHP standards, with HPO contributing more than FDHP (Figure 3.8). The existence of FDHP was also confirmed by spectrophotometry, in which FDHP has a characteristic absorption peak at 420 nm (data not shown).

*GC/MS Confirmation of GA.* Since the major product of the SaY54F-catalyzed reaction was DHXP, not HP, it was necessary to confirm the identity of GA as indicated by the NMR analysis (Figure 3.3). To this end, we derivatized the reaction products of SaDHNA and SaY54F with methoxyamine and MTBSTFA to form the *tert*-butyldimethylsilyl ether of the methoxime. GA was then detected by GC/MS as shown in Figure 3.9. The enzymatic reaction product (Figure 3.9B) was identified by comparison with the commercially available standard GA (Figure 3.9A). The retention time of GA standard is 12.3 min (data not shown). The molecular weight of the GA derivative is 203 Da, but the molecular ion was too weak to be observed as is typical for these derivatives. The dominant fragment ions in the mass spectrum appeared at  $m/z$  146 ( $[M-C_4H_9]^+$ ) and 188 ( $[M-CH_3]^+$ ). Both reaction mixtures generated by SaDHNA and SaY54F contained a peak with the same retention time as that of standard GA. The mass spectrum of the

**Figure 3.7: Multistage tandem mass spectrometry identification of the substrate DHNP.** (A) CID MS/MS product ion spectrum of the ion at  $m/z$  256 obtained from the reaction of DHNP with SaDHNA at 0 min. (B) CID MS/MS product ion spectrum of the  $m/z$  256 precursor ion obtained from a solution of commercially available DHNP. (C) CID MS<sup>3</sup> product ion spectrum of the ion at  $m/z$  154 in panel A. (D) CID MS<sup>3</sup> product ion spectrum of the ion at  $m/z$  154 in panel B.

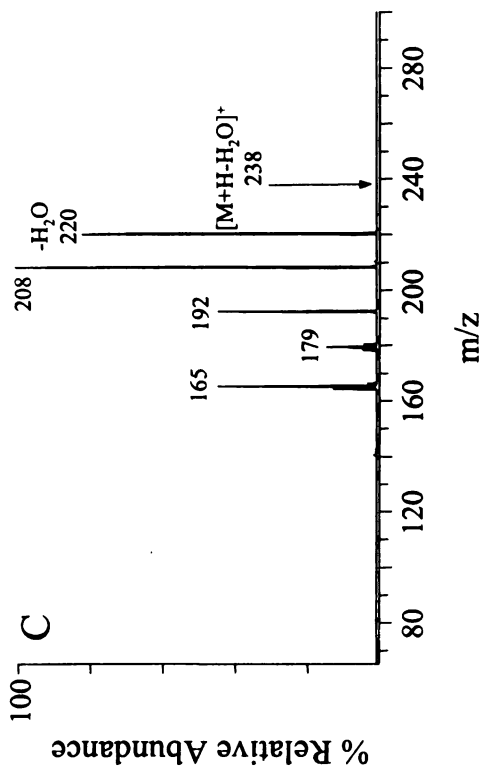
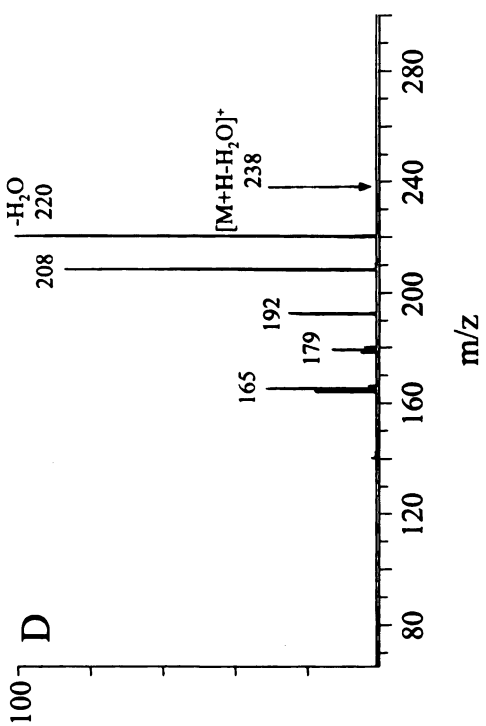
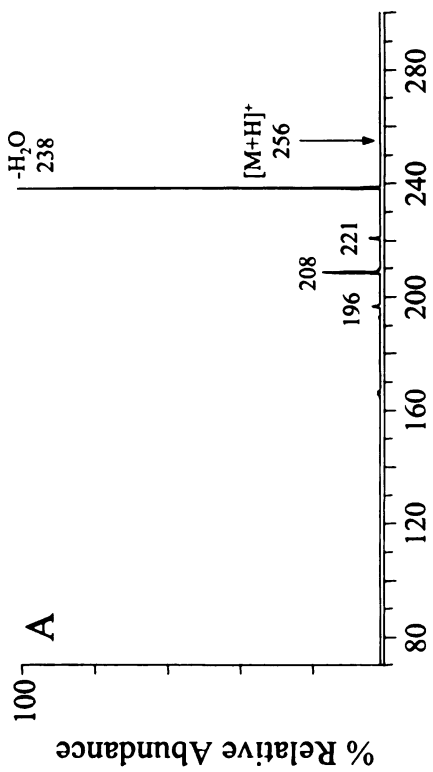
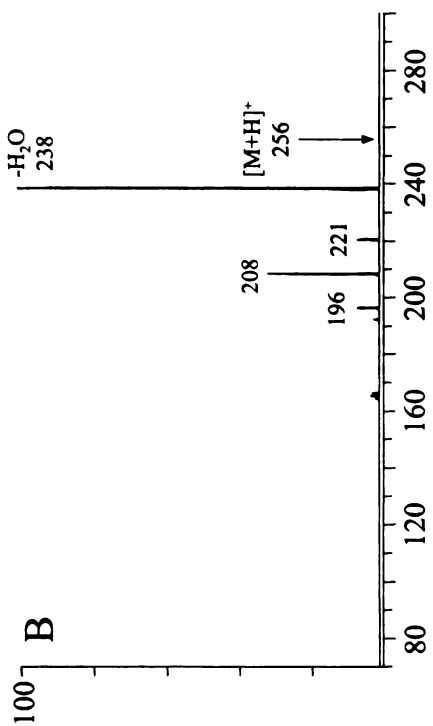


**Figure 3.8: Multistage tandem mass spectrometry identification of the m/z 194 products from the DHNP reaction catalyzed by SaY54F.** (A) CID MS/MS product ion spectrum of the ion at m/z 194 obtained from the Figure 3.4B. (B) CID MS/MS product ion spectrum of the m/z 194 precursor ion obtained from a solution of commercially available HPO. (C) CID MS/MS product ion spectrum of the m/z 194 precursor ion obtained from a solution of commercially available 6-formyl-7,8-dihydropterin (FDHP). (D) CID MS<sup>3</sup> product ion spectrum of the ion at m/z 176 in panel A. (E) CID MS<sup>3</sup> product ion spectrum of the ion at m/z 176 in panel B. (F) CID MS<sup>3</sup> product ion spectrum of the ion at m/z 165 in panel A. (G) CID MS<sup>3</sup> product ion spectrum of the ion at m/z 165 in panel C.

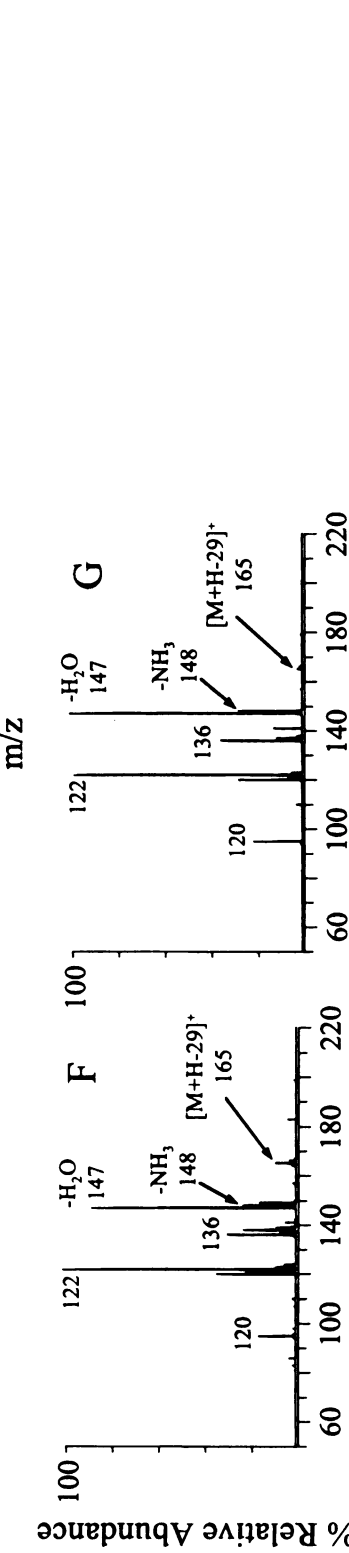
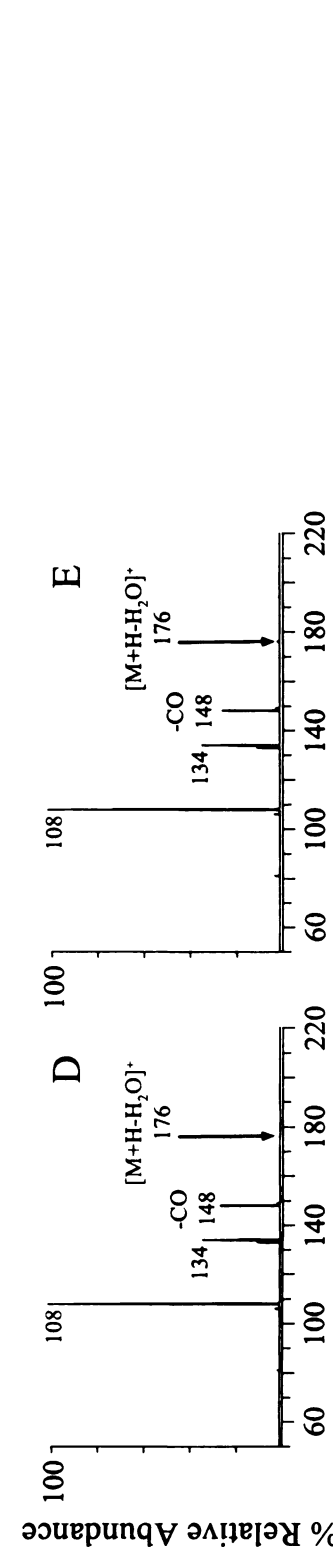
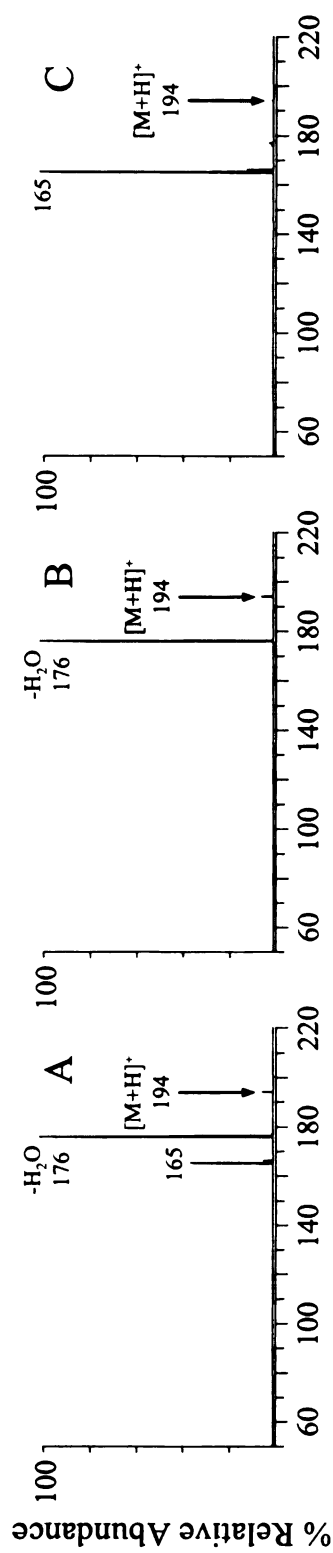
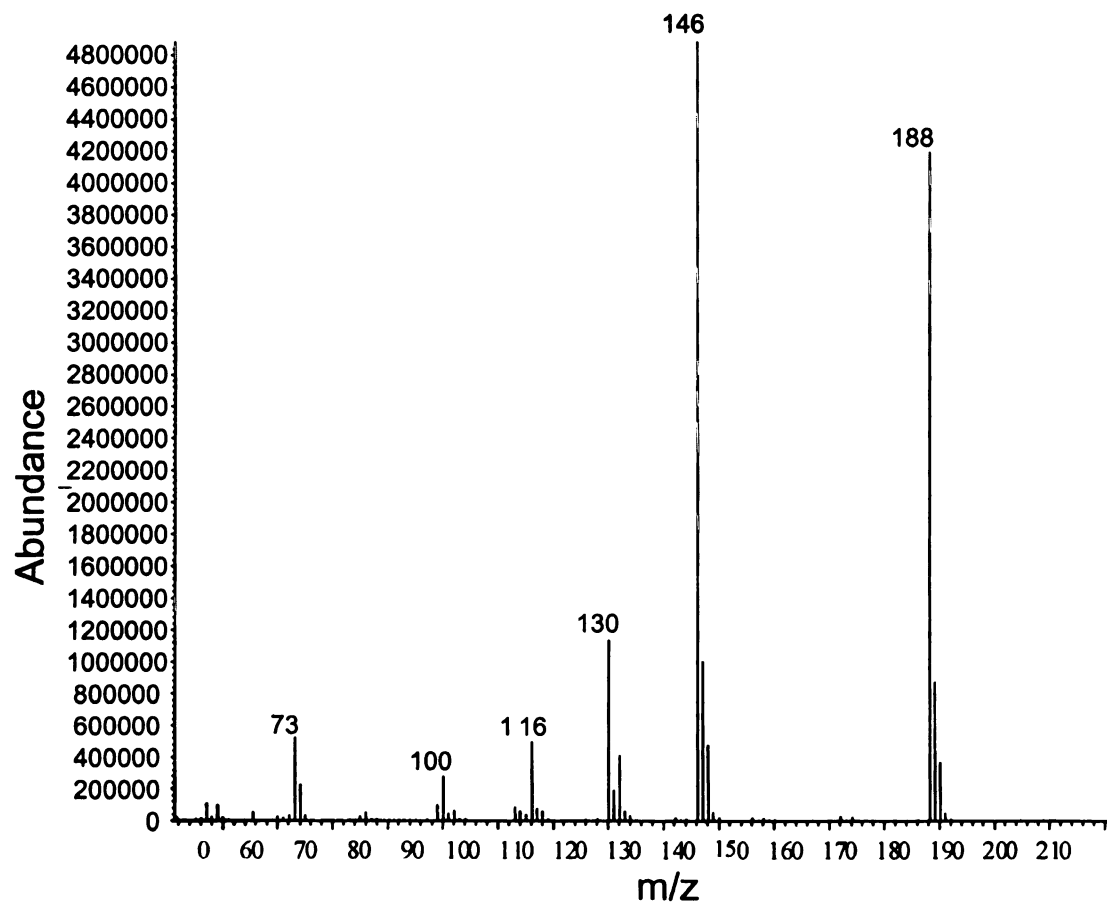
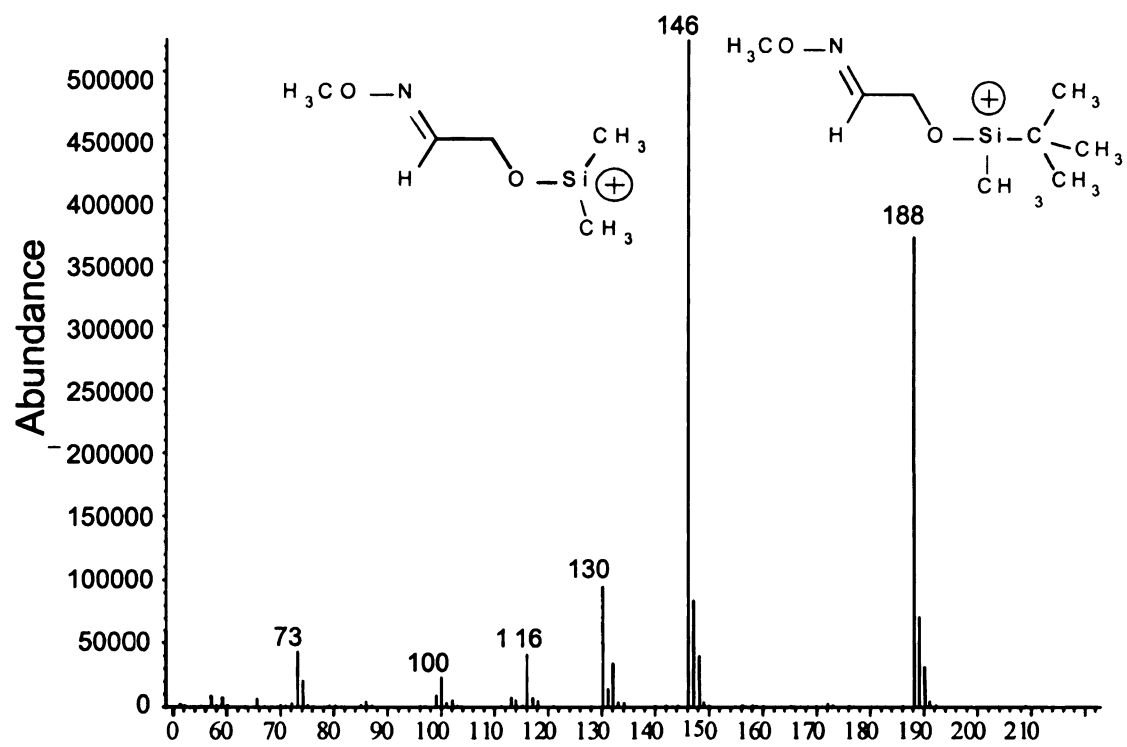


**Figure 3.7: Electron ionization mass spectra of the tert-butyltrimethylsilyl/methoxime derivatives of GA standard (A) and the DHNP reaction mixture generated by SaY54F (B). The chromatographic retention times of the derivatives were 12.3 min.**



derivative (the peak at 12.3 min) from the SaY54F-catalyzed reaction (Figure 3.9B), which was identical to that of the SaDHNA-catalyzed reaction (data not shown), also showed two dominant ions at  $m/z$  146 and 188. This result and that of the NMR analysis clearly indicated that the SaY54F-catalyzed reaction generates GA as the SaDHNA-catalyzed reaction.

*HPLC Identification of Formic Acid.* Because DHXP contains one carbon less than HP, the SaY54F-catalyzed reaction must generate a one-carbon species, most likely formic acid. In order to identify the one-carbon species, we analyzed the DHNP reaction mixtures generated by SaDHNA and SaY54F by HPLC using an Aminex HPX-87H column. The unknown compounds in the reaction mixtures were identified by comparing their retention times with those of the standard compounds as shown in Figure 3.10. This HPLC run of standard compounds (blue line) included succinic acid at 13.5 min, formic acid at 14.9 min, and acetic acid at 16 min. It also showed a peak at 17.5 min, probably due to the HEPES buffer, which also appeared in all chromatograms, including those of the SaY54F solution (green line), the reaction mixture generated by SaY54F (red line), the reaction mixture generated by SaDHNA (cyan line), and the buffer alone (data not shown). The chromatogram of the reaction mixture generated by SaY54F showed an intense peak at 14.9 min, which was the same as the retention time for standard formic acid. The small shoulder at the left side was probably due to the protein. The intense peak in the chromatogram of the reaction mixture generated by SaY54F was absent in the chromatogram of the reaction mixture generated by SaDHNA. The result indicated that the mutant-catalyzed reaction generates formic acid but the wild-type enzyme-catalyzed reaction does not.

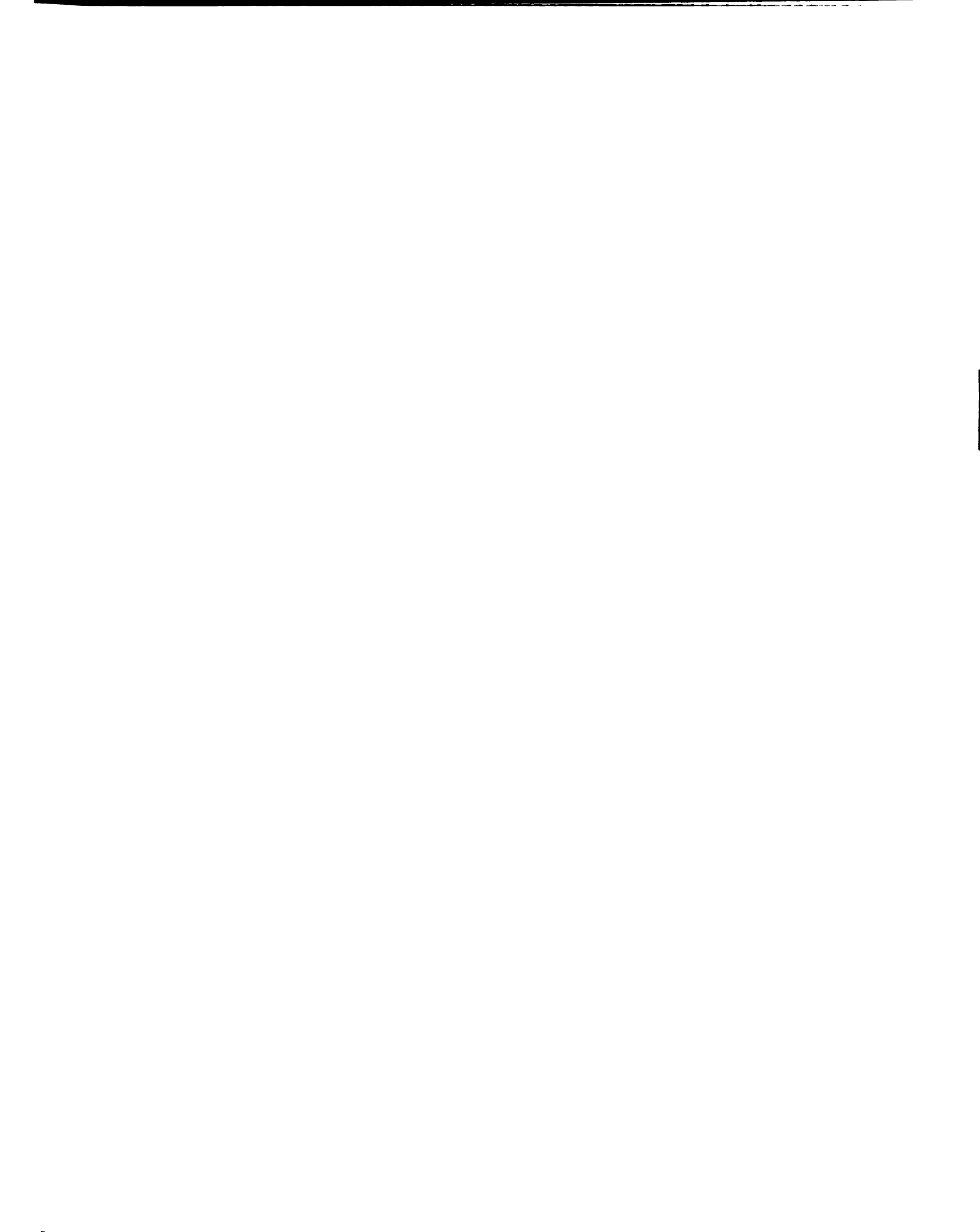
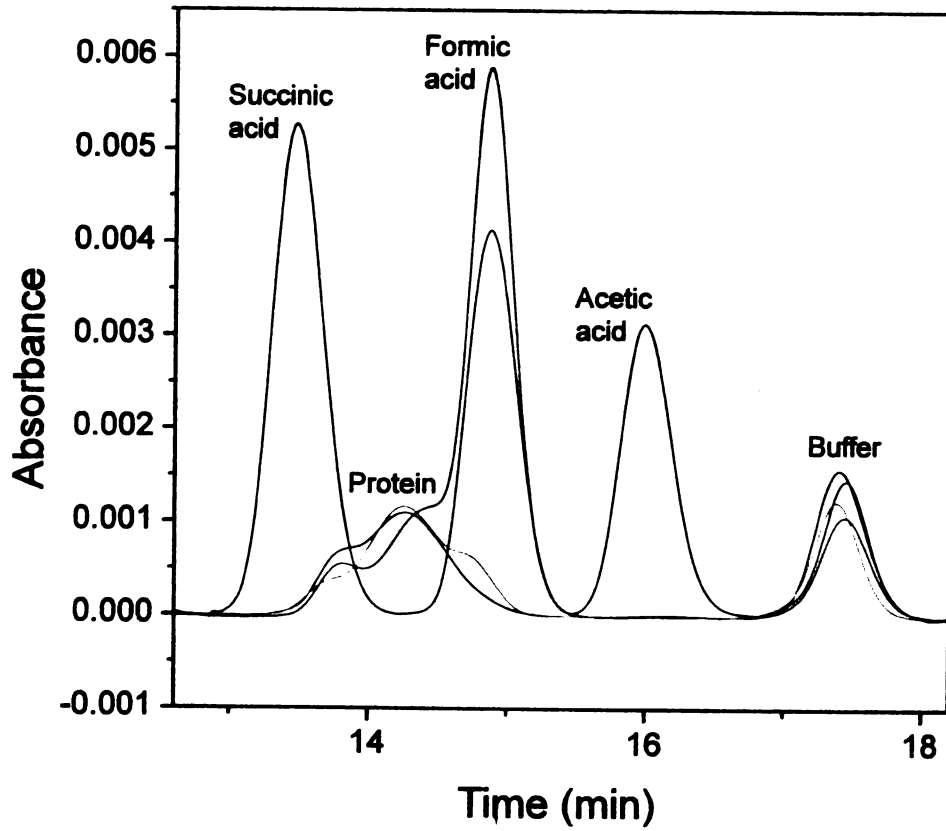


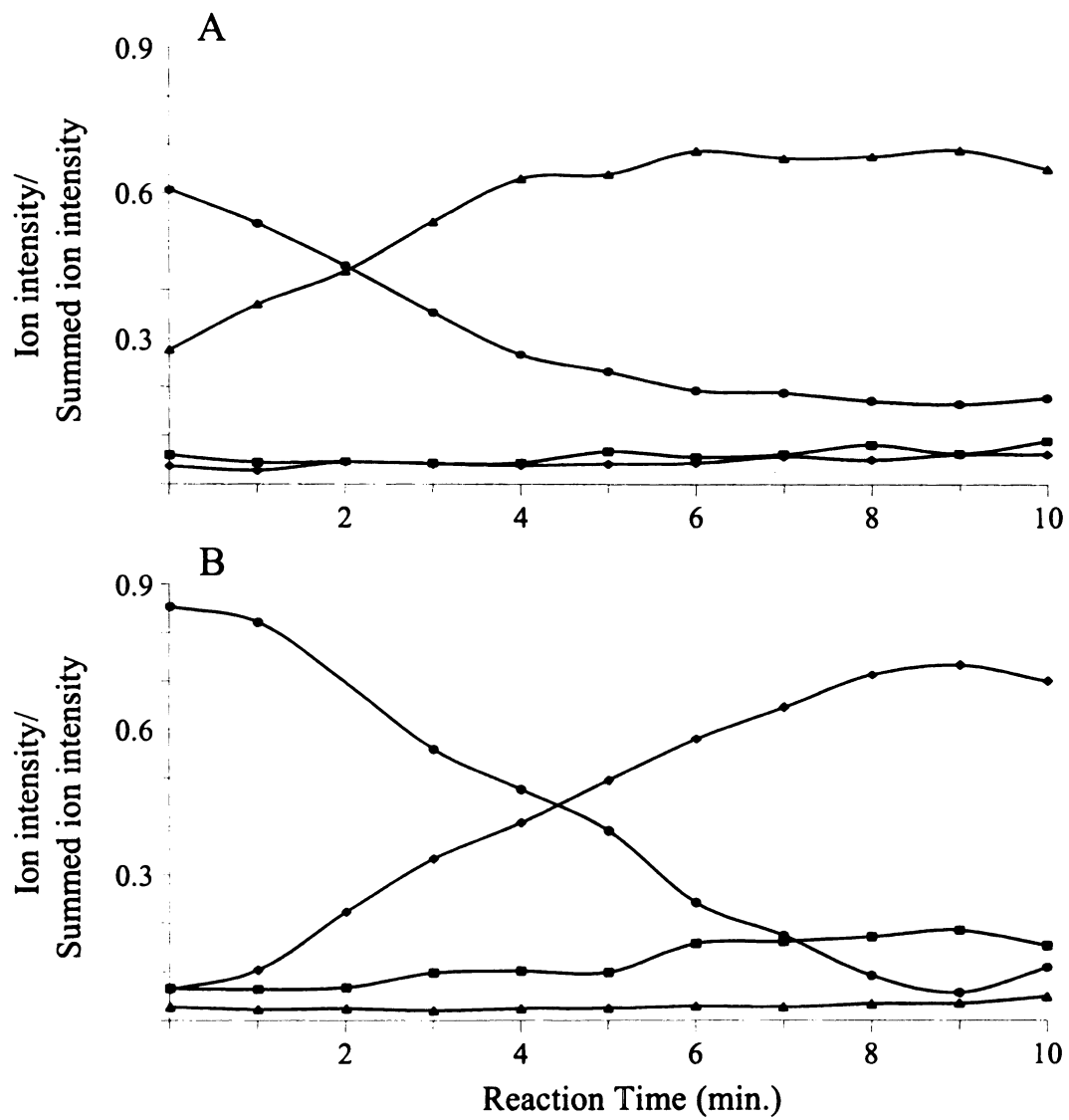
**Figure 3.10: Identification of formic acid by HPLC.** The red, cyan, green, and blue lines are the chromatogram of the SaY54F-catalyzed DHNP reaction mixture, the SaDHNA-catalyzed DHNP reaction mixture, the SaY54F solution, and a standard organic acid solution, respectively. The standard organic acid solution contained formic acid, acetic acid, and succinic acid.



*Is DHXP Derived from HP?* Since the C1'-C2' bond is cleaved first in the generation of DXHP, which is the same for the normal aldolase reaction for the formation of HP, it is logical to ask whether DHXP is derived from HP. To address this question, we analyzed the time course of the DHNP reaction by MS. The results are shown in Figure 3.11. The ions at  $m/z$  256, 196, and 182 were due to DHNP, HP, and DHXP, respectively, as described earlier. The  $m/z$  194 ions were to a large part from HPO and to a small part from FDHP. The results showed again that the major product of the wild-type enzyme-catalyzed reaction was HP as expected, but the major product of the mutant-catalyzed reaction was DHXP. Furthermore, there was no accumulation of HP in the mutant-catalyzed reaction, suggesting that DHXP was not derived from HP, unless the conversion of HP to DHXP was much faster than the formation of HP. In order to confirm that DHXP was not formed from the rapid conversion of HP, HP was incubated with SaY54F and analyzed by MS. If DHXP was derived from the rapid conversion of HP, then over time, these spectra should show a decrease in the intensity of  $m/z$  196 and an increase in the intensity of  $m/z$  182. There was not, however, any production of the ion at  $m/z$  182 seen in these spectra (not shown), indicating that DXHP was not derived from HP.

*The Source of Oxygen.* Finally we considered the source of the new oxygen at the C-6 position of DHXP. Was it from water or from the oxygen molecules dissolved in the buffer? To address this issue, we ran the DHNP reaction in buffer prepared with  $^{18}\text{O}$ -water and analyzed the reaction mixture with MS. With  $^{18}\text{O}$ -water, if the oxygen was from the solvent, the mass spectrum should show a shift in the  $m/z$  of the protonated

**Figure 3.11: ESI-MS time course analysis of the DHNP reactions catalyzed by SaDHNA (A) and SaY54F (B). (● = m/z 256, ■ = m/z 194, ▲ = m/z 196, ◆ = m/z 182)**

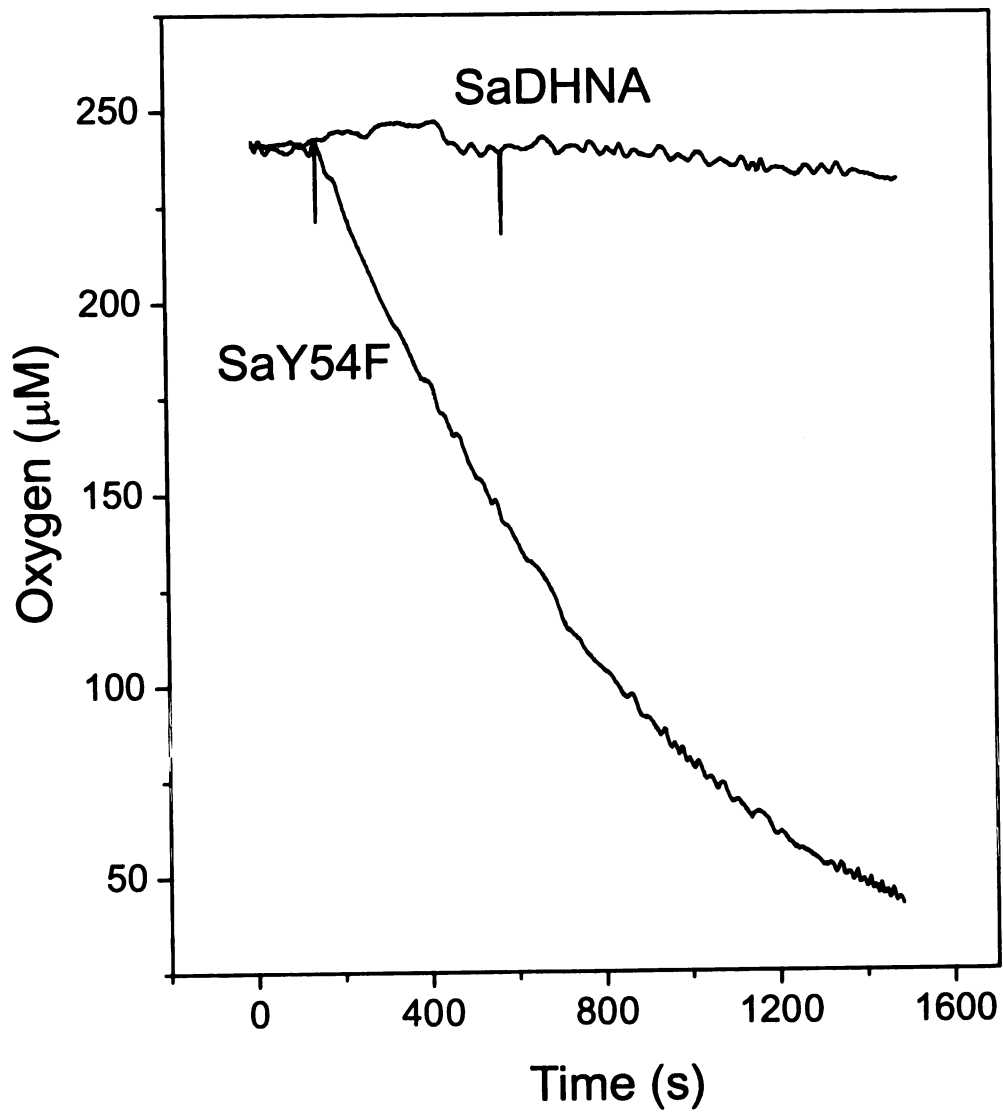


product ion from 182 to 184. The MS spectra of the reaction mixtures obtained with  $^{18}\text{O}$ -water as the solvent, however, were the same as the spectra obtained when the reaction was run in unlabelled solvent (data not shown), indicating that there was no  $^{18}\text{O}$  incorporation in any of the products and the oxygen incorporated in the product DHXP does not come from water. Then we measured the oxygen consumption of the reactions catalyzed by SaY54F and SaDHNA. The results are shown in Figure 3.12. The amounts of wild-type and mutant enzymes were both  $8\ \mu\text{M}$ . Under the conditions, nearly all DHNP was converted to products. The results showed that only the mutant-catalyzed reaction consumes a significant amount of oxygen, indicating that SaY54F is an oxygenase and the source of oxygen for the oxygenation reaction is molecular oxygen dissolved in the buffer. We calculated the turnover number for the oxygenation reaction from the linear portion of the oxygen consumption curve, which was  $0.027\ \text{s}^{-1}$ . We also calculated the turnover number for the formation of DHXP from the NMR time course of the SaY54F-catalyzed reaction, which was  $0.018\ \text{s}^{-1}$ . The two turnover numbers were in close agreement, indicating that one oxygen molecule is used in the formation of one molecule of DHXP. The extra oxygen consumption was probably due to the formation of FDHP and HPO.

## DISCUSSION

*SaY54 and EcY53F Are Oxygenases.* By a variety of means we have shown that the major product of the mutant (either SaY54F or EcY53F)-catalyzed reaction is DHXP, rather than HP of the wild-type enzyme-catalyzed reaction. The turnover number for the

**Figure 3.12: Oxygen consumption by the reactions catalyzed by SaDHNA and SaY54F.** The initial samples contained 200  $\mu\text{M}$  DHNP in 100 mM HEPES-KOH, pH 8.2, and the reactions were initiated by 8  $\mu\text{M}$  SaDHNA or SaY54F as marked by the vertical lines.



formation of DHXP is >50-fold that for the formation of the normal product HP for SaY54F. The initial clue to the surprising properties of the mutant enzymes was a dramatic drop of the fluorescence intensities of the reaction mixtures. The NMR analysis of the reaction mixtures revealed that the mutant enzymes generate a new compound with a  $^1\text{H}$  NMR signal at 4.12 ppm and little of the normal product HP (Figure 3.3). The new compound was also a major product in the MS analysis of the reaction mixtures generated by the mutant SaY54F (Figure 3.4) and was identified to be DHXP by comparing its MS/MS and MS<sup>3</sup> spectra with those of a DHXP standard (Figure 3.6). This raises the immediate question of how DHXP is generated. Is DHXP generated via the cleavage of the C6-C1' bond or the C1'-C2' bond as in the aldolase reaction? The fact that either mutant-catalyzed reaction generates GA and furthermore that about equal moles of GA and DHXP are generated (Figure 3.3) strongly indicates that DHXP is generated via the cleavage of the C1'-C2' bond. The formation of GA was confirmed by the derivatization of the reaction mixtures followed by GC-MS analysis (Figure 3.9). Since the first step in the generation of DHXP is the cleavage of the C1'-C2' bond as in the wild-type enzyme-catalyzed reaction, the next question is whether DHXP is derived from HP. The MS analysis of the time course of the mutant-catalyzed reaction shows that there is no accumulation of HP in the reaction (Figure 3.12). This indicates that DHXP is not derived from HP, unless the conversion of HP to DHXP is very rapid relative to the generation of HP. This was addressed by mixing HP standard with the mutant and following the possible reaction by MS. The result indicates that HP cannot be converted to DHXP under the experimental conditions. Since the cleavage of the C1'-C2' bond generates an intermediate with one carbon more than DHXP, the conversion of the

intermediate to DHXP must generate a one-carbon species, which was identified as formic acid by comparing the HPLC chromatogram of the reaction mixtures generated by the mutant and wild-type enzymes with those of standard organic acids and aldehydes (Figure 3.10). The remaining question is where the oxygen at the C-6 position of DHXP comes from. Is it from water or from oxygen molecules dissolved in the buffer? This issue was addressed by the O<sup>18</sup>-water experiment and the oxygen consumption assay. The O<sup>18</sup>-water experiment eliminates water as the source for the oxygen newly attached to the pterin ring. The oxygen consumption assay indicates that molecular oxygen is the source for the oxygenation reaction, because significant oxygen consumption only occurs in the mutant catalyzed reaction (Figure 3.11) and the turnover number calculated from the oxygen consumption data is comparable to that for the formation of DHXP calculated from the NMR data.

The above analysis leads us to propose a chemical mechanism for the mutant-catalyzed reaction as depicted in Figure 3.13. The initial step in the formation of DHXP is the generation of the same enol intermediate as in the wild-type enzyme-catalyzed reaction, which involves the cleavage of the C1'-C2' bond and yields approximately equal moles of GA and DHXP, as described earlier. Deprotonation of N5 of the enol intermediate generates a carbanion species, which donates a single electron to molecular oxygen to form a caged radical pair. The caged radicals react to generate the peroxide ion, which leads to the formation of DHXP and formic acid. The participation of molecular oxygen in the mutant-catalyzed reaction has been confirmed by the oxygen consumption assay. The reaction path for the formation of DHXP from the enol intermediate is speculative, but the formation of formic acid has been confirmed by

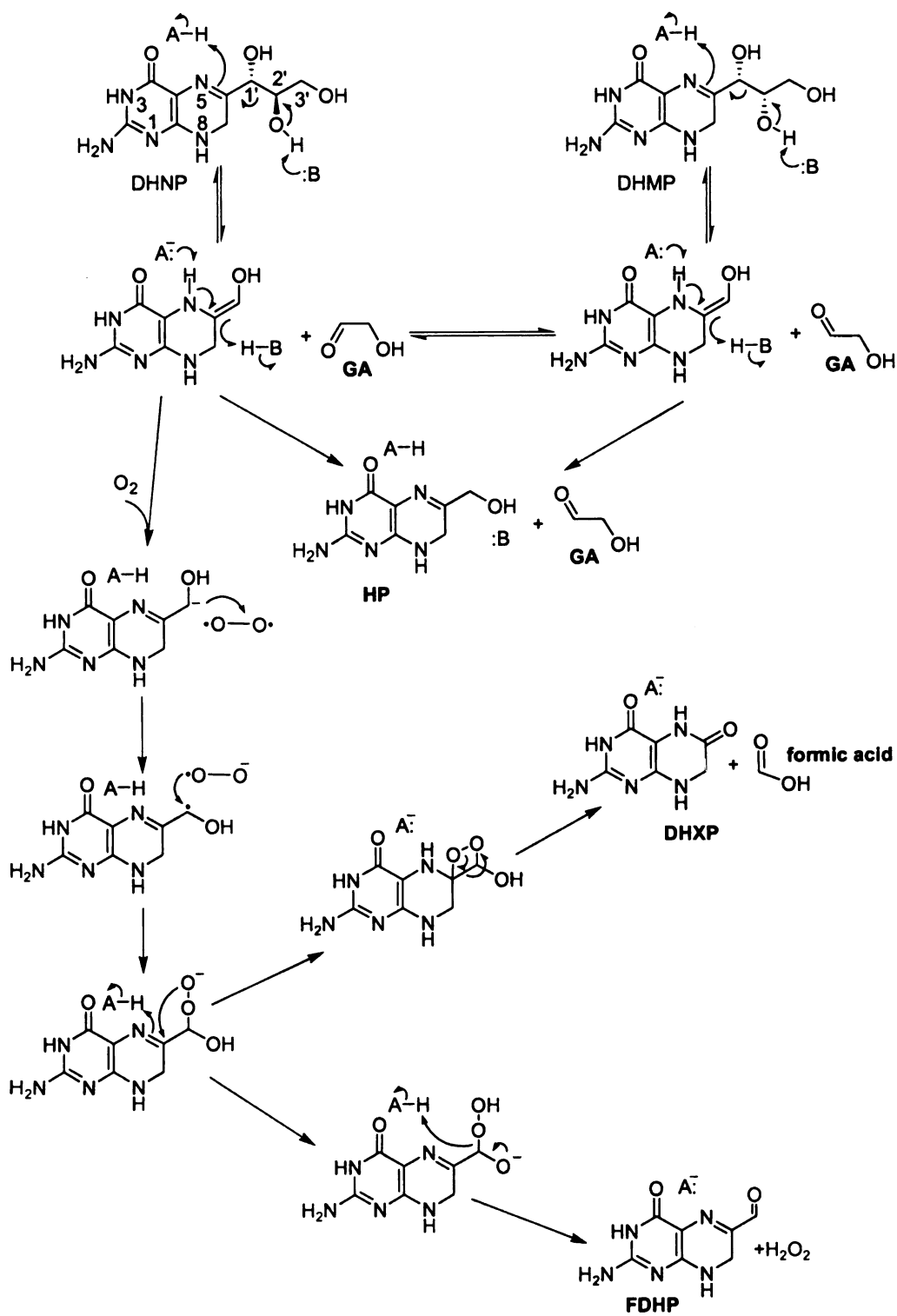
HPLC. The proposed mechanism also accounts for the formation of the minor product FDHP. Alternative mechanisms involve protein radicals (in contrast to just substrate radicals). Both mechanisms have been proposed for cofactor-independent oxygenases (10), but the proposed mechanism or variations thereof that involve mainly general acid and base catalysis are more likely, particularly considering that DHNA is evolved for general acid and base catalysis.

The key step in the formation of DHXP from the enol intermediate is the generation of the carbanion species, which involves the deprotonation of N5 as in the wild-type enzyme-catalyzed reaction and the block of the protonation of the hydroxymethylene group by the mutation of the active site tyrosine residue. Carbanions are prone to react with oxygen, and several enzymatic reactions involving carbanion intermediates indeed have oxygen-consuming side reactions (11, 12). The formation of the peroxide ion is reminiscent of the initial steps of the reactions catalyzed by 1H-3-hydroxy-4-oxoquinoline 2,4-dioxygenase (13) and urate oxidase (14, 15), both of which do not have any cofactor. These enzymes seem to evolve to utilize carbanion reactivity toward dioxygen for the oxygenation reactions (10), which might be a general catalytic strategy for the family of cofactor-independent oxygenases. Interestingly, both DHNA (4, 7, 16, 17) and urate oxidase (18, 19) have a tunnel-like structure called “T-fold” with active sites located between subunits (20). The bound ligands are stacked with a conserved phenylalanine residue in urate oxidase and the conserved tyrosine in DHNA that was substituted with a phenylalanine residue in this study.

*The Role of the Conserved Tyrosine Residue.* The biochemical analysis of the two mutants SaY54F and EcY53F indicates that the hydroxyl group of the phenol ring of the

conserved tyrosine residue plays only a minor role in the physical steps of the enzymatic reaction. In contrast, the hydroxyl group plays a critical role in catalysis. The hallmark of the DHNA-catalyzed reaction is general acid and base catalysis. The general acid and base involved in the protonation and deprotonation of N5 are most likely a water molecule and its conjugated base based on the published crystal structures (7) and our own unpublished crystal structures. The deprotonation of 2'-hydroxyl group is most likely the function of the conserved lysine residue, K100 in SaDHNA and K98 in EcDHNA. The conserved tyrosine residue may play a minor role if any in this step, because the formation of the enol intermediate is not impaired by the mutations to any great extent as evidenced by the high  $k_{\text{cat}}$  for the formation of DHXP by the mutant SaY54F, which is 1/10 of the  $k_{\text{cat}}$  value for the formation of HP by the wild-type enzyme. On the other hand, the major product of the mutant-catalyzed reaction is DHXP, not HP, suggesting that the protonation of the enol intermediate to generate HP is greatly impaired and the conserved tyrosine residue may play a critical role in this step. The high oxygenase activities of the mutants are likely due to the tendency of the enol intermediate to react with molecular oxygen and the available general acid and base for the generation of the enol intermediate and its subsequent oxygenation as illustrated in Figure 3.13. The conserved tyrosine residue is located at the bottom of the active site. The active site is likely to be accessible to molecular oxygen even in the wild-type enzyme. The wild-type enzyme is an efficient aldolase rather than an oxygenase, because it has a general acid that can efficiently protonate the enol intermediate to form HP.

**Figure 3.13: The proposed chemical mechanism for the generation of DHXP and FDHP by SaY54F and EcY53F. For simplicity, many steps are indicated by single arrows irrespective of their reversibility.**



## REFERENCES

- (1) Walsh, C. (2003) Where will new antibiotics come from? *Nature Rev. Microbiol.* *1*, 65-70.
- (2) Bermingham, A., and Derrick, J. P. (2002) The folic acid biosynthesis pathway in bacteria: Evaluation of potential for antibacterial drug discovery. *Bioessays* *24*, 637-648.
- (3) Kompis, I. M., Islam, K., and Then, R. L. (2005) DNA and RNA synthesis: Antifolates. *Chem. Rev.* *105*, 593-620.
- (4) Sanders, W. J., Nienaber, V. L., Lerner, C. G., McCall, J. O., Merrick, S. M., Swanson, S. J., Harlan, J. E., Stoll, V. S., Stamper, G. F., Betz, S. F., Condroski, K. R., Meadows, R. P., Severin, J. M., Walter, K. A., Magdalinos, P., Jakob, C. G., Wagner, R., and Beutel, B. A. (2004) Discovery of potent inhibitors of dihydroneopterin aldolase using crystallead high-throughput X-ray crystallographic screening and structure-directed lead optimization. *J. Med. Chem.* *47*, 1709-1718.
- (5) Mathis, J. B., and Brown, G. M. (1970) The biosynthesis of folic acid XI. Purification and properties of dihydroneopterin aldolase. *J. Biol. Chem.* *245*, 3015-3025.
- (6) Haußmann, C., Rohdich, F., Schmidt, E., Bacher, A., and Richter, F. (1998) Biosynthesis of pteridines in *Escherichia coli* - structural and mechanistic similarity of dihydroneopterin-triphosphate epimerase and dihydroneopterin aldolase. *J. Biol. Chem.* *273*, 17418-17424.
- (7) Hennig, M., D'Arcy, A., Hampele, I. C., Page, M. G. P., Oefner, C., and Dale, G. E. (1998) Crystal structure and reaction mechanism of 7,8- dihydroneopterin aldolase from *Staphylococcus aureus*. *Nature Struct. Biol.* *5*, 357-362.
- (8) Scherperel, G., Yan, H. G., Wang, Y., and Reid, G. E. (2006) 'top-down' characterization of site-directed mutagenesis products of *Staphylococcus aureus* dihydroneopterin aldolase by multistage tandem mass spectrometry in a linear quadrupole ion trap. *Analyst* *131*, 291-302.
- (9) Li, Y., Gong, Y., Shi, G., Blaszczyk, J., Ji, X., and Yan, H. (2002) Chemical transformation is not rate-limiting in the reaction catalyzed by *Escherichia coli* 6-hydroxymethyl-7,8-dihydropterin pyrophosphokinase. *Biochemistry* *41*, 8777-8783.
- (10) Fetzner, S. (2002) Oxygenases without requirement for cofactors or metal ions. *Appl. Microbiol. Biotechnol.* *60*, 243-257.

- (11) Abell, L. M., and Schloss, J. V. (1991) Oxygenase side reactions of acetolactate synthase and other carbanion-forming enzymes. *Biochemistry* 30, 7883-7887.
- (12) Hixon, M., Sinerius, G., Schneider, A., Walter, C., Fessner, W. D., and Schloss, J. V. (1996) Quo vadis photorespiration: A tale of two aldolases. *FEBS Lett.* 392, 281-284.
- (13) Frerichs-Deeken, U., Rangelova, K., Kappl, R., Huttermann, J., and Fetzner, S. (2004) Dioxygenases without requirement for cofactors and their chemical model reaction: Compulsory order ternary complex mechanism of 1*H*-3-hydroxy-4-oxoquinoline 2,4-dioxygenase involving general base catalysis by histidine 251 and single-electron oxidation of the substrate dianion. *Biochemistry* 43, 14485-14499.
- (14) Sarma, A. D., and Tipton, P. A. (2000) Evidence for urate hydroperoxide as an intermediate in the urate oxidase reaction. *J. Am. Chem. Soc.* 122, 11252-11253.
- (15) Imhoff, R. D., Power, N. P., Borrok, M. J., and Tipton, P. A. (2003) General base catalysis in the urate oxidase reaction: Evidence for a novel Thr-Lys catalytic diad. *Biochemistry* 42, 4094-4100.
- (16) Bauer, S., Schott, A. K., Illarionova, V., Bacher, A., Huber, R., and Fischer, M. (2004) Biosynthesis of tetrahydrofolate in plants: Crystal structure of 7,8-dihydroneopterin aldolase from *Arabidopsis thaliana* reveals a novel adolase class. *J. Mol. Biol.* 339, 967-979.
- (17) Goulding, C. W., Apostol, M. I., Sawaya, M. R., Phillips, M., Parseghian, A., and Eisenberg, D. (2005) Regulation by oligomerization in a mycobacterial folate biosynthetic enzyme. *J. Mol. Biol.* 349, 61-72.
- (18) Colloc'h, N., ElHajji, M., Bachet, B., Lhermite, G., Schiltz, M., Prange, T., Castro, B., and Mornon, J. P. (1997) Crystal structure of the protein drug urate oxidase-inhibitor complex at 2.05 angstrom resolution. *Nat. Struct. Biol.* 4, 947-952.
- (19) Retailleau, P., Colloc'h, N., Vivares, D., Bonnete, F., Castro, B., El Hajji, M., Mornon, J. P., Monard, G., and Prange, T. (2004) Complexed and ligand-free high-resolution structures of urate oxidase (Uox) from *aspergillus flavus*: A reassignment of the active-site binding. *Acta Crystallogr. D. Biol. Crystallogr.* 60, 453-462.
- (20) Colloc'h, N., Poupon, A., and Mornon, J. P. (2000) Sequence and structural features of the T-fold, an original tunnelling building unit. *Proteins* 39, 142-154.

## CHAPTER 4: THE FUNCTIONAL ROLES OF THE CONSERVED ACTIVE SITE GLUTAMATE AND LYSINE RESIDUES

### ABSTRACT

Dihydroneopterin aldolase (DHNA) catalyzes the conversion of 7,8-dihydroneopterin (DHNP) to 6-hydroxymethyl-7,8-dihydropterin (HP) in the folate biosynthetic pathway. There are four conserved active site residues at the active site, E22, Y54, E74, and K100 in *Staphylococcus aureus* DHNA (SaDHNA), corresponding to E21, Y53, E73, and K98 in *Escherichia coli* DHNA (EcDHNA). Previously we have shown that the conserved tyrosine residue plays a critical role in the protonation of the enol reaction intermediate to form HP. The functional roles of the conserved glutamate and lysine residues have been investigated by site-directed mutagenesis in this work. E22 and E74 of SaDHNA and E21, E73, and K98 of EcDHNA were replaced by alanine. K100 of SaDHNA was replaced by alanine and glutamine. The mutant proteins were characterized by equilibrium binding, stopped-flow binding, and steady-state kinetic analyses. The results showed that E74 of SaDHNA and E73 of EcDHNA are important for substrate binding, but their roles in catalysis are minor. In contrast, E22 and K100 of SaDHNA are important for catalysis, but their roles in substrate binding are minor. On the other hand, E21 and K98 of EcDHNA are important for both substrate binding and catalysis.

## INTRODUCTION

Dihydroneopterin aldolase (DHNA) catalyzes the conversion of the 7,8-dihydroneopterin (DHNP) to 6-hydroxymethyl-7,8-dihydropterin (HP) in the folate biosynthetic pathway, one of principal targets for developing antimicrobial agents (1). Folate cofactors are essential for life (2). Most microorganisms must synthesize folates *de novo*. In contrast, mammals cannot synthesize folates because of the lack of three enzymes in the middle of the folate pathway and obtain folates from the diet. DHNA is the first of the three enzymes that are absent in mammals and therefore an attractive target for developing antimicrobial agents (3).

DHNA is a unique aldolase in two respects. First, DHNA requires neither the formation of a Schiff base between the substrate and enzyme nor metal ions for catalysis (4). Aldolases can be divided into two classes based on their catalytic mechanisms (5, 6). Class I aldolases require the formation of a Schiff base between an amino group of the enzyme and the carbonyl of the substrate, whereas class II aldolases require a  $Zn^{2+}$  ion at their active sites for catalysis. The proposed catalytic mechanism for DHNA is similar to that of class I aldolases, but the Schiff base is embedded in the substrate. Secondly, in addition to the aldolase reaction, DHNA also catalyzes the epimerization at the 2'-carbon of DHNP to generate 7,8-dihydromonapterin (DHMP) (Figure 1.3) (7), but the biological function of the epimerase reaction is not known at present.

Interestingly, DHNAs from Gram-positive and Gram-negative bacteria have some unique sequence motifs. Figure 1.2 shows the amino acid sequence alignment of DHNAs from 11 bacteria. The first five enzymes are from Gram-positive bacteria, and the rest are

from Gram-negative bacteria. The identities between enzymes from Gram-positive bacteria range from 39% to 45% and those between Gram-negative bacteria are 49-91%, but the identities between Gram-positive and Gram-negative bacterial enzymes are <30%. Many differences between these enzymes from Gram-positive and Gram-negative bacteria are at or near their active centers (8). We have recently shown that DHNAs from *Staphylococcus aureus* (SaDHNA) and *Escherichia coli* (EcDHNA) indeed have significant differences in their binding and catalytic properties (Wang et al., unpublished), suggesting that it is possible to develop antimicrobial agents targeting a specific class of bacteria.

DHNA consists of eight identical subunits. The atomic structures of SaDHNA (3, 8), *Mycobacterium tuberculosis* DHNA (MtDHNA) (9), and *Arabidopsis thaliana* DHNA (AtDHNA) (10) have been determined by X-ray crystallography. The octameric structures look like two stacked donuts with a large hole in the middle, ~13 Å in SaDHNA. Each donut consists of four subunits. There are eight active sites, all formed by residues from two adjacent subunits. At the active sites, there are four conserved residues that interact with the bound product HP as revealed by the crystal structures (8, 9) (Figure 1.7). These four residues are E22, Y54, E74, and K100 in SaDHNA, corresponding to E21, Y53, E73, and K98 in EcDHNA, respectively (Figure 1.2). Previously we showed that the conserved tyrosine residue plays a critical role in DHNA catalysis. Substitution of the conserved tyrosine residue in SaDHNA or EcDHNA with phenylalanine turned the target enzyme into an oxygenase. In this paper, we describe a site-directed mutagenesis study of the functional roles of the other conserved, active-site residues in SaDHNA and EcDHNA. The results provide important insight into the

catalytic mechanisms of the enzymes and valuable information for designing inhibitors targeting these enzymes.

## EXPERIMENTAL PROCEDURES

*Materials.* 6-Hydroxymethylpterin (HPO), 6-Hydroxymethyl-7,8-dihydropterin (HP), 7,8-dihydro-D-neopterin (DHNP), 7,8-dihydro-L-monapterin (DHMP), D-neopterin (NP), and L-monapterin (MP) were purchased from Schircks Laboratories. *Pfu* DNA polymerase was purchased from Stratagene. Other chemicals were from Sigma or Aldrich.

*Site-Directed Mutagenesis and Protein Purification.* The site-directed mutants were made by a PCR-based method using high-fidelity *pfu* DNA polymerase according to a protocol developed by Stratagene. The forward and reverse primers for the PCR-based mutagenesis experiments are listed in Table 4.1. The mutants were selected by DNA sequencing. In order to ensure that there were no unintended mutations in the mutants, the entire coding sequences of the mutated genes were determined.

The mutant proteins were purified as described previously (Wang et al., unpublished). Briefly, SaE22A, SaE74A, SaK100A, and SaK100Q were purified to homogeneity by a Ni-NTA column followed by a Bio-Gel A-0.5m gel column. EcE21A, EcE73A, and EcK98A were purified by a DEAE-cellulose column followed by a Bio-Gel A-0.5m gel column. The purities of the protein preparations were checked by SDS-PAGE. The purified proteins were concentrated, dialyzed, lyophilized, and stored at -80 °C.

**Table 4.1: The Forward and Reverse Primers for the PCR-Based Mutagenesis**

**Experiments**

<sup>a</sup>SaE22A, SaE74A, and SaK100A are mutants of SaDHNA in which E22, E74, and K100 are replaced by alanine respectively. SaK100Q is a SaDHNA mutant with K100 replaced by glutamine. EcE21A, EcE73A, and EcK98A are mutants of EcDHNA in which E21, E73, and K98 are replaced by alanine respectively.

<sup>b</sup>The forward primers are listed first with the mutations underlined. The mutations in the reverse primers are not indicated.

Mutant <sup>a</sup>	Primer <sup>b</sup>
SaE22A	5'-GGTGCTTTATCAGCTG <u>C</u> AAATGAAATAGGGCAAATTTTC-3' 5'-GAAAATTTGCCCTATTTCAATTTGCAGCTGATAAAGCACC-3
SaE74A	5'-GCCGTTAATTTACTTG <u>C</u> GCATCTAGCTGAACGTATTGC-3' 5'-GCAATACGTTTCAGCTAGATGCGCAAGTAAATTAACGGC-3'
SaK100A	5'- GAAACGAAAGTGAGAATCACTG <u>C</u> AGAAAACCCACCGATTCCG-3' 5'-CGGAATCGGTGGGTTTTCTGCAGTGATTCTCACTTTCGTTTC- 3'
SaK100Q	5'-CGAAAGTGAGAATCACT <u>C</u> AAGAAAACCCACCGATTCC-3' 5'-GGAATCGGTGGGTTTTCTTGAGTGATTCTCACTTTC G -3'
EcE21A	5'-GTGTTTACGACTGGG <u>C</u> ACAGACCATCGAACAG-3' 5'-CTGTTCGATGGTCTGTGCCAGTCGTAAACAC-3'
EcE73A	5'-GCGCTGGTGG <u>C</u> ACGCGTGGCTG-3' 5'-CAGCCACGCGTGCCACCAGCGC-3'
EcK98A	5'-CGTATCAAACCTCAGC <u>G</u> CGCCAGGCGCAGTGG-3' 5'-CCACTGCGCCTGGCGCGCTGAGTTTGATACG-3'

*Equilibrium Binding Studies.* The procedures for the equilibrium binding studies of DHNAs were essentially the same as previously described for the similar studies of 6-hydroxymethyl-7,8-dihydropterin pyrophosphokinase using a Spex FluoroMax-2 fluorometer (11, 12). Briefly, proteins and ligands were all dissolved in 100 mM Tris-HCl, pH 8.3 and the titration experiments were performed in a single cuvette at 24 °C. The equilibrium binding experiments were performed by titrating either ligands or the proteins. In ligand titrations, fluorescence intensities were measured at an emission wavelength of 446 nm with a slit of 5 nm. The excitation wavelength and slit were 400 nm and 1 nm, respectively. A set of control data was obtained in the absence of the protein. The data set obtained in the absence of the protein was then subtracted from the corresponding data set obtained in the presence of the protein after correcting inner filter effects. The  $K_d$  value was obtained by nonlinear least square fitting of the titration data as previously described (11). All  $K_d$  values for SaDHNA mutants except that of SaE22A for HPO were obtained by titrating ligands.

In protein titration experiments, a ligand solution was titrated with a stock solution of one of the mutant proteins. Fluorescence intensities were measured at an emission wavelength of 430 nm and an excitation wavelength of 330 nm. The emission and excitation slits were both 5 nm. A control titration experiment was performed in the absence of the ligand. The control data set obtained in the absence of HP was subtracted from the corresponding data set obtained in the presence of the ligand. The  $K_d$  value was obtained by nonlinear least square fitting of the titration data as previously described (11). All  $K_d$  values for EcDHNA mutants and that of SaE22A for HPO were obtained by titrating proteins.

*Stopped-Flow Analysis.* Stopped-flow experiments were performed on an Applied Photophysics SX.18MV-R stopped-flow spectrofluorometer at 25 °C. One syringe contained one of the mutant proteins, and the other contained NP, MP, HP or HPO. The protein concentrations were 1 or 2  $\mu\text{M}$ , and the ligand concentrations ranged from 5-60  $\mu\text{M}$ . All concentrations were those after the mixing of the two syringe solutions. Fluorescence traces for NP, MP and HPO were obtained with an excitation wavelength of 360 nm and a filter with a cutoff of 395 nm for emission. Fluorescence traces for HP were obtained with an excitation wavelength of 330 nm and the same filter for emission. Apparent rate constants were obtained by nonlinear squares fitting of the data to a single exponential equation and were re-plotted against the ligand concentrations. The association and dissociation rate constants were obtained by linear regression of the apparent rate constants vs. ligand concentration data.

*Steady-State Kinetic Assay.* All components were dissolved in a buffer containing 100 mM Tris-HCl, 1 mM EDTA, and 5 mM DTT, pH 8.3. The reactions were initiated by mixing with the mutant enzymes and quenched with 1 N HCl. The quenched reaction mixtures were processed as previously described (7). Briefly, the reaction mixtures (115  $\mu\text{l}$  each) were mixed with 50  $\mu\text{l}$  1%  $\text{I}_2$  (w/v) and 2% (w/v) KI in 1 N HCl for 5 min at room temperature to oxidize the pterin compounds. Excess iodine was reduced by mixing with 25  $\mu\text{l}$  2% ascorbic acid (w/v). The samples were then centrifuged at room temperature for 5 min using a microcentrifuge. The oxidized reactant and products in the supernatants were separated by HPLC using a Vydac RP18 column. The column was equilibrated with 20 mM  $\text{NaH}_2\text{PO}_4$  made with MilliQ water and eluted at the flow rate of 0.8 ml/min with the same solution. The oxidized reactant and products were quantified by

online fluorometry with excitation and emission wavelengths of 365 and 446 nm, respectively. The enzyme and substrate concentrations were adjusted appropriately on the basis of initial estimations of the kinetic constants. When the substrate concentrations were in large excess of the enzyme, the normal Michaelis-Menten equation was used to obtain kinetic constants by nonlinear least square regression. When the enzyme concentration is comparable to the substrate concentrations because of the extremely low activity of the enzyme, a modified steady state kinetic equation (Equation 1) was used to obtain kinetic constants.

$$v = \frac{k_{cat}}{2} (E_t + S_t + K_m - \sqrt{(E_t + S_t + K_m)^2 - 4E_t S_t}) \quad (1)$$

where  $E_t$  and  $S_t$  are the total enzyme and substrate concentrations, respectively,  $k_{cat}$  and  $K_m$  have the usual meanings.

## RESULTS

*Binding Studies.* Previously we established the thermodynamic and kinetic framework for the structure-function studies of SaDHNA and EcDHNA by equilibrium measurements and stopped-flow and quench-flow analyses (Wang et al., unpublished). A similar strategy was used for the characterization of the site-directed mutants. The binding steps were mimicked with the substrate and product analogues NP, MP, and HPO. The only difference between the substrate and product analogues and the corresponding substrate and products is that between C7 and N8 is a double bond in the analogues and a single bond in the substrate and products. NP, MP, and HPO are excellent substrate and product analogues, as described previously. The  $K_d$  values were

**figure 4.1: Binding of MP to SaE22A at equilibrium.** A 2 mL solution containing 10  $\mu\text{M}$  SaE22A in 100 mM Tris-HCl, pH 8.3, was titrated with MP by adding aliquots of a 1.03 mM MP stock solution at 24 °C. The final enzyme concentration was 9.3  $\mu\text{M}$ . The top axis indicates the MP concentrations during the titration. A set of control data was obtained in the absence of the enzyme and was subtracted from the corresponding data set obtained in the presence of the enzyme. The solid line was obtained by nonlinear least-squares regression as previously described (11).

g 10

s of a

The

was

data

ar

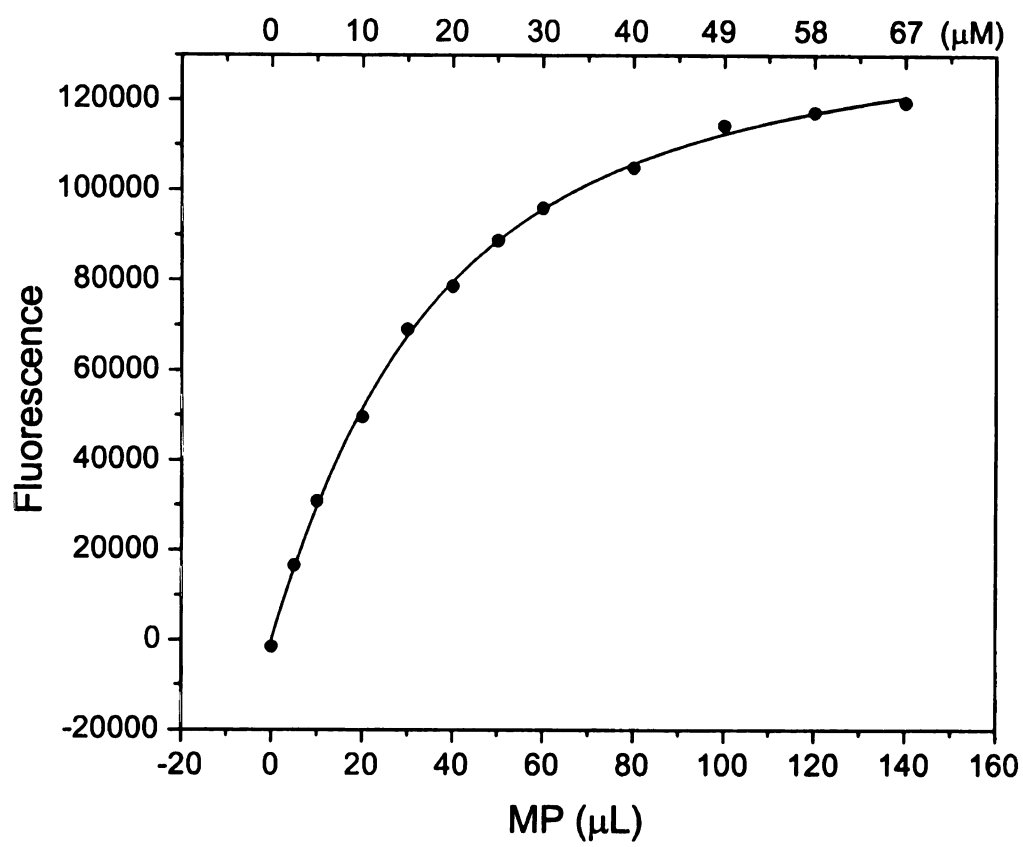
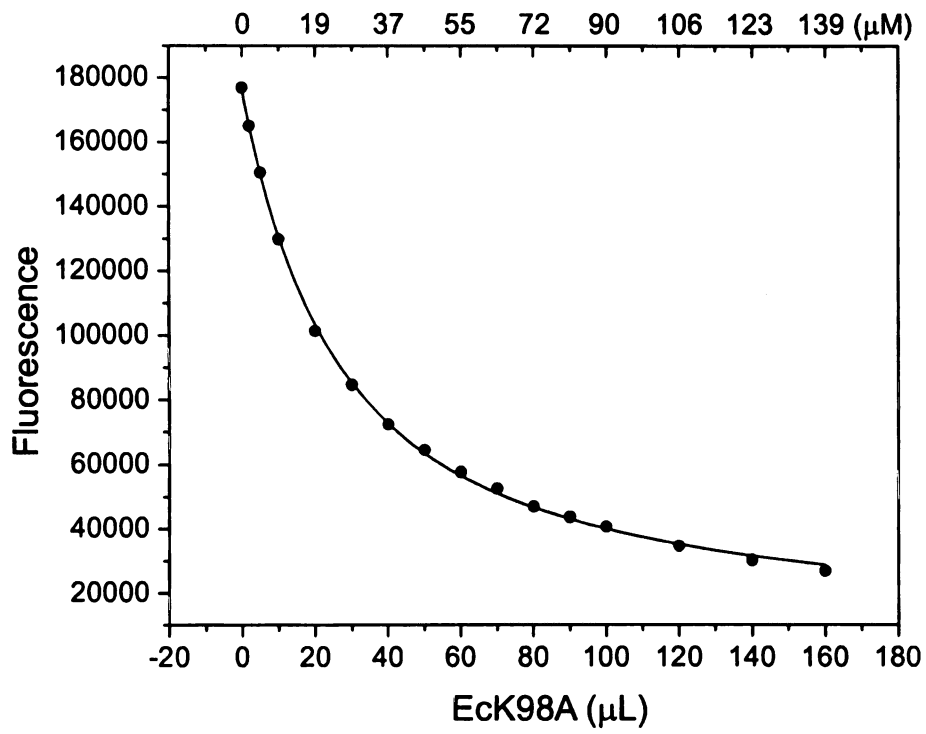


**Figure 4.2: Binding of HPO to EcK98A at equilibrium.** A 2 mL solution containing 5  $\mu\text{M}$  HPO in 100 mM Tris-HCl, pH 8.3, was titrated with EcK98A by adding aliquots of a 1.9 mM EcK98A stock solution at 24 °C. The final HPO concentration was 4.6  $\mu\text{M}$ . The top axis indicates the EcK98A concentrations during the titration. A set of control data was obtained in the absence of HPO and was subtracted from the corresponding data set obtained in the presence of HPO. The solid line was obtained by nonlinear least-squares regression as previously described (11).



measured by equilibrium binding experiments using fluorometry by either titrating the ligands or the proteins. Representative results of the equilibrium binding studies are shown in Figures 4.1 and 4.2. The association and dissociation rate constants were determined by kinetic binding experiments using stopped-flow fluorometry. A representative result of the kinetic binding studies is shown in Figures 4.3. For technical reasons, the binding constants for SaE74A and the association and dissociation rate constants for EcE73A could not be measured. The complete results of the binding studies are summarized in Tables 4.2 and 4.3 for SaDHNA and EcDHNA, respectively. In general, the thermodynamic data are in good agreement with the kinetic data, as the measured  $K_d$  values are in good agreement with those calculated from the association and dissociation rate constants. High  $K_d$  values are, for the most part, due to high dissociation rate constants. For SaDHNA, none of the mutations except E74A caused dramatic changes in the affinities of the enzyme for the substrate or product analogues or the rate constants. The  $K_d$  values for SaE74A were estimated to be  $>3000 \mu\text{M}$ , suggesting that the  $K_d$  values of the mutant is at least 100 times those of the wild-type enzyme. The results indicated that for SaDHNA, of the three conserved residues, only E74 is important for the binding of the analogues. For EcDHNA, similarly, the mutation of E73, corresponding E74 in SaDHNA, had the most dramatic effects on the ligand binding. The E73A mutation caused increases in the  $K_d$  values for the binding of NP, MP and HPO by factors of 340, 160, and 5600, respectively, relative to those of the wild-type enzyme, suggesting that E73 is critically important for the binding of these substrate or product analogues. In addition, the K98A mutation caused increases in the  $K_d$  values for the binding of NP, MP, and HPO by factors of 14, 3.6, and 230, respectively, suggesting that K98 is important for

**Figure 4.3: Stopped-flow fluorometric analysis of the binding of HPO to SaE22A.**

The concentration of SaE22A was 1  $\mu\text{M}$ , and the concentrations of HPO were 5, 10, 20 and 40  $\mu\text{M}$  for traces 1, 2, 3, and 4, respectively. All concentrations were those immediately after the mixing of the two syringe solutions. Both SaE22A and HPO were dissolved in 100 mM 100 mM Tris-HCl, pH 8.3. The fluorescent signals were rescaled so that they could be fitted into the figure with clarity. The solid lines were obtained by nonlinear regression as described in the Experimental Procedures section. Panel B is a replot of the apparent rate constants vs. the HPO concentrations. The solid line was obtained by linear regression.

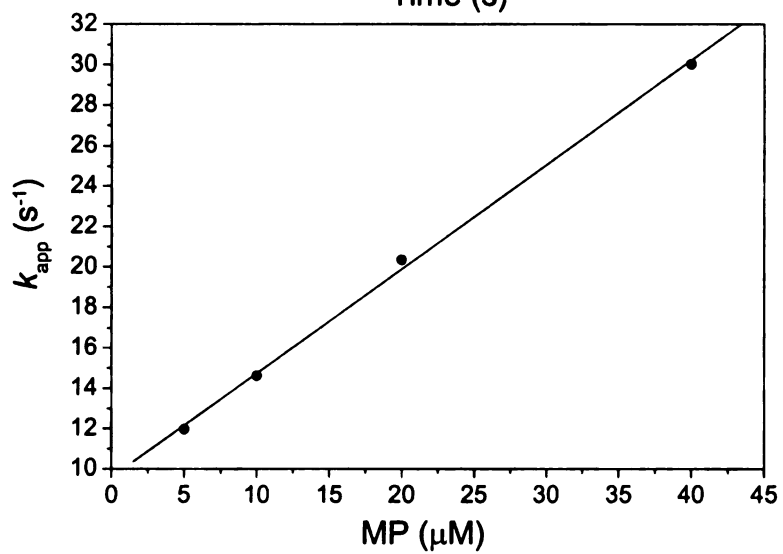
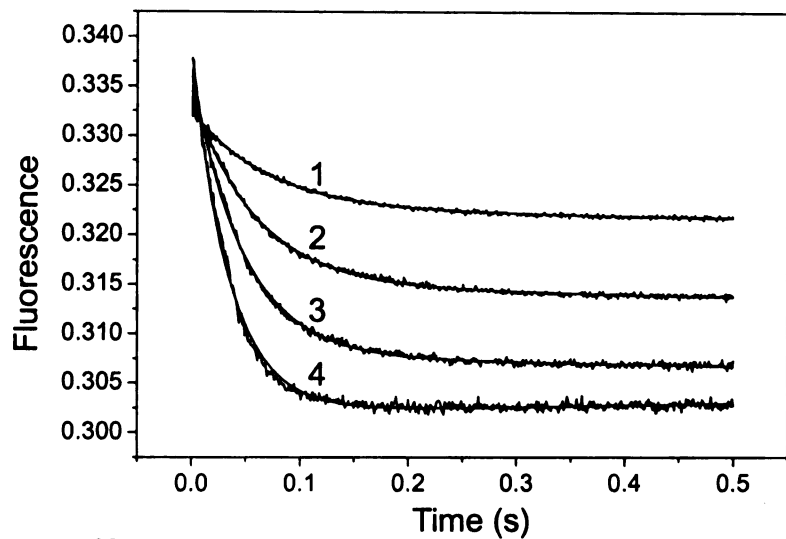


Table 4.2: Binding Constants of SaDHNA and Site-Directed Mutants<sup>a</sup>

		SaDHNA	SaE22A	SaE74A	SaK100A	SaK100Q
NP	$K_d$ ( $\mu\text{M}$ )	18 $\pm$ 2	13 $\pm$ 0.6	> 4000	6.9 $\pm$ 0.7	11 $\pm$ 0.3
	$k_1$ ( $\mu\text{M}^{-1}\text{s}^{-1}$ )	0.24 $\pm$ 0.01	0.29 $\pm$ 0.008	n.d.	0.22 $\pm$ 0.004	0.19 $\pm$ 0.007
	$k_{-1}$ ( $\text{s}^{-1}$ )	4.5 $\pm$ 0.1	4.0 $\pm$ 0.1	n.d.	1.2 $\pm$ 0.07	2.0 $\pm$ 0.08
MP	$K_d$ ( $\mu\text{M}$ )	13 $\pm$ 1	11 $\pm$ 0.9	>3000	9.1 $\pm$ 0.6	13 $\pm$ 1
	$k_1$ ( $\mu\text{M}^{-1}\text{s}^{-1}$ )	0.29 $\pm$ 0.02	0.31 $\pm$ 0.01	n.d.	0.27 $\pm$ 0.006	0.28 $\pm$ 0.002
	$k_{-1}$ ( $\text{s}^{-1}$ )	4.2 $\pm$ 0.2	4.0 $\pm$ 0.1	n.d.	2.1 $\pm$ 0.1	4.3 $\pm$ 0.1
HPO	$K_d$ ( $\mu\text{M}$ )	24 $\pm$ 0.2	17 $\pm$ 2	>6000	6.0 $\pm$ 0.1	8.8 $\pm$ 0.4
	$k_1$ ( $\mu\text{M}^{-1}\text{s}^{-1}$ )	0.45 $\pm$ 0.02	0.56 $\pm$ 0.03	n.d.	0.64 $\pm$ 0.03	0.68 $\pm$ 0.04
	$k_{-1}$ ( $\text{s}^{-1}$ )	10 $\pm$ 0.5	10 $\pm$ 0.2	n.d.	5.8 $\pm$ 0.3	5.8 $\pm$ 0.1

<sup>a</sup>Both the wild-type SaDHNA and mutants have a His-tag at the N-terminus. We have shown previously that the His-tag has no effects on the binding and catalytic properties of the enzyme. The chemical structures of the measured compounds are as follows.

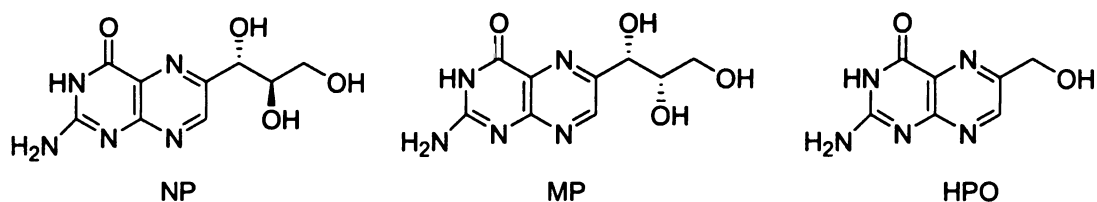


Table 4.3: Binding Constants of EcDHNA and Site-Directed Mutants

		EcDHNA	EcE21A	EcE73A	EcK98A
NP	$K_d$ ( $\mu\text{M}$ )	0.77±0.06	1.7±0.01	260±40	11±0.3
	$k_1$ ( $\mu\text{M}^{-1}\text{s}^{-1}$ )	0.32±0.02	0.46±0.02	n.d. <sup>a</sup>	0.66±0.007
	$k_{-1}$ ( $\text{s}^{-1}$ )	0.29±0.03	0.82±0.02	n.d.	7.2±0.3
MP	$K_d$ ( $\mu\text{M}$ )	2.6±0.06	0.80±0.01	420±20	9.4±0.09
	$k_1$ ( $\mu\text{M}^{-1}\text{s}^{-1}$ )	0.26±0.01	0.43±0.02	n.d.	0.91±0.04
	$k_{-1}$ ( $\text{s}^{-1}$ )	0.58±0.03	0.47±0.02	n.d.	9.1±0.6
HPO	$K_d$ ( $\mu\text{M}$ )	0.10±0.007	4.2±0.01	560±20	23±2
	$k_1$ ( $\mu\text{M}^{-1}\text{s}^{-1}$ )	0.55±0.04	1.4±0.04	n.d.	1.2±0.03
	$k_{-1}$ ( $\text{s}^{-1}$ )	0.062±0.006	6.3±0.2	n.d.	27±1

<sup>a</sup>n.d.: not determined.

the binding of these ligands, particularly for the binding of HPO and NP. The E21A mutation caused increases in the  $K_d$  values for the binding of NP and HP by factors of 2.2 and 42, respectively, but a decrease in the  $K_d$  value for the binding of MP by a factor of 3.3, suggesting that E21 is only important for the binding of HPO.

*Steady-State Kinetic Studies.* The catalytic properties of the mutants were determined by steady-state kinetic measurements. Because the reactions were slow, no quench-flow apparatus was needed. For technical reasons, mainly because of the solubility limits of DHNP and DHMP, only  $k_{cat}/K_m$  could be estimated for SaF74A. Also, only  $k_{cat}$  could be estimated for SaK100Q, because the fluorescence of some unknown small molecules associated with the protein preparation caused significant errors in the reaction rates at low substrate concentrations. The steady-state kinetic parameters of the SaDHNA and EcDHNA mutants are summarized in Tables 4.4 and 4.5, respectively. Probably because of the complicated kinetic mechanism (Figure 2.1), there appears to be no correlation between the  $K_m$  values measured by the steady-state kinetic experiments and the corresponding  $K_d$  values measured by the binding studies. Thus, our analysis of the steady-state kinetic data focuses on the  $k_{cat}$  values of the mutants. For SaDHNA, the E22A mutation caused a decrease in  $k_{cat}$  by a factor of  $4.8 \times 10^3$  with DHNP as the substrate and  $1.5 \times 10^3$  with DHMP as the substrate, in comparison with those of the wild-type enzyme. The K100A and K100Q mutations caused decreases in  $k_{cat}$  by factors of  $2 \times 10^4$  and  $2.8 \times 10^3$ , respectively, with DHNP as the substrate, and by factors of  $2 \times 10^3$  and  $1.8 \times 10^3$ , respectively, with DHMP as the substrate. The effects of the two mutations were very similar. The results suggest that both E22 and K100 are important for catalysis. The  $k_{cat}$  value of SaE74A mutant could not be determined, but its  $k_{cat}/K_m$  value could be

Table 4.4: Steady State Kinetic Constants of SaDHNA and Site-Directed Mutants

	SaDHNA	SaE22A	SaE74A	SaK100A	SaK100Q
DHNP $k_{\text{cat}}$ ( $\text{s}^{-1}$ )	0.045±0.002	(9.3±0.4)×10 <sup>-6</sup>	n.d. <sup>a</sup>	(2.2±0.1)×10 <sup>-6</sup>	(1.6±0.3)×10 <sup>-5</sup>
$K_{\text{m}}$ ( $\mu\text{M}$ )	4.6±0.3	3.9±0.6	n.d.	5.8±1.1	n.d.
$k_{\text{cat}}/K_{\text{m}}$ ( $\text{s}^{-1}\mu\text{M}^{-1}$ )	9.7×10 <sup>-3</sup>	2.4×10 <sup>-6</sup>	(1.7±0.09)×10 <sup>-5</sup>	3.7×10 <sup>-7</sup>	
DHMP $k_{\text{cat}}$ ( $\text{s}^{-1}$ )	0.01±0.001	(6.5±0.2) ×10 <sup>-6</sup>	n.d.	(5.1±0.1) ×10 <sup>-6</sup>	(5.7±0.9)×10 <sup>-6</sup>
$K_{\text{m}}$ ( $\mu\text{M}$ )	5.5±0.2	4.0±0.6	n.d.	9.5±0.7	n.d.
$k_{\text{cat}}/K_{\text{m}}$ ( $\text{s}^{-1}\mu\text{M}^{-1}$ )	1.8×10 <sup>-3</sup>	1.6×10 <sup>-6</sup>	(8.0± 0.08)×10 <sup>-5</sup>	5.4×10 <sup>-7</sup>	

<sup>a</sup>n.d.: not determined.

Table 4.5: Steady State Kinetic Constants of EcDHNA and Site-Directed Mutants

	EcDHNA	EcE21A	EcE73A	EcK98A
DHNP $k_{\text{cat}}$ ( $\text{s}^{-1}$ )	0.082±0.001	(6.5±0.3)×10 <sup>-5</sup>	(7.3±0.6)×10 <sup>-3</sup>	(4.3±0.03)×10 <sup>-6</sup>
$K_{\text{m}}$ ( $\mu\text{M}$ )	7.4± 0.3	1.6± 0.3	9700±1000	2.4±0.1
$k_{\text{cat}}/K_{\text{m}}$ ( $\text{s}^{-1}\mu\text{M}^{-1}$ )	1.1×10 <sup>-2</sup>	4.2×10 <sup>-5</sup>	7.6×10 <sup>-7</sup>	1.8×10 <sup>-6</sup>
DHMP $k_{\text{cat}}$ ( $\text{s}^{-1}$ )	0.089±0.004	(2.3±0.2)×10 <sup>-5</sup>	(6.0±1)×10 <sup>-3</sup>	(5.3±0.05)×10 <sup>-6</sup>
$K_{\text{m}}$ ( $\mu\text{M}$ )	8.0±0.6	0.76±0.2	9800±3000	2.9±0.2
$k_{\text{cat}}/K_{\text{m}}$ ( $\text{s}^{-1}\mu\text{M}^{-1}$ )	1.1×10 <sup>-2</sup>	3.1×10 <sup>-5</sup>	6.1×10 <sup>-7</sup>	1.8×10 <sup>-6</sup>

estimated from the linear part of the reaction rate vs. substrate concentration curve, which decreased by a factor of 570 with DHNP as the substrate and a factor of 23 with DHMP as the substrate. The decreases in the  $k_{\text{cat}}/K_m$  values are probably largely due to the increases in  $K_m$ , considering that the mutation caused dramatic decreases in the affinities of the enzyme for all substrate or product analogues. The result suggests that E74 plays no great role in catalysis. This was confirmed by the mutation of the corresponding residue (E73) of EcDHNA. The E73A mutation of EcDHNA caused a decrease in  $k_{\text{cat}}$  by only a factor of  $\sim 10$ . The EcE21A and EcK98A mutants behaved like the corresponding SaDHNA mutants (SaE22A and SaK100A) in terms of their  $k_{\text{cat}}$  values. Thus, the  $k_{\text{cat}}$  of EcE21A decreased by a factor of  $1.3 \times 10^3$  with DHNP as the substrate and by a factor of  $3.9 \times 10^3$  with DHMP as the substrate, in comparison with those of the wild-type *E. coli* enzyme. The  $k_{\text{cat}}$  of EcK98A decreased by a factor of  $1.9 \times 10^4$  with DHNP as the substrate and by a factor of  $1.7 \times 10^4$  with DHMP as the substrate. The results suggest that the conserved glutamate and lysine residues both are important as well for the catalysis by EcDHNA.

## DISCUSSION

Figure 2.1 illustrates the proposed chemical mechanism for the DHNA-catalyzed reaction. It is understood that the enzymatic reaction takes place in the confines of the eight active sites of the octomeric enzyme. For simplicity, the physical steps of substrate binding and product dissociation are omitted. The epimerization reaction is proposed to occur via the intermediate for the retroaldol reaction, which is supported by our NMR

analysis of the reaction in D<sub>2</sub>O that shows no deuteration of 2'H of DHMP (Wang et al., unpublished). However, little is known about how DHNA catalyzes the reaction.

Of the published crystal structures DHNAs (3, 8-10), the most informative structures are the binary HP complexes of SaDHNA and MtDHNA, which reveal the atomic interactions between the pterin moiety of the substrate and the enzymes. Four conserved residues and an important water molecule are found at the active site as illustrated in Figure 1.7 for SaDHNA. The structure of SaDHNA in complex with the substrate analogue NP (3) should provide the structural information about the interaction between the trihydroxypropyl moiety and the enzyme. Unfortunately, the occupancy value is 0 with an R factor of 100 for all trihydroxypropyl atoms of the bound NP, suggesting that the trihydroxypropyl moiety of NP was not seen in the crystal and no structural information about the interaction between the trihydroxypropyl moiety and the enzyme can be deduced from the crystal structure.

The interactions between pterin and DHNA are reminiscent of those of dihydrofolate reductase (DHFR) with dihydrofolate, which also contains a pterin moiety. The common features include two hydrogen bonds between a carboxylate group of a glutamate or aspartate and the 2-NH<sub>2</sub> and 3-NH groups of the pterin and a hydrogen bond between a water molecule and N5 of the pterin. Replacement of D27 of *E. coli* DHFR, a residue corresponding to E74 of SaDHNA and E73 of EcDHNA, with asparagine or serine causes a significant decrease in  $k_{\text{cat}}$  and a significant increase in  $K_m$  or  $K_d$ , suggesting that the aspartate is important for both substrate binding and catalysis (13). On the other hand, replacement of D26 of *Lactobacillus casei* DHFR, which corresponds to D27 of *E. coli* DHFR, with asparagine causes a <10-fold decrease in  $k_{\text{cat}}$  and essentially

no change in  $K_m$  or  $K_d$ , suggesting that the carboxyl group is not important for substrate binding but may play a minor role in catalysis (14). For DHNA, the biochemical properties of SaE74A and EcE73A indicate that the conserved glutamate is very important for substrate binding and its role in catalysis is a minor one if any. It contributes to the binding of the pterin compounds by 3-5 kcal/mol on the basis of the binding data of the two mutants.

The hallmark of the DHNA-catalyzed reaction is general acid and base catalysis (Figure 2.1). The formation of the intermediate of the retroaldol reaction requires the protonation of N5 and the deprotonation of 2'-OH of DHNP. The formation of HP requires the deprotonation of 5-NH and the protonation of the enol group of the reaction intermediate. The epimerization reaction is basically the reversal of the chemical step for the formation of the reaction intermediate following the flip of GA. We have recently shown that the conserved active site tyrosine residue, corresponding to Y54 in SaDHNA and Y53 in EcDHNA, plays a critical role in the protonation of the enol group of the reaction intermediate to form HP (Wang et al., unpublished). Replacement of either Y54 of SaDHNA or Y53 of EcDHNA causes a dramatic decrease in the rate for the formation of HP but no significant change in the rate for the formation of the reaction intermediate. Either mutation converts the aldolase to an oxygenase. The water molecule that is hydrogen bonded to N5 of HP in the crystal structures (8, 9) is probably the general acid for the protonation of N5 of DHNP and its conjugated base for the deprotonation of 5-NH of the reaction intermediate, because no amino acid residue is in a position to play such a role according to the crystal structures. There are several candidate residues that may act as a general base for the deprotonation of 2'-OH of DHNP according to the crystal

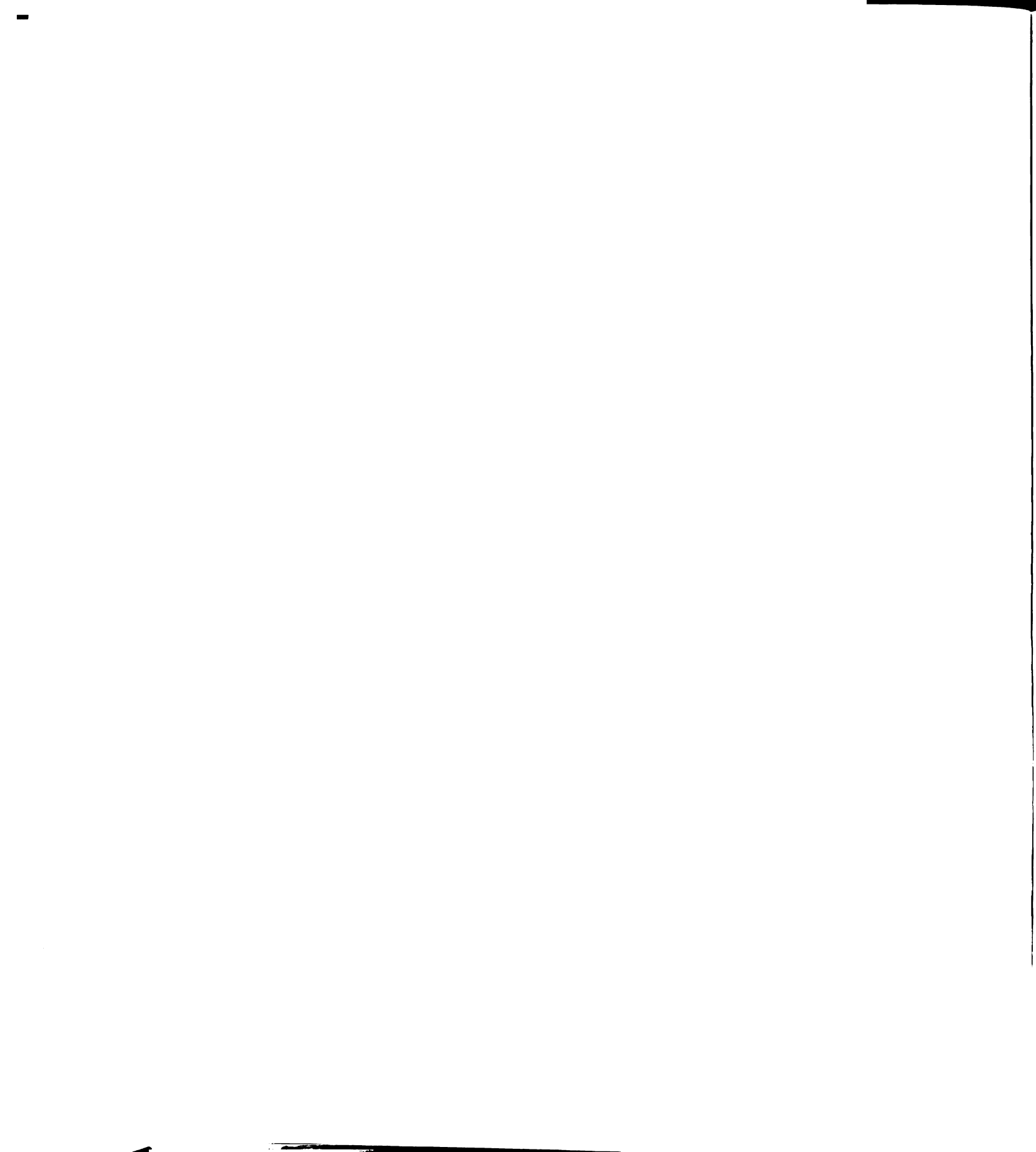
structures, including E22, Y54, and K100 (SaDHNA numbering). Y54 can be excluded on the basis of our previous site-directed mutagenesis of the conserved tyrosine residue (Wang et al., unpublished). The present site-directed mutagenesis study suggests that both E22 and K100 are important for catalysis, with K100 contributing a bit more to the transition state stabilization. The larger contribution by K100 is probably due to its hydrogen bond with the water molecule that serves as a general acid in the first chemical step of the enzymatic reaction. However, from the chemical perspective, K100 is much more likely to serve as a general base for the deprotonation of 2'-OH of DHNP. The optimal pH for the DHNA-catalyzed reaction is 9.6 (4, 15). In the crystal structure of the product complex of SaDHNA, K100 is hydrogen bonded to the carboxyl group of E22, the hydroxyl group of Y54, and the water molecule that serves as a general acid. It probably has a normal  $pK_a$  of  $\sim 10$ , which matches closely with the optimal pH of the enzymatic reaction. On the other hand, the carboxyl group of E22 is hydrogen bonded to the hydroxyl of HP, the main-chain NH of L19, and the side-chain amide of Q27. The  $pK_a$  of E22 is unlikely to be higher than 4.5, the  $pK_a$  of model peptides, which is too far away from the optimal pH of the enzymatic reaction.

While E74 of SaDHNA and the corresponding residue E73 in EcDHNA play a common role in the enzymatic reaction, namely in the binding of the substrate, the roles of E22 and K100 of SaDHNA are slightly different from those corresponding residues E21 and K98 in EcDHNA. Both E22 and K100 of SaDHNA are involved in catalysis but neither contributes to the binding of the substrate. On the other hand, in addition to their roles in catalysis, both E21 and K98 are also involved in the binding of the substrate. The different biochemical properties between SaDHNA and EcDHNA revealed by the

previous study of the wild-type enzymes and this site-directed mutagenesis study suggest that it is possible to develop specific inhibitors for these two enzymes.

## REFERENCES

- (1) Walsh, C. (2003) Where will new antibiotics come from? *Nature Rev. Microbiol.* 1, 65-70.
- (2) Blakley, R. L., and Benkovic, S. J. (1984) in *Folates and pterins*, John Wiley & Sons, New York.
- (3) Sanders, W. J., Nienaber, V. L., Lerner, C. G., McCall, J. O., Merrick, S. M., Swanson, S. J., Harlan, J. E., Stoll, V. S., Stamper, G. F., Betz, S. F., Condroski, K. R., Meadows, R. P., Severin, J. M., Walter, K. A., Magdalinos, P., Jakob, C. G., Wagner, R., and Beutel, B. A. (2004) Discovery of potent inhibitors of dihydroneopterin aldolase using crystallead high-throughput X-ray crystallographic screening and structure-directed lead optimization. *J. Med. Chem.* 47, 1709-1718.
- (4) Mathis, J. B., and Brown, G. M. (1970) The biosynthesis of folic acid XI. Purification and properties of dihydroneopterin aldolase. *J. Biol. Chem.* 245, 3015-3025.
- (5) Horecker, B. L., Tsolas, O., and Lai, C.-Y. (1975) Aldolases, in *The enzymes* (Boyer, P. D., Ed.) pp 213-258, Academic Press, San Diego.
- (6) Allen, K. N. (1998) Reactions of enzyme-derived enamines, in *Comprehensive biological catalysis* (Sinnott, M., Ed.) pp 135-172, Academic Press, San Diego.
- (7) Haußmann, C., Rohdich, F., Schmidt, E., Bacher, A., and Richter, F. (1998) Biosynthesis of pteridines in *Escherichia coli* - structural and mechanistic similarity of dihydroneopterin-triphosphate epimerase and dihydroneopterin aldolase. *J. Biol. Chem.* 273, 17418-17424.
- (8) Hennig, M., D'Arcy, A., Hampele, I. C., Page, M. G. P., Oefner, C., and Dale, G. E. (1998) Crystal structure and reaction mechanism of 7,8- dihydroneopterin aldolase from *Staphylococcus aureus*. *Nature Struct. Biol.* 5, 357-362.
- (9) Goulding, C. W., Apostol, M. I., Sawaya, M. R., Phillips, M., Parseghian, A., and Eisenberg, D. (2005) Regulation by oligomerization in a mycobacterial folate biosynthetic enzyme. *J. Mol. Biol.* 349, 61-72.
- (10) Bauer, S., Schott, A. K., Illarionova, V., Bacher, A., Huber, R., and Fischer, M. (2004) Biosynthesis of tetrahydrofolate in plants: Crystal structure of 7,8- dihydroneopterin aldolase from arabisopsis thaliana reveals a novel adolase class. *J. Mol. Biol.* 339, 967-979.



- (11) Li, Y., Gong, Y., Shi, G., Blaszczyk, J., Ji, X., and Yan, H. (2002) Chemical transformation is not rate-limiting in the reaction catalyzed by *Escherichia coli* 6-hydroxymethyl-7,8-dihydropterin pyrophosphokinase. *Biochemistry* 41, 8777-8783.
- (12) Shi, G., Gong, Y., Savchenko, A., Zeikus, J. G., Xiao, B., Ji, X., and Yan, H. (2000) Dissecting the nucleotide binding properties of *Escherichia coli* 6-hydroxymethyl-7,8-dihydropterin pyrophosphokinase with fluorescent 3'(2)'-o-anthraniloyladenine 5'-triphosphate. *Biochim. Biophys. Acta* 1478, 289-299.
- (13) Howell, E. E., Villafranca, J. E., Warren, M. S., Oatley, S. J., and Kraut, J. (1986) Functional role of aspartic acid-27 in dihydrofolate-reductase revealed by mutagenesis. *Science* 231, 1123-1128.
- (14) Birdsall, B., Casarotto, M. G., Cheung, H. T. A., Basran, J., Roberts, G. C. K., and Feeney, J. (1997) The influence of aspartate 26 on the tautomeric forms of folate bound to lactobacillus casei dihydrofolate reductase. *FEBS Lett.* 402, 157-161.
- (15) Mathis, J. B., and Brown, G. M. (1980) Dihydroneopterin aldolase from *Escherichia coli*. *Methods Enzymol.* 66, 556-560.

MICHIGAN STATE UNIVERSITY LIBRARIES



3 1293 02845 0652